

FUJI ELECTRIC REVIEW

2018
Vol.64 No.



Power Semiconductors Contributing in Energy Management



FUJI ELECTRIC REVIEW

2018
Vol.64 No.

4

Power Semiconductors Contributing in Energy Management

The use of energy-saving technologies and renewable energy has been progressing in order to prevent global warming. Many countries have already declared to completely abolish the sale of gasoline-powered vehicles over the next few decades; and they have been aggressively adopting electric vehicles (xEV) as a means of reducing CO₂ among other rapidly growing initiatives to achieve decarbonization. In response to the need to improve efficiency and miniaturize power electronics devices to ensure the efficient and stable use of electrical energy, power semiconductors have been receiving much attention as the key devices capable of contributing greatly to this goal. At Fuji Electric, we have been developing and commercializing power semiconductors for a variety of different fields. In this special issue we'll be introducing the latest Fuji Electric power semiconductor technologies and products.

Cover Photo:

(1)"XS Series" 650-V discrete IGBT, (2)"Dual XT M254" high speed hybrid module, (3) 3.3-kV 400-A All-SiC module



FUJI ELECTRIC REVIEW vol.64 no.4 2018

date of issue: December 30, 2018

editor-in-chief and publisher KONDO Shiro

Corporate R & D Headquarters
Fuji Electric Co., Ltd.
Gate City Ohsaki, East Tower,
11-2, Osaki 1-chome, Shinagawa-ku,
Tokyo 141-0032, Japan
<http://www.fujielectric.co.jp>

editorial office Fuji Electric Journal Editorial Office
c/o Fuji Office & Life Service Co., Ltd.
1, Fujimachi, Hino-shi, Tokyo 191-8502,
Japan

Fuji Electric Co., Ltd. reserves all rights concerning the republication and publication after translation into other languages of articles appearing herein.

All brand names and product names in this journal might be trademarks or registered trademarks of their respective companies.

The original Japanese version of this journal is "FUJI ELECTRIC JOURNAL" vol.91 no.4.

Contents

Power Semiconductors Contributing in Energy Management	
[Preface] Power Devices and Peripheral Technologies FUNAKI, Tsuyoshi	166
Power Semiconductors: Current Status and Future Outlook FUJIHARA, Tatsuhiko MIYASAKA, Tadashi IKAWA, Osamu	168
High Speed Hybrid Modules Combining High Speed IGBTs with SiC-SBDs USUI, Ryosuke KATO, Yoshiharu TAKAHASHI, Seiichi	176
Line-Up of 2nd-Generation Small IPM with 650 V / 50 A, 75 A OKAYAMA, Kenichi SIRAKAWA, Toru TANAKA, Masanori	181
On-Chip Sensor Built-In IGBT Modules for Driving xEV Motors NAKAYAMA, Tomoya NAKANO, Hayato YOSHIDA, Soichi	186
3.3-kV All-SiC Module with Trench-Gate MOSFETs for Electric Distribution Equipment KANAI, Naoyuki HOYA, Masashi TSUJI, Takashi	190
SiC-MOSFET with High Threshold Voltage and Low On-Resistance Using Halo Structure KOBAYASHI, Yusuke OHSE, Naoyuki KOJIMA, Takahito	195
Estimation of Power Losses, Temperatures and Power Cycle Lifetime for IGBT Modules by Using IGBT Simulator TAKAKU, Taku YUKAWA, Fumio IKENOUCHI, Shun	199
“FA1B00 Series” 4th-Generation Critical Conduction Mode, Power Factor Correction Control ICs ENDO, Yuta YAGUCHI, Yukihiro HIASA, Nobuyuki	205
“XS Series” 650-V Discrete IGBTs HARA, Yukihito KATO, Yoshiharu TAMURA, Takahiro	211
6.5th-Generation Automotive High Pressure Sensors SATO, Eisuke UENO, Fumiya UZAWA, Ryohei	215
Regular Paper	
“UPS7000HX Series” and “UPS6000DX Series,” Using Lithium Ion Batteries YASUMOTO, Koji KITANO, Akihiro GOTO, Mizuho	221
New Products	
“XS Series” 650-V Discrete IGBTs	227
7th-Generation “X Series” RC-IGBT Module “Small-2B”	229
High Speed Hybrid Modules Combining High Speed IGBTs with SiC-SBDs	232

Power Devices and Peripheral Technologies



FUNAKI, Tsuyoshi*

It is believed that the evolution of power devices is driven by the requirement of improving power electronics performance. The material and process for Si semiconductor material has been matured, and power devices employing Si are approaching performance limitation of material. Accordingly, wide bandgap semiconductors SiC (silicon carbide) and GaN (gallium nitride) are believed to invoke game change in power device development. News report simply addresses that the replacement of Si device to wide band gap semiconductor device, e.g. SiC device, achieves loss reduction. However, the replacement of device structure from bipolar to unipolar realizes loss reduction. Though, conventional Si semiconductor material employs a bipolar structure to realize both high breakdown voltage and low conduction loss at high voltages, but SiC semiconductor material can employ unipolar structure. Unipolar devices, such as metal-oxide-semiconductor field-effect transistor (MOSFET), have no loss due to knee voltage of PN junction. Moreover, unipolar devices do not employ conductivity modulation, then fast switching operation is achieved, and there is almost no loss resulting from reverse recovery or tail current. The wide bandgap is beneficial in maintaining breakdown voltage at high temperatures.

A large distance between conductors is required to secure insulation for high voltage circuit. This increases parasitic inductance in wiring. Fast switching operations increase the time rate of change in circuit current and increase surge voltage with interacting parasitic inductance. In this way, there is a trade-off between employing higher circuit voltage and adopting high-speed switching. Modularization of multiple power devices and circuit components is necessary to improve this trade-off.

Passive components such as inductors, transformers, and capacitors dominate large volumes and weights in power electronics systems, and high-frequency switching operation is required to miniaturize them. The fast switching capability of MOSFET enables high-frequency switching operations. But, it must be careful about high-frequency switching operation of MOSFET with hard switching. It is believed that the faster the switching speed is, the lower the switching loss is. However, during MOSFET is turning-on, the stored electric charge

in the depletion layer is shorted via a channel, resulting in switching loss. This loss is constant, regardless of switching speed. Therefore, the loss increases in proportion to switching frequency in hard switching operation, which makes it difficult to increase the switching frequency. It is therefore necessary to apply soft switching with zero voltage turn-on to increase switching frequency. It is necessary to detect zero cross timing of voltage and current to ensure reliable soft switching, and sensing devices must also be integrated into power modules.

The miniaturization of power modules to reduce parasitic inductance also leads to an increase in heat generation density due to loss at power devices, and it is therefore necessary to improve heat dissipation and thermal resistance. Power device die^{*1} are attached to a module substrate for current output and heat dissipation. Die attachment^{*2} with solder offers high thermal resistance, however, mitigates the stress generated as a result of the difference in thermal expansion coefficient with the copper plate on the module substrate, and by temperature changes. The process temperature of sintered metal die attach, such as silver, is lower than the melting point, and it results in low thermal resistance. However, thin bonding layers to ensure low thermal resistance is difficult to mitigate thermal stress. There are many difficulties in sintering die attach process to be overcome such as requiring pressurization in the bonding process in order to ensure sufficient bonding strength and reliability. Moreover, the miniaturization of high-voltage power modules results in high electric field inside module. Consequently, in addition to power devices, insulating substrate materials and sealing material must also have high critical electric field. Insulating materials are required to have not only high dielectric breakdown capability, but also electrical characteristics such as no space charge accumulation and maintain volume resistivity at high temperatures, as well as free from partial discharge due to void formation. We must therefore simultaneously satisfy mechanical and chemical properties such as degassing in the sealing process and substrate material adhesion. Furthermore, the miniaturization

* Ph.D (Engineering), Professor, Graduate School of Engineering, Osaka University

*1: Die: semiconductor chip

*2: Die attachment: bonding semiconductor chips to a substrate

of power modules reduces the thermal conduction area. Consequently, further improvements in cooling performance using methods such as double side cooling or direct water cooling are also required at the same time.

As discussed above, we must simultaneously develop and apply a variety of peripheral technologies to effectively utilize the performance of evolving power devices.

In other words, we need to integrate technologies and knowledges across different fields such as power devices, metallurgy and dielectric materials, as well as thermodynamics and mechanical engineering. To achieve this, we need to see development from the perspective of these issues involving the cooperation of industry, government, and university.



Power Semiconductors: Current Status and Future Outlook

FUJIHIRA, Tatsuhiko* MIYASAKA, Tadashi* IKAWA, Osamu*

1. Introduction

Energy consumption has been steadily increasing as populations and economies grow worldwide. In addition to measures for conserving energy, the use of renewable energies, such as photovoltaic power and wind power, has been expanding in an attempt to suppress CO₂ emissions and prevent global warming. Many countries have already declared their desire to completely ban the sale of gasoline powered vehicles in a few decades and been employing electric vehicles (xEV) as a means of reducing CO₂ and rapidly growing initiatives to achieve decarbonization.

Fuji Electric has been working on innovating energy technology for a long time. We have been contributing to the realization of a responsible and sustainable society by developing and commercializing power semiconductors as key devices in the power electronics products used in achieving energy stability and optimization.

2. Power Semiconductors and Application Examples

Figure 1 shows some application examples of Fuji Electric's power semiconductor products. Fuji Electric is developing power semiconductors to meet various needs. We offer power discrete devices*¹

* Electronic Devices Business Group, Fuji Electric Co., Ltd.

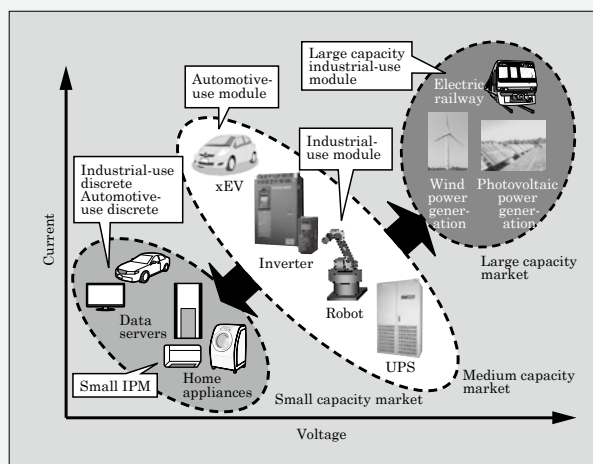


Fig.1 Examples of Fuji Electric power semiconductor product applications

and small intelligent power modules (IPM)*² for small capacity markets and power modules*³ for medium and large capacity markets, and they have industrial and automotive applications respectively. We are also developing products that use silicon (Si) and silicon carbide (SiC)*⁴ as materials for power semiconductor devices.

It is important to adopt designs that ensure long-term reliability for power semiconductors. This includes not only semiconductor chip design, but also package electrical design, heat dissipation design, insulation design, and the design guarantees initial characteristics over a certain period of time. Fuji Electric has repeatedly innovated technologies

*1: Power discrete device

This power semiconductor device consists of a single IGBT or MOSFET power semiconductor device, or a circuit referred to as a 1-in-1 in which the device is supplemented with a diode inserted in an inverse parallel manner. The shape is generally determined by the pin layout and it adopts a package such as TO-220 or TO-3P. It is used in small capacity PC power supplies, uninterruptible power systems, LCD displays and small motor control circuits.

*2: IPM

Abbreviation for intelligent power module. This is a power module that incorporates a power semiconductor device, drive circuit and protection circuit. Circuit design can be facilitated and the performance of the power semiconductor device can be maximized by using a dedicated drive circuit.

*3: Power module

This is a package in an easy-to-use form that is created by routing multiple

power semiconductors, corresponding to diode and transistor based applications, to construct an electrical circuit. It is referred to as a 1-in-1, 2-in-1, 6-in-1 or likewise, depending on the number of devices in the module (usually an IGBT + inverse parallel connected FWD). A module mounted with a drive circuit for controlling the power semiconductor device is called an intelligent power module (IPM).

as it develops power semiconductors that meet the requirements of high functionality, large capacity, and eco-friendliness.

In this chapter, we will provide an overview of the power semiconductor products developed by Fuji Electric.

2.1 Power module products (Si)

In the field of power module products, small IPMs are used in household appliances, such as air conditioners, and in the small capacity applications of inverters and servos. The demand for energy savings is also increasing in the applications that small IPMs are targeted at. For example, air conditioners are required to exhibit low noise characteristics in Europe and other countries in order to meet the standards related to energy consumption efficiency and comply with EMC standards for preventing radio wave interference. To meet these energy-saving demands, Fuji Electric has commercialized a 2nd-generation small IPMs⁽¹⁾⁻⁽³⁾. In addition, we have developed a line-up of 650-V/50-A, 75-A products based on this 2nd-generation small IPMs that is capable of being used in applications typified by large air conditioners and industrial-use inverters.

For medium capacity industrial applications such as inverters, robots and uninterruptible power systems (UPS), we have developed the “X Series” as a line-up of the latest modules and IPMs that uses 7th-generation chip technology and packaging technology^{(4),(5)}.

In the medium capacity, we have also commercialized modules and IPMs for xEV, such as hybrid electric vehicles and electric vehicles⁽⁶⁾. IGBT*⁵ modules are key components in the inverters used to control xEV motors. In addition to reducing loss

to achieve efficient use of battery power, it is also important to achieve miniaturization, weight savings and capacity gains since mounting space is limited in engine rooms. To meet these requirements, we have developed 3rd generation high-power direct liquid cooling modules⁽⁷⁾⁻⁽⁹⁾ for automotive applications that are equipped with RC-IGBTs*⁶. In addition to this 3rd-generation direct liquid cooling technology, we have developed large-capacity automotive modules that make use of lead frame technology instead of conventional wiring for the main circuit wiring in order to achieve further miniaturization and high reliability^{(10),(11)}. In addition, in the field of temperature sensing for overheating protection, we have made use of on-chip temperature sensors instead of conventional negative temperature coefficient (NTC) thermistors in the development of on-chip sensors-integrated IGBT modules for xEV motor drives that seek to achieve miniaturization, weight savings and enhanced current capacity.

We have developed X-Series high-capacity modules to meet the demands of further miniaturization and increased efficiency in power conversion equipment⁽¹²⁾. Moreover, we have been developing hybrid modules suitable for electric railways that secure a higher degree of efficiency and reliability by employing new packages that utilize low-loss SiC-SBDs*⁷ instead of an FWDs*⁸⁽¹³⁾.

In order to use IGBT in applications characterized by frequent and repeated acceleration and deceleration, such as xEV, it is necessary to adopt a design that sufficiently takes into consideration power loss and temperature rise in the complex operation patterns related to the lifetime and reliability of the equipment.

Fuji Electric has released an IGBT simulator

*4: SiC

SiC is a compound of silicon (Si) and carbon (C). It is characterized by a multi-crystal polymorph such as 3C, 4H and 6H. It is referred to as a wide-gap semiconductor with a band gap of 2.2 to 3.3 eV depending on the structure. Since it has physical properties advantageous to power devices, such as high dielectric breakdown voltage and high thermal conductivity, it is contributing to the development of devices characterized by high withstand voltage, low loss and high temperature operation.

*5: IGBT

Abbreviation for insulated gate bipolar transistor. The gate has the same structure as MOSFET. It is a voltage control device that has a gate insulated with an oxide insulating film. It makes use of the strong points of MOSFET and bipolar transistors. It can make use of conductivity modulation because of its bipolar operation. As a result, it

is able to achieve the high switching speed, high withstand voltage and low on-state resistance required by inverter applications.

*6: RC-IGBT

Abbreviation for reverse-conducting IGBT. This device integrates an IGBT and FWD, which are used together as a pair, on a single chip in the module. It exhibits excellent heat dissipation characteristics since the IGBT and FWD operate in alternation, and it facilitates IGBT module miniaturization and improved power density since it can reduce the number of chips in the module.

*7: SBD

Abbreviation for Schottky barrier diode. This is a diode characterized by a rectifying action that makes use of a Schottky barrier formed through metal and semiconductor bonding. Its excellent electrical characteristics have made it an object of study in the application to SiC-SBD based FWD.

Compared with P-intrinsic-N (PiN) diodes that also use of a small number of carriers, SBD diodes, which operate only with a large number of carriers, speed up reverse recovery and reduce reverse recovery loss.

*8: FWD

Abbreviation for free wheeling diode. It is also referred to as a circulation diode. This device is connected in parallel with the IGBT in power conversion circuits of inverters, and is responsible for recirculating the energy stored in inductance to the power supply side when the IGBT is turned off. PiN diodes are mainstream for Si based FWD. Since it is a bipolar type that also uses a small number of carriers, the voltage drop during forward current flow can be reduced. However, this will also result in a larger reverse recovery loss.

that is available free of charge on our website to calculate power loss and temperature in IGBT modules⁽¹⁴⁾. It has been updated to enable characteristics such as the temperature dependence of loss, which is a characteristic more closely reflects actual situations.

2.2 Power module products (SiC)

SiC is expected to proliferate as a next-generation power semiconductor material. Since SiC has about 3 times the band gap and thermal conductivity of Si, it has very few thermally excited carrier and thus can diffuse generated heat more easily, thereby contributing to high-temperature operation. Moreover, it also has the benefit of reducing loss.

In order to reduce the switching loss of power semiconductors, it is effective to replace IGBT with MOSFET^{*9}. However, increase in the conduction loss of a Si-MOSFET is the problem we have to work on. SiC has a dielectric breakdown electric field strength approximately 10 times that of Si, and thereby exhibits that a high withstand voltage can be secured even in devices that are thinner. Furthermore, it also has the benefit of reducing conduction loss because heavy doping can be done at the drift layer. Therefore, by utilizing SiC-MOSFET for the switching element, it is possible to reduce loss in power conversion equipment to a greater extent than can be done using Si-IGBT. By taking advantage of the superiorities of high operation temperature, low loss, and high withstand voltage exhibited in these types of SiC devices, it is possible to achieve miniaturized, high power density modules.

Fuji Electric is developing small and medium capacity products to which a low-inductance high-output packaging technology is applied to derive these superiorities from SiC devices. Furthermore, we are also developing large capacity products such as power distribution equipment.

We are confident that our modules with SiC trench gate MOSFETs have world-class low-loss characteristics^{(15),(16)}. In order to achieve further improvement, we have developed an application technology for halo structure vertical SiC trench gate MOSFET that suppresses the short channel effect⁽¹⁷⁾. This development was conducted as part of a project of the joint research body Tsukuba Power Electronics Constellation (TPEC).

As mentioned in Section 2.1, we have developed

products that utilize 7th-generation chip technology and packaging technology using Si that can be applicable to medium capacity industrial fields such as inverters, robots and UPS. Demand is increasing for power conversion equipment with further miniaturization and efficiency using high carrier frequency regions for power conversion. To meet this demand, Fuji Electric has developed high-speed hybrid modules that combine high-speed IGBTs and SiC-SBDs capable of lowering loss in high carrier regions of 20 kHz or higher.

2.3 Power discrete, power ICs, pressure sensors

In recent years, the use of the Internet of Things (IoT), big data and artificial intelligence (AI) has been increasing the amount of data used worldwide. As a result, UPSs for servers and data centers have been becoming more efficient. In addition, there has been increasing demand for high-efficiency power conditioning systems (PCSs) that convert DC to AC to use renewable energies such as photovoltaic power generation. Fuji Electric has been developing discrete IGBTs that achieve high efficiency for UPS and PCS. We have also recently developed the “XS Series” as a line-up that improves the $V_{CE(sat)}$ responsible for steady-state loss as well as switching loss compared with previous “High-Speed W Series” products⁽¹⁸⁾.

Against the backdrop of fuel efficiency and exhaust gas regulations, the number of pressure sensors for automotive applications has been increasing. In intake systems, pressure sensors are used to highly control the air and fuel mixture ratio in order to improve fuel efficiency. In exhaust systems, pressure sensors are used to highly control the amount of gas recirculated after combustion in order to clean the exhaust gas. Pressure sensors are also used to detect fuel leaking from a tank. Fuji Electric has developed pressure sensors for these types of applications for low pressure^{(19),(20)}. The demand has also been greatly increasing for high-pressure sensors for brakes, transmissions and hydraulic control of engine oil. Fuji Electric improved its 5th-generation automotive high-pressure sensors for conventional engine oil pressure applications and has developed 6.5th-generation automotive pressure sensors that ensure accuracy under the high temperature environments accompanying engine downsizing.

Switching power supplies of 75 W or more used

*9: MOSFET

Abbreviation for metal-oxide-semiconductor field-effect transistor. This voltage control device is a type of field-effect transistor that has a gate insulated with an oxide insulating film. It is the most common

structure in LSI. Its unipolar operation enables operation at high speeds, but it is used as a low withstand voltage, high frequency device since on-state resistance rises according to withstand voltage. In contrast to planar gate MOSFET where the gate is located

on the surface of the device and the channel is parallel to the surface of the device, trench gate MOSFET are characterized by the gate being embedded in a groove formed on the device and the channel perpendicular to the surface of the device.

in electronic devices must be equipped with a power factor correction (PFC) circuit that suppresses harmonic current in accordance with the international standard IEC 61000-3-2. In order to achieve energy savings, PFC circuits are continuously required to reduce standby power and improve efficiency at light loads. To meet these requirements, Fuji Electric has developed 4th-generation critical mode PFC control ICs⁽²¹⁾ that exhibit less standby power and higher efficiency at light loads than previous 3rd-generation critical mode PFC control ICs.

3. Power Semiconductor Development Status

In this chapter, we will provide an overview of the development status of Fuji Electric power semiconductors. For details, please refer to the subsequent papers in this journal.

3.1 2nd-generation small IPM 650 V/50 A, 75 A series

Fuji Electric has been developing small IPM products that integrate the power devices and control ICs necessary for inverter circuit configurations that require energy savings and low noise characteristics. In 2015, we launched the 2nd-generation small IPM (2G-IPM) series rated at 600 V/10 to 30 A, which uses X-Series IGBT chip technology. This series achieves lower loss than conventional products, expands maximum operating temperature T_{vjop} from 125 °C to 150 °C and enhances over-current detection and overheating protection functions⁽²⁾. In addition, we have added to this a line-up of 650-V/50-A, 75-A products which are mainly applicable to large air conditioners and industrial-use inverters (see Fig. 2). In order to ensure the same level as conventional products had, the products were designed to suppress the heat generation that accompanies allowable current expansion and reduction in the internal stress that accompanies package size enlargement (refer to “Line-Up of 2nd-Generation Small IPM with 650 V / 50 A, 75 A” on page 181).

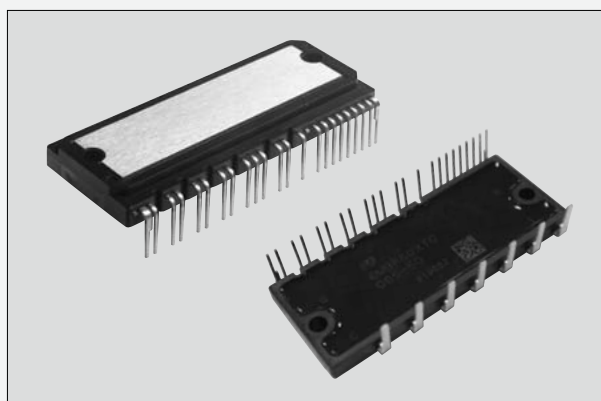


Fig.2 Small IPM (650 V/50 A, 75 A)

3.2 On-chip sensor-integrated IGBT module for xEV motor drive applications

Fuji Electric has developed products that make use of technologies of RC-IGBT chips and cooler integrated structures that meet the needs of low loss, miniaturization, weight-savings and large capacity for automotive modules⁽⁷⁾⁻⁽¹⁰⁾. We have also developed on-chip sensor integrated IGBT modules to meet the demand for further miniaturization. Conventionally, NTC thermistors were arranged near the chip as temperature sensors for overheating protection. However, an on-chip sensor integrated IGBT module, incorporating a temperature sensor diode on the power semiconductor chip, can monitor chip temperature accurately. Compared with NTC thermistors, it is possible to increase allowable current by 13% reducing the safety margin of various characteristics that affect the thermal design features such as device characteristic variation and package thermal resistance variation. A comparison of the allowable current of an automotive IGBT module equipped with an on-chip temperature sensor and an NTC thermistor at a switching frequency of 8 kHz is shown in Fig. 3. The figure shows that modules equipped with an on-chip temperature sensor can be miniaturized more than modules equipped with a conventional NTC thermistor, provided that the allowable current is the same (refer to “On-Chip Sensor Built-In IGBT Modules for Driving xEV Motors” on page 186).

3.3 Simulator based IGBT module generated loss, temperature and lifetime estimation

Fuji Electric has released software that is available free of charge on its website to simulate generated loss and semiconductor chip temperature when incorporating a Fuji Electric IGBT product into a power electronics system such as an inverter. We have recently released Ver. 6, which comes with newly added functionality. Ver. 6 supports 3-level circuits and commonly used PWM^{*10} methods. In

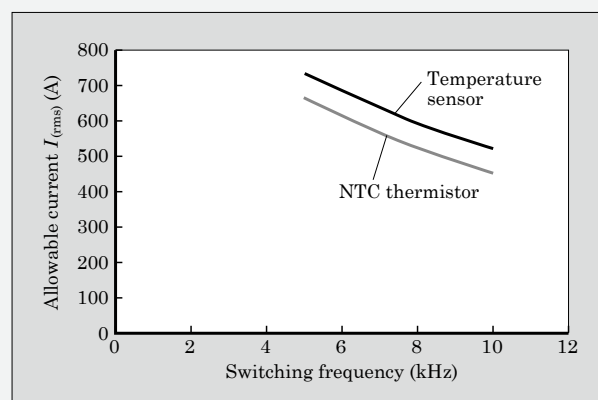


Fig.3 Automotive IGBT on-chip temperature sensor and NTC thermistor allowable current

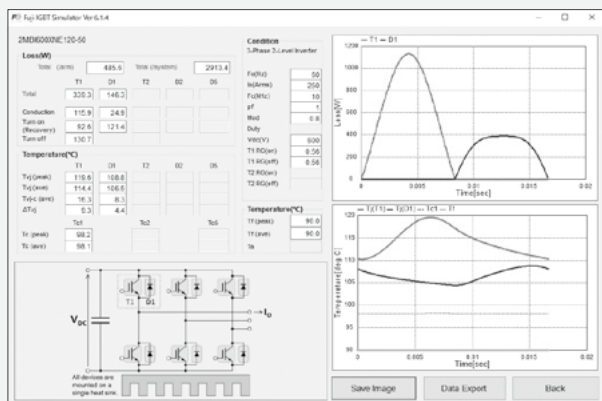


Fig.4 IGBT Simulator Ver. 6 operation screen example (calculation of steady-state loss)

previous version's loss calculations were performed assuming a uniform junction temperature T_{vj} of 125°C. However, in Ver. 6, we incorporated a calculation function that takes into account T_{vj} dependency, thereby making simulations more realistic. Compared with commercially available circuit simulators, it is more user friendly and makes it easy to obtain results with the same level of accuracy as the commercially available circuit simulators show. It also newly supports applications such as automotive modules, which are characterized by complex output and T_{vj} fluctuations. Figure 4 shows the operation screen of IGBT Simulator Ver. 6 (refer to “Estimation of Power Losses, Temperatures and Power Cycle Lifetime for IGBT Modules by Using IGBT Simulator” on page 199).

3.4 Trench gate MOSFET equipped 3.3-kV All-SiC module for distribution equipment

Since September 2014, Fuji Electric has been participating in the “Demonstration Project for Constructing a Next-Generation Distributed Energy Electric Power Network” launched by New Energy and Industrial Technology Development Organization (NEDO). In this project, we have been developing next-generation voltage regulators (distribution equipment) and applicable control systems that use SiC power semiconductors in order to support the expanded use of renewable energies such as photovoltaic power generation, and maintain and improve our international competitiveness in the electric power equipment and systems industry. So far we have successfully developed 3.3-kV All-SiC 200-A 1-in-1 module for next-generation distribution equipment⁽²²⁾. In order to further reduce the size and weight of distribution equipment, we have developed modules that expanded rated

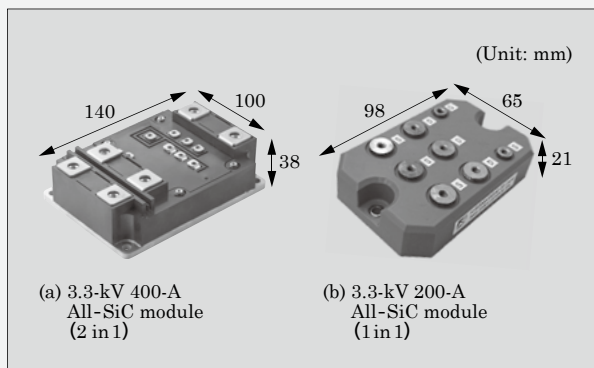


Fig.5 3.3-kV All-SiC module

capacity to 400 A (see Fig. 5). The use of the SiC trench gate MOSFET significantly reduced generated loss when compared with conventional SiC planar-gate MOSFET. The footprint size has been reduced by 45% compared with previous 200-A 1-in-1 modules that have an equivalent circuit configuration (4 units required) (refer to “3.3-kV All-SiC Module with Trench-Gate MOSFETs for Electric Distribution Equipment” on page 190).

3.5 High-speed hybrid modules combining high-speed IGBTs and SiC-SBDs

Fuji Electric has developed high-speed hybrid modules that reduce loss in high frequency regions that are characterized by a switching frequency of 20 kHz or higher, as required by power conversion equipment in the renewable energy field. The products contain combinations of high-speed IGBTs suitable for high-speed switching and low loss SiC-SBDs. The products are compatible with conventional Si modules with 2-in-1 circuit configurations having the same package as that of the conventional Si modules. Figure 6 shows the inverter generated loss simulation results for a distributed small capacity PCS equipped with a high-speed 1,200-V/200-A hybrid module that utilizes an M276 package. Compared with X Series Si modules, total generated loss can be reduced by approximately 50%. Moreover, the rate of reduction increases at high switching frequencies. It can contribute to high efficiency operation and miniaturization through the high-frequency operation of the inverter (refer to “High Speed Hybrid Modules Combining High Speed IGBTs with SiC-SBDs” on page 176).

3.6 SiC-MOSFETs achieving high threshold voltage and low on-state resistance with halo structure

Fuji Electric has been contributing to energy savings of power electronics equipment by develop-

*10: PWM

Abbreviation for pulse width modulation. It is a power control method that uses

switching elements. Given a DC input, it changes output by varying the on-state time width while repeatedly powering on and off

at a constant frequency. It is generally used when converting DC to AC with an inverter.

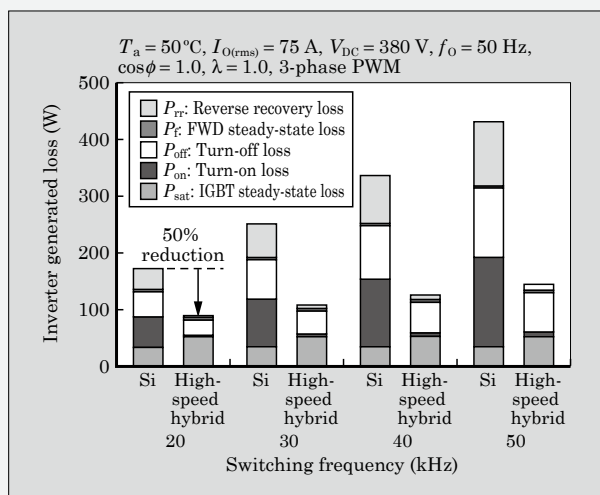


Fig.6 Simulation based comparison of inverter generated loss

ing and commercializing SiC-MOSFET equipped compact and lightweight PCS⁽²³⁾ and mega solar PCS⁽²⁴⁾. Power semiconductor modules play an important role in these products. In order to reduce loss, we have been developing modules that utilize trench-gate MOSFETs in place of conventional planar gate MOSFETs⁽¹⁵⁾. As a measure to further reduce loss, we have recently developed a technology to apply the halo structure used with Si horizontal MOSFET to vertical trench MOSFET. It reduces the on-state resistance that contributes to low loss while maintaining a high threshold voltage. Figure 7 shows the relationship between on-state resistance and threshold voltage. Channel shortening is an effective way to reduce on-state resistance. However, in conventional structures, threshold voltage drops significantly due to the shortened channel, thereby making it susceptible to malfunction (short channel effect). In order to avoid the short channel effect, we applied a halo structure and verified that on-state resistance could be reduced at a high threshold voltage (refer to "SiC-MOSFET with

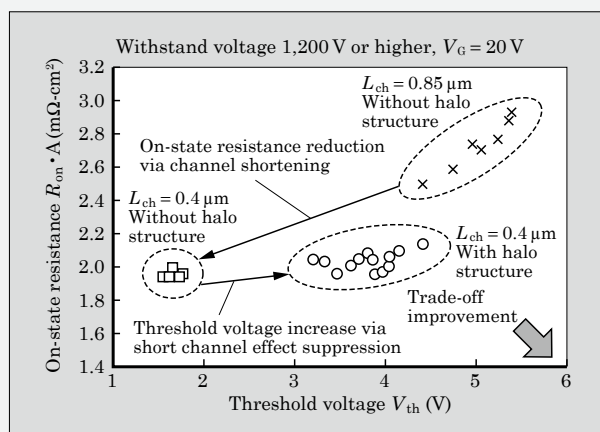


Fig.7 Effect of applying halo structure in trench gate SiC-MOSFET

High Threshold Voltage and Low On-Resistance Using Halo Structure" on page 195).

3.7 "XS Series" 650-V discrete IGBT

Fuji Electric has developed the "XS Series" 650-V discrete IGBT. This product can be widely used for the power circuits of industrial equipment and the PFC circuits of switching power supplies for UPSs and PCSs, demand for which has been increasing accompanying social trends including increased data usage worldwide and the development of renewable energies. Compared with the conventional "High-Speed W Series⁽¹⁸⁾", these modules improve the trade-off between on-voltage and switching loss and meet the demand for low loss. Figure 8 shows the results of measuring efficiency when using the XS Series with a UPS composed of a 3-level inverter I-type circuit as an application example. The UPS output capacity was 3 kW, and IGBT switching frequency was 4 kHz. Compared with the High-Speed W Series, the XS Series improves efficiency by up to 0.12 points in all load regions (refer to "XS Series 650-V Discrete IGBTs" on page 211).

3.8 6.5th-generation automotive high-pressure sensors

High pressure sensors used for measuring engine oil pressure are required to ensure accuracy at high temperatures due to the higher density mounting accompanying engine downsizing implemented to improve fuel efficiency in automobiles. By optimizing the diaphragm diameter, thickness and position of the gauge resistor, Fuji Electric has successfully developed a 6.5th-generation automotive high-pressure sensor that improves output characteristic linearity and circuit temperature characteristics, while ensuring accuracy at high temperatures (see Fig. 9). As a result, the accuracy guaranteed temperature is increased to 150°C, while that of the previous 5th-generation products is 125°C (refer to "6.5th-Generation Automotive High Pressure Sensors" on page 215).

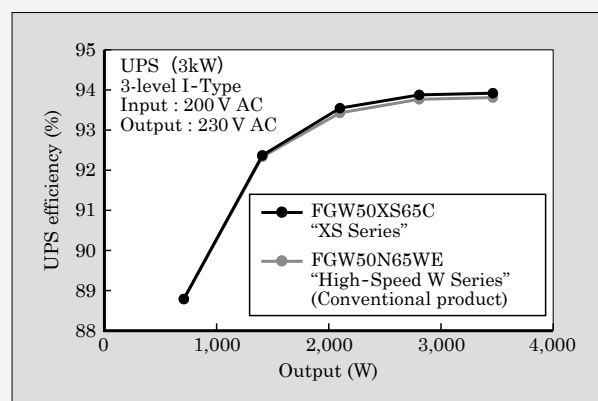


Fig.8 UPS efficiency when applying an "XS Series" 650 V discrete IGBT

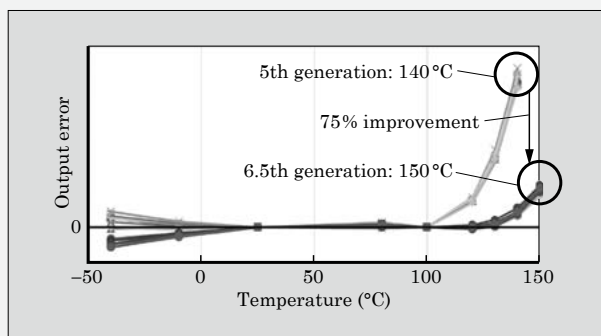


Fig.9 Output error temperature characteristics in 6.5th-generation automotive high-pressure sensors

3.9 “FA1B00 Series” 4th-Generation critical conduction mode, power factor correction control ICs

Switching power supplies are widely used with electronic equipment since they can achieve greater miniaturization, a lighter weight and higher efficiency than conventional linear power supplies. The harmonic current of switching power supplies leads to operation failure and power factor degradation in equipment and distribution facilities, as well as an increase in apparent power. Therefore, power source harmonic current is regulated by the international standard IEC 61000-3-2. Active filter type PFC circuits are widely used to eliminate harmonic current induced power factor problems. Fuji Electric has commercialized ICs that control PFC circuits, thereby contributing to reducing the cost and improving the energy savings of switching power supplies. Fuji Electric has developed the “FA1B00 Series” 4th-generation critical mode PFC control IC, which enables highly efficient power control during light loads and standby. This product is the successor to the “FA1A00 Series” 3rd-generation critical mode PFC control IC. The PFC control IC can comply with power source harmonic current regulations and miniaturize the output capacitor of the PFC circuit. In addition, it makes use of a newly conceived control method that suppresses output voltage ripple and reduce power source harmonic current. The new method can suppress output voltage ripple to 70% of that of conventional methods over the entire input voltage range (see Fig. 10). Basic characteristics such as efficiency and power factor are the same as conventional methods, but in addition, it satisfies power source harmonic current characteristics. It also reduces output voltage ripple with the new control method and miniaturizes smoothing capacitors, which have large footprints in the PFC circuit (refer to “FA1B00 Series 4th-Generation Critical Conduction Mode, Power Factor Correction Control ICs” on page 205).

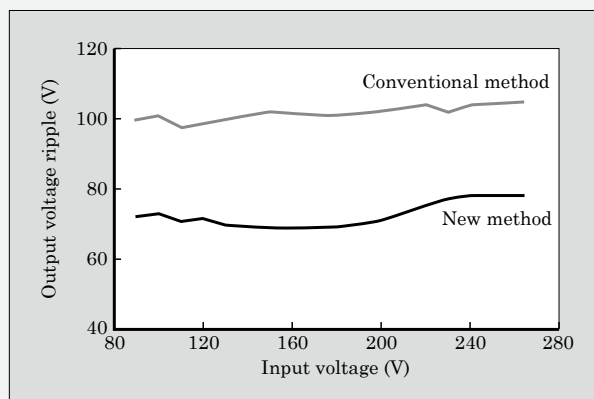


Fig.10 Output voltage ripple comparison (smoothing capacitor: 15 μ F)

4. Postscript

Fuji Electric has continuously pursued innovation of energy technologies on the basis of its management policy of “contributing to the realization of a responsible and sustainable society through innovation of electric and thermal energy technologies.” Power electronics are a driving force behind meeting the increasing demand for energy savings, decarbonization and environmental conservation. Through our technological innovation in power semiconductors, key devices in this field, we are contributing to the achievement of a sustainable society.

References

- (1) Tezuka, S. et al. 2nd-Generation Small IPM Series. FUJI ELECTRIC REVIEW. 2016, vol.62, no.4, p.246-250.
- (2) Araki, R. et al. 2nd-Generation Small IPM. FUJI ELECTRIC REVIEW. 2015, vol.61, no.4, p.242-246.
- (3) Ohashi, H. et al. “The 2nd Generation Small Intelligent Power Module for General-purpose Inverter”. proc. 2016 PCIM Asia.
- (4) Kawabata, J. et al. 7th-Generation “X Series” IGBT Module. FUJI ELECTRIC REVIEW. 2015, vol.61, no.4, p.237-241.
- (5) Heinzl, T. et al. “The New High Power Density 7th Generation IGBT Module for Compact Power Conversion Systems”, Proc. PCIM Europe 2015.
- (6) Gohara, H. et al. Packing Technology of IPMs for Hybrid Vehicles. FUJI ELECTRIC REVIEW. 2013, vol.59, no.4, p.235-240.
- (7) Arai, H. et al. 3rd-Generation Direct Liquid Cooling Power Module for Automotive Applications. FUJI ELECTRIC REVIEW. 2015, vol.61, no.4, p.252-257.
- (8) Koge, T. et al. Speed Enhancement for the 3rd-Generation Direct Liquid Cooling Power Modules for Automotive Applications with RC-IGBT. FUJI ELECTRIC REVIEW. 2016, vol.62, no.4, p.251-255.
- (9) Sato, K. et al. Functionality Enhancement of 3rd-Generation Direct Liquid Cooling Power Module

- for Automotive Applications Equipped with RC-IGBT. FUJI ELECTRIC REVIEW. 2016, vol.62, no.4, p.256-260.
- (10) Osawa, A. et al. "M660" High-Power IGBT Module for Automotive Applications. FUJI ELECTRIC REVIEW. 2017, vol.63, no.4, p.228-231.
 - (11) Nakano, H. et al. "Impact of I2t Capability of RCIGBT and Leadframe Combined Structure in xEV Active Short Circuit Survival", Proc. PCIM Europe 2018.
 - (12) Yamamoto, T. et al. "PrimePACK™" of 7th-Generation "X Series" 1,700-V IGBT Modules. FUJI ELECTRIC REVIEW. 2017, vol.63, no.4, p.214-217.
 - (13) Sekino, Y. et al. "HPnC" High-Current SiC Hybrid Module. FUJI ELECTRIC REVIEW. 2017, vol.63, no.4, p.218-222.
 - (14) Fuji IGBT Simulator. <https://www.fujielectric.com/products/semiconductor/model/igbt/simulation/index.html>, (accessed 2018-09-20).
 - (15) Nakazawa, M. et al. All-SiC Modules Equipped with SiC Trench Gate MOSFETs. FUJI ELECTRIC REVIEW. 2017, vol.63, no.4, p.204-208.
 - (16) Harada, S. et al. "1200 V SiC IE-UMOSFET with Low On-resistance and High Threshold Voltage", Materials Science Forum, 2017, vol. 897, p.497-500.
 - (17) Kobayashi, Y. et al. "Low on-resistance SiC trench MOSFET with suppressed short channel effect by halo implantation" ICSCRM, FR.D2.1, 2017.
 - (18) Hara, Y. et al. High-Speed Discrete IGBT "High-Speed W-Series". FUJI ELECTRIC REVIEW. 2015, vol.61, no.4, p.280-284.
 - (19) Nishikawa, M. et al. 6th Generation Small Pressure Sensor. FUJI ELECTRIC REVIEW. 2011, vol.57, no.3, p.103-107.
 - (20) Uzawa, R. et al. 6.5th-Generation Automotive Pressure Sensors. FUJI ELECTRIC REVIEW. 2017, vol.63, no.4, p.232-236.
 - (21) Sugawara, T. et al. 3rd-Gen. Critical Mode PFC Control IC "FA1A00 Series". FUJI ELECTRIC REVIEW. 2014, vol.60, no.4, p.233-237.
 - (22) Taniguchi, K. et al. 3.3-kV All-SiC Modules for Electric Distribution Equipment. FUJI ELECTRIC REVIEW. 2017, vol.63, no.4, p.209-213.
 - (23) Matsumoto, Y. et al. Power Electronics Equipment Applying SiC Devices. FUJI ELECTRIC REVIEW. 2015, vol.58, no.4, p.212-216.
 - (24) Oshima, M. et al. Mega Solar PCS Incorporating All-SiC Module "PVI1000 AJ-3/1000". FUJI ELECTRIC REVIEW. 2015, vol.61, no.1, p.11-16.



High Speed Hybrid Modules Combining High Speed IGBTs with SiC-SBDs

USUI, Ryosuke* KATO, Yoshiharu* TAKAHASHI, Seiichi*

ABSTRACT

In recent years, there have been an increasing number of power converter applications that require power conversion in the high frequency region to achieve further compactness, weight savings and high efficiency for their power converters. Switching devices are thus greatly demanded for high speed and low loss. Fuji Electric has developed a high speed hybrid module combining IGBTs with SiC-SBDs, both of which operate with low loss and high speed in the high frequency region, significantly reducing switching loss. As a result, power dissipation during high-frequency inverter operation can be reduced by approximately 50% compared with existing products, thereby increasing expectations that it can be utilized with applications that require compactness, weight savings and high efficiency.

1. Introduction

In recent years, there has been increasing demand to reduce emissions of the greenhouse gas CO₂ as a measure to suppress global warming. Against this background, renewable energies, such as photovoltaic power generation and wind power generation, not only require proliferation, but also need to be efficiently converted to power at sites that face various limitations. Moreover, in order to realize further miniaturization and better efficiency in power conversion equipment typified by inverters, an increasing number of applications are performing power conversion at high frequencies of 20 kHz or higher.

Therefore, Fuji Electric has developed high-speed hybrid modules that incorporate low-loss high-speed insulated gate bipolar transistors (IGBT) that can operate in a high switching frequency region of 20 kHz or higher and silicon carbide Schottky barrier diodes (SiC-SBD) into a conventional package.

In this paper, the product's features, application effects and benefits to power conversion equipment are described.

2. Overview of the High-Speed Hybrid Modules

Figure 1 shows applications targeting power device switching frequency and power capacity. Some of the main applications of high-speed hybrid modules include power conversion equipment, such as those used for renewable energies, automotive applications and uninterruptible power systems (UPS), which need to convert power at high frequencies.

Table 1 shows the external appearance of the high-speed hybrid modules, and Table 2, product line-up.

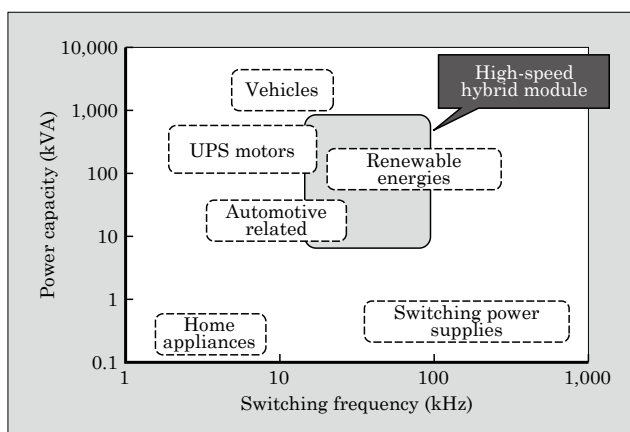

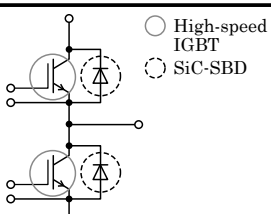

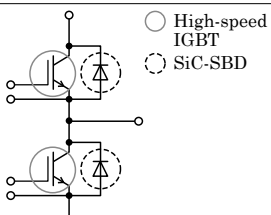


Fig.1 Main applications of high-speed hybrid modules

Table 1 High-speed hybrid module

Package	Equivalent circuit
 Standard 2-in-1 M276	 ○ High-speed IGBT ○ SiC-SBD
 Dual XT M254	 ○ High-speed IGBT ○ SiC-SBD

The high-speed hybrid modules make use of the same package as conventional Si modules in order to main-

* Electronic Devices Business Group, Fuji Electric Co., Ltd.

Table 2 High-speed hybrid module product line-up

Package	Circuit configuration	Dimensions	Rated voltage (V)	Rated current (A)
		W × D × H (mm)		
Standard 2 in 1	2 in 1	62.0 × 108.0 × 30.9	1,200	200
				300
Dual XT	2 in 1	62.0 × 150.0 × 20.5	1,200	300

tain compatibility and consist of a 2-in-1 circuit configuration that combines high-speed IGBTs and SiC-SBDs. The IGBT utilizes a chip optimized for high-speed switching on the basis of the conventional IGBTs while using a SiC-SBD chip as the free wheeling diode (FWD).

3. Features of the High-Speed Hybrid Modules

It is important to improve the generated loss of IGBT modules in order to achieve miniaturization and better efficiency for devices that perform high-speed switching. The generated loss depends largely on the characteristics of IGBT and FWD semiconductor chips. In this chapter, the characteristics of the high-speed IGBT and SiC-SBD chip used for high-speed switching are described.

3.1 High-speed IGBT based turn-off loss improvement

Figure 2 shows the trade-off characteristic between the 1,200-V high-speed IGBT collector-emitter saturation voltage $V_{CE(sat)}$ and turn-off loss E_{off} . The high-speed IGBT, developed on the basis of the existing IGBT, uses the active structure that significantly reduces parasitic capacitance and reduces the concentration of impurities in the collector layer responsible for suppressing hole injection. Compared with the 7th-generation “X Series IGBT,” it further reduce turn-off loss and has the $V_{CE(sat)}$ - E_{off} trade-off characteristic that is suitable for high-speed switching⁽¹⁾. Figure 3 shows a comparison between the turn-off waveforms of a 1,200-V/200-A high-speed hybrid module and

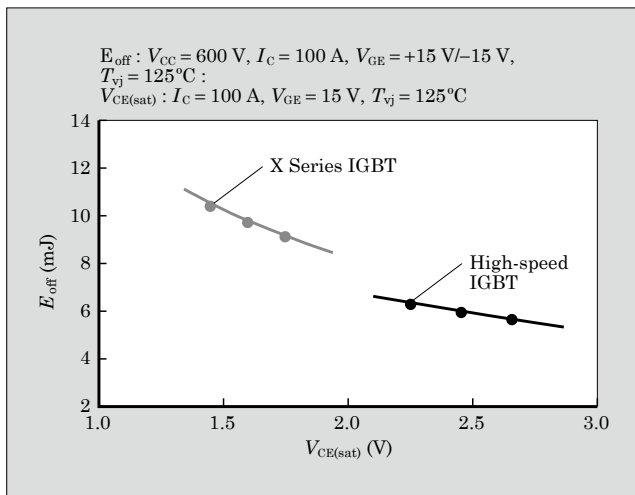


Fig.2 1,200 V high-seed IGBT $V_{CE(sat)}$ - E_{off} characteristic

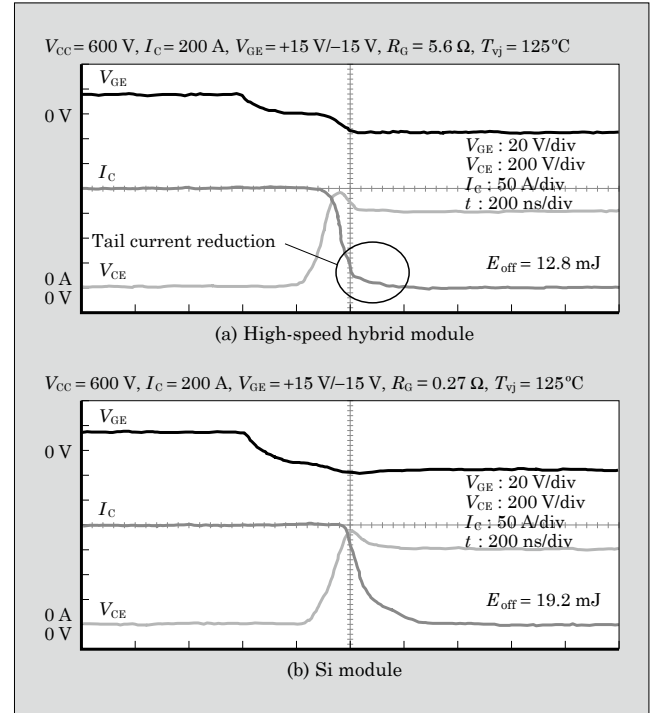


Fig.3 Turn-off waveforms

X Series Si module. Compared with the X Series Si module, the high-speed hybrid module achieves a 33% reduction in turn-off loss E_{off} by greatly improving tail current during turn-off.

3.2 SiC-SBD based improvement in reverse recovery loss and turn-on loss

Figure 4 shows a comparison between the reverse

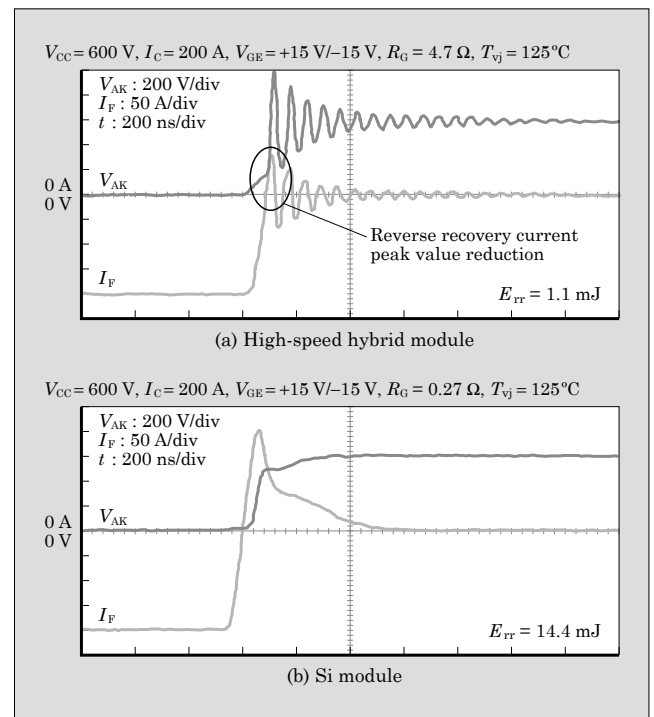


Fig.4 Reverse recovery waveforms

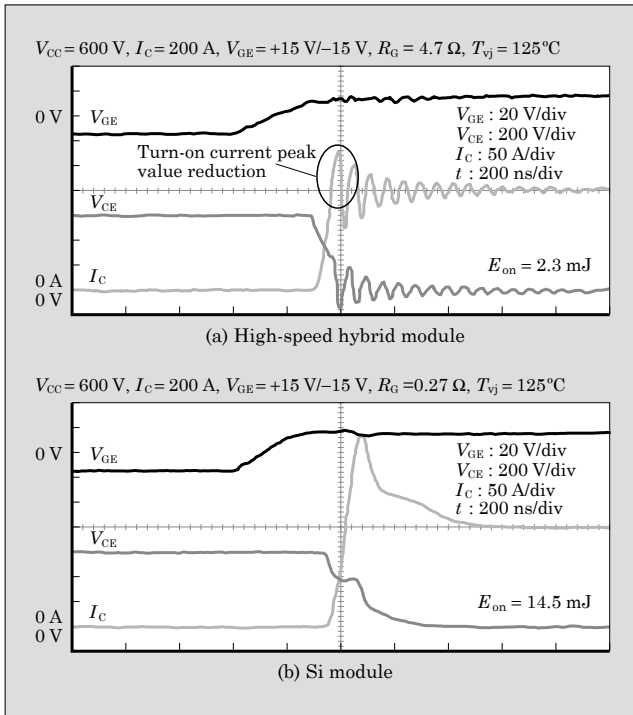


Fig.5 Turn-on waveforms

recovery waveforms of a 1,200-V/200-A high-speed hybrid module and the X Series Si module. The high-speed hybrid module can reduce reverse recovery current peak value by about 60%. This is explained by the fact that SiC-SBD is unipolar device, and so it causes no minority carrier injection. Compared with the X Series Si modules, the high-speed hybrid modules are reduced in reverse recovery loss E_{rr} by 92%.

Furthermore, the peak value of the reverse recovery current in the FWD is reflected in the peak value of the turn-on current in the IGBT of the opposing arm. Since the peak value of the turn-on current reduces as the peak value of the reverse recovery current gets smaller, it has become possible to reduce turn-on loss⁽²⁾. Figure 5 shows a comparison between the turn-on waveforms of a 1,200-V/200-A high-speed hybrid module and X Series Si module. Similar to the reverse recovery waveforms, the peak value of the turn-on current can be reduced by about 60%, thereby demonstrating the superiority of the SiC-SBD. Compared with X Series Si modules, the high-speed hybrid modules are reduced in turn-on loss E_{on} by 84%.

3.3 Switching loss reduction effect

Table 3 shows a comparison of loss between a high-speed hybrid module and X Series Si module. Compared with the X Series Si module, the high-speed hybrid module, which combines a high-speed IGBT and SiC-SBD, achieves a significant reduction in total loss of 66%.

Table 3 Switching loss comparison

	E_{on} (mJ)	E_{off} (mJ)	E_{rr} (mJ)	Total loss (mJ)
X Series Si module	14.5	19.2	14.4	48.1
High-speed hybrid module	2.3	12.8	1.1	16.2
Reduction rate	84%	33%	92%	66%

4. High-Speed Hybrid Module Effect

In this section, as an example, the inverter generated loss and chip junction temperature of a distributed small capacity power conditioning system (PCS) equipped with a 1,200-V/200-A hybrid module that utilizes an M276 package are described.

Figure 6 shows The result of simulating generated loss in the inverter. Compared with the inverter equipped with the X Series Si module at switching frequencies of 20 kHz or higher, the one equipped with the high-speed hybrid module was greatly reduced in switching loss, despite the slight increase in IGBT steady-state loss P_{sat} due to a high $V_{CE(sat)}$.

As a result, total generated loss can be reduced by about 50%. Furthermore, the rate of reduction increased in correlation with increases in switching frequency, and therefore, it can contribute to high-efficiency operation and miniaturization via the high-frequency operation of the inverter.

Figure 7 shows the junction temperature of the chip when mounted to the inverter. The junction temperature of the chip for the high-speed hybrid module at a switching frequency of 20 kHz was lower than that of the X Series Si module with temperature of about 18°C for the IGBT and 19°C for the FWD, enabling the inverter to increase the output current during high-frequency.

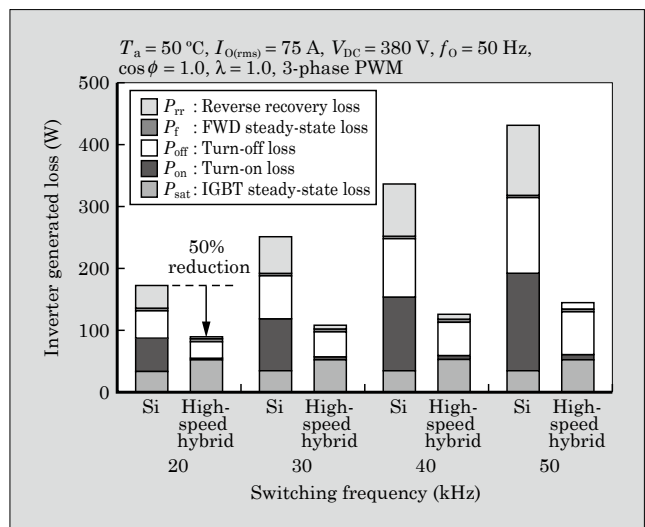


Fig.6 Simulation based comparison of inverter generated loss

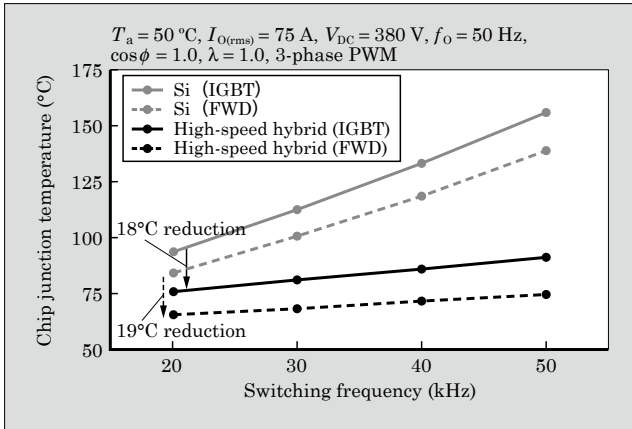


Fig.7 Chip junction temperature when mounted to inverter

5. Contribution to Power Conversion Equipment

Figure 8 shows the dependence of reactor volume on switching frequency. When switching frequency is increased from 10 kHz to 30 kHz, reactor volume can be reduced by about 50%. By miniaturizing passive components, such as reactors, via high-speed switching, the size of the entire unit can be reduced, and this can most likely lead to cost reduction.

Figure 9 and Fig. 10 show examples of using the high-speed hybrid module in a PCS and UPS respectively. The demand for small, lightweight PCS has been increasing due to the proliferation of distributed photovoltaic power generation. Parallel redundant UPS configurations are necessary to ensure high reliability for servers and data centers. There is a growing need for miniaturized UPS since parallel redundant configurations require the use of multiple systems. By using the high-speed hybrid modules, equipment can be compact and lightweight because increased operating frequency help miniaturize capacitors and reactors for filter circuits, which have been large in volume and mass. Furthermore, low loss in the high frequency region is expected to help improve power conversion efficiency.

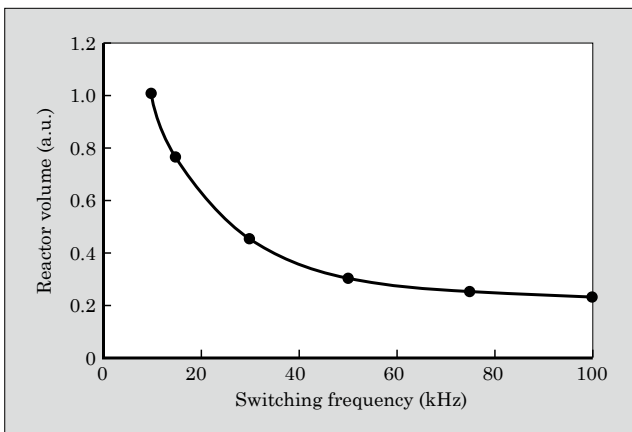


Fig.8 Dependence of reactor volume on switching frequency

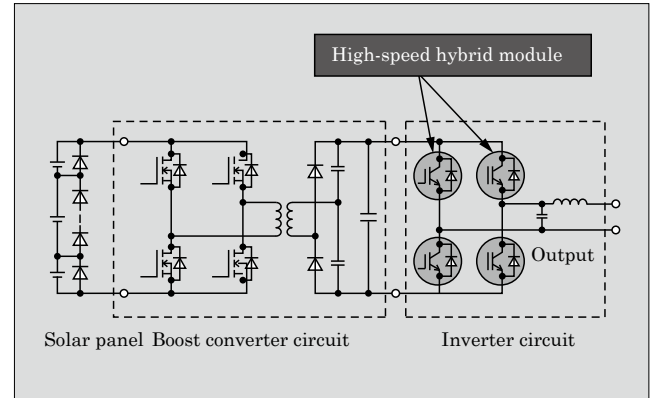


Fig.9 Configuration of PCS power supply using high-speed hybrid modules

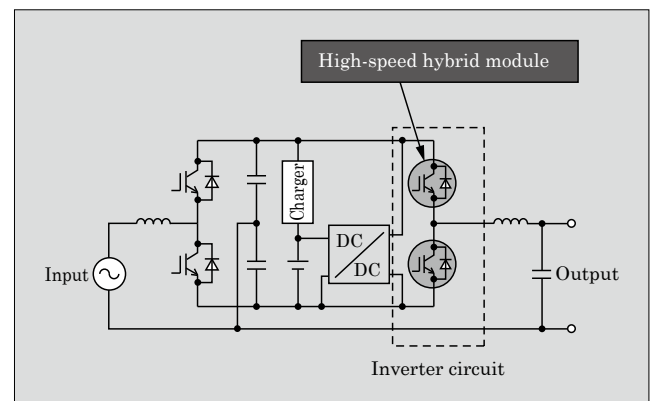


Fig.10 Configuration of UPS power supply using high-speed hybrid modules

Figure 11 shows an example of using the high-speed hybrid module to a power conversion unit used with a welding machine. High-speed switching is required to miniaturize a transformer in power conversion equipment with a high-frequency isolation system, such as welding machines, plasma cutters, and induction heaters (IH). In these types of applications, a resonant circuit system is used to reduce high-speed switching loss and noise. By using a high-speed hybrid module, this circuit system can contribute to the min-

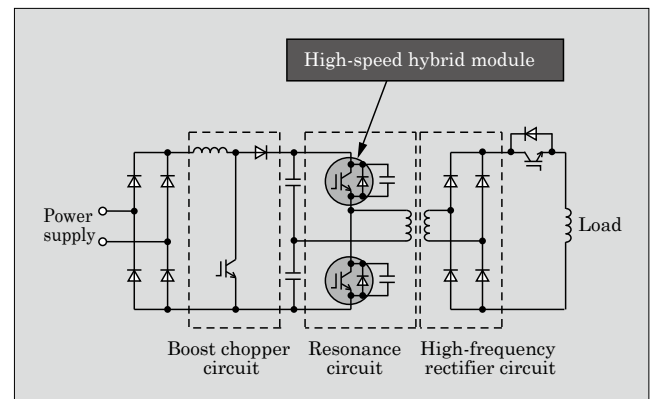


Fig.11 Configuration of welding machine power supply using high-speed hybrid modules

miniaturization and efficiency of power conversion equipment because high-speed switching of 20 kHz or higher is used in the circuit.

In addition, the module is expected to be applied to medical device power supplies such as those for X-rays, as well as EV quick chargers and gas turbines, all of which are requiring further miniaturization, weight savings and enhanced efficiency.

6. Postscript

In this paper, Fuji Electric introduced our high-speed hybrid modules that combine a high-speed IGBTs and SiC-SBDs. The high-speed IGBT reduces turn-off loss, and the SiC-SBD reduces turn-on loss, thereby enabling the module to achieve low loss char-

acteristics during high-frequency operation.

As the demand for applications that perform power conversion at high frequencies increases, Fuji Electric plans to continue pursuing ways to reduce loss so that Fuji Electric can contribute to energy savings through the development of products that meet market demands.

References

- (1) Hara, Y. et al. High-Speed Discrete IGBT “High-Speed W-Series”. FUJI ELECTRIC REVIEW. 2015, vol.61, no.4, p.280-284.
- (2) Onezawa, T. et al. 1,700-V Withstand Voltage SiC Hybrid Module. FUJI ELECTRIC REVIEW. 2015, vol.61, no.4, p.228-231.



Line-Up of 2nd-Generation Small IPM with 650 V / 50 A, 75 A

OKAYAMA, Kenichi* SIRAKAWA, Toru* TANAKA, Masanori*

ABSTRACT

In recent years, to deal with global environmental problems, there has been increasing demand for energy conservation to cope with greenhouse gas emission regulations and size reduction to save on resources. Fuji Electric developed a line-up of 2nd-generation Small-IPM with 650 V / 50 A and 75 A that integrate the power devices and control ICs to compose inverter circuits. The products adopting “X Series” IGBT chip technology reduce their power dissipation compared to conventional products and increase the maximum operating temperature from 125 °C to 150 °C by using a high heat-resistant packaging technology. These enhancements will contribute to saving energy, downsizing of power conversion systems and increasing their output current.

1. Introduction

In recent years, to deal with global environmental problems, there has been increasing demand for energy conservation to cope with greenhouse gas emission regulations and size reduction to save on resources. Inverter air conditioners, motor drives, and servos amp, which are the target of Small-IPM (intelligent power modules), also need to meet these requirements.

Especially, for the inverter air conditioners in principal countries, energy saving standard is established on the basis of the annual performance factor (APF), which represents the energy consumption efficiency estimated under actual usage.

In addition to an energy saving characteristic, equipment needs to have a low noise characteristic that conforms to standards related to electro magnetic compatibility (EMC) specified by the special committee of IEC, Comité international spécial des perturbations radioélectriques (CISPR).

In order to meet market demands, Fuji Electric has provided Small IPM integrated with power devices and control ICs to compose inverter circuits.⁽¹⁾

The Small IPM includes a 3-phase inverter bridge circuit, a control circuit and a protection circuit on one package, contributing to a size reduction of inverter circuits. The 2nd-generation Small IPM (2G-IPM) with rated values 600 V/10 A to 30 A, which was released in 2015, applies the chip technology⁽²⁾ of the “X-series” insulated gate bipolar transistor (IGBT). The product achieved lower power dissipation compared with the conventional types, further saving energy. Furthermore, this product realized increase of maximum operating temperature T_{vjop} from 125 °C to

150 °C based on the high heat-resistant package technology. In addition, thus, the easiness to design and the expansion of the application area of inverters are achieved by improving the accuracy of the over-current detection and the overheat protection function.

The product series of rated 650 V / 50 A, 75 A, which is developed on the basis of 2G-IPM technology, is added to the product line-up this time. In this paper, the features of 2G-IPM technology are described hereinafter.

2. Product Outline

Figure 1 and Table 1 show an external view of the product and its main characteristics respectively. The product has outer dimension of 79.0 × 31.0 × 7.8 (mm) and adopts a dual in-line structure. The safety standard of insulation conforms to the UL1557. The rated voltage is 650 V, and the rated currents is 50 A or 75 A. Each type has a line-up with or without the overheat protection function.

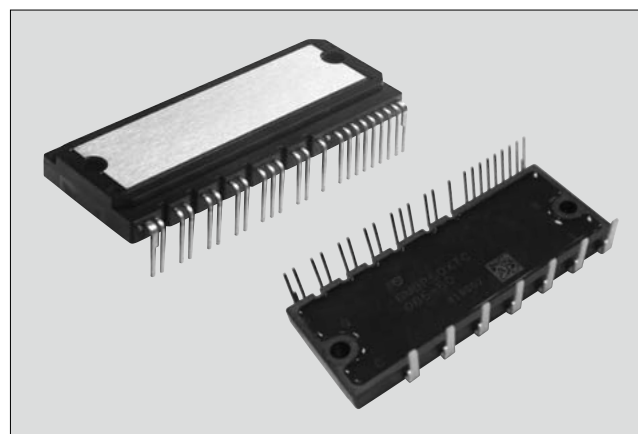


Fig.1 Product appearance

* Electronic Devices Business Group, Fuji Electric Co., Ltd.

Table 1 Main characteristics of product

Voltage	Type name	I_C	I_{CP}	$V_{CE(sat)}$	V_F	Guaranteed operating temperature	Over-temperature protection function
650 V	6MBP50XTA065-50	50 A	100 A	1.30 V (typ.)	1.55 V (typ.)	$T_{vjop} \leq 150\text{ }^{\circ}\text{C}$	None
	6MBP50XTC065-50						Yes
	6MBP75XTA065-50	75 A	150 A	1.30 V (typ.)	1.80 V (typ.)		None
	6MBP75XTC065-50						Yes

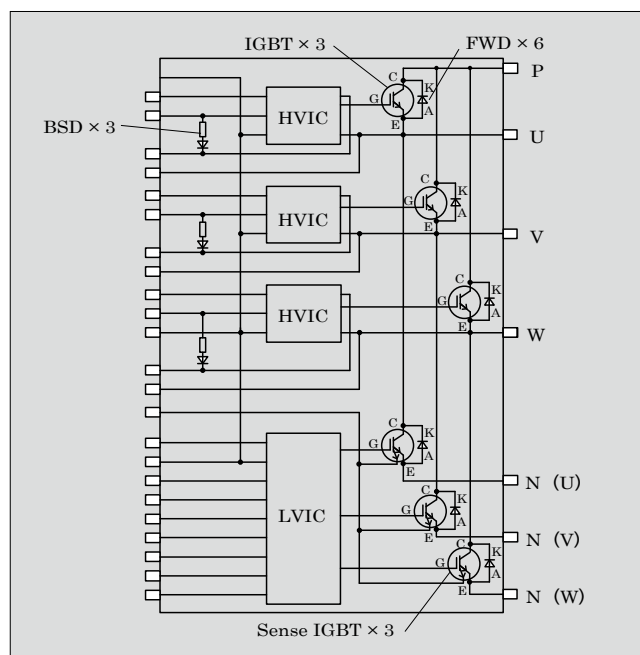


Fig.2 Internal equivalent circuit

Figure 2 shows the circuit configuration of the 2G-IPM. The 2G-IPM includes a 3-phase inverter bridge circuit, which consists of 6 pairs of low-loss IGBTs and high-speed free wheeling diodes (FWD). Each low side IGBT has a shunt current sense IGBT^{*1}. The 2G-IPM has a chip of low-voltage integrated circuit (LVIC) for driving the low-side IGBT and 3 chips high-voltage integrated circuits (HVIC) for driving high-side IGBTs. And this 2G-IPM has a 3 chips of the boot-strap diode (BSD) with current limiter resistors. These make it easy to compose high side power supply by only connecting the external capacitors. Therefore, an external insulating power supply is unnecessary, and the space of print circuit boards can be saved.

3. Product Design

3.1 Device design

(1) IGBT

Figure 3 shows the cross section structures of the IGBT chip for 1st-generation Small IPM (1G-IPM) and that for 2G-IPMs. The IGBT chip for 2G-IPMs is

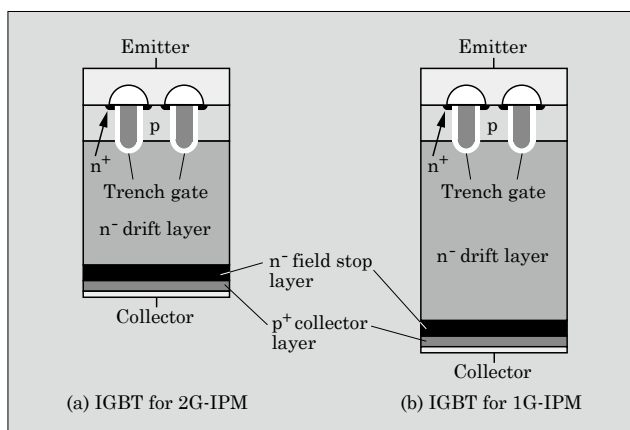


Fig.3 Comparison of cross section structures of IGBT chips

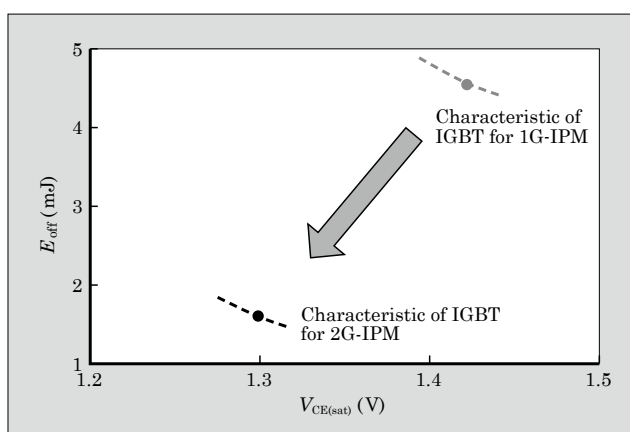


Fig.4 Trade-off relationship of $V_{CE(sat)}$ - E_{off}

based on the X-Series IGBT technology, such as fine cell technology and thinner wafer technology. Those IGBT chips include a newly developed current sensing part, and the IGBT cells for sensing the current are shunted from those of the main current part. Figure 4 shows trade-off relationship between saturated voltage $V_{CE(sat)}$ and turn-off loss E_{off} . The $V_{CE(sat)}$ and turn-off loss of 2G-IPMs are improved by 0.5 V and about 56% respectively compared with 1G-IPMs by optimizing the resistivity and thickness of the drift layer, doping profile of the filed stop (FS) layer and channel density.

(2) FWD

For the improvement of FWD chip characteristics, it is necessary to suppress the dv_r/dt during the reverse recovery resulting in noise generation and to reduce the reverse recovery loss.

Figure 5 and Fig. 6 show trade-off relationship be-

*1: Sense IGBT: IGBT with a current sensing function for over-current protection

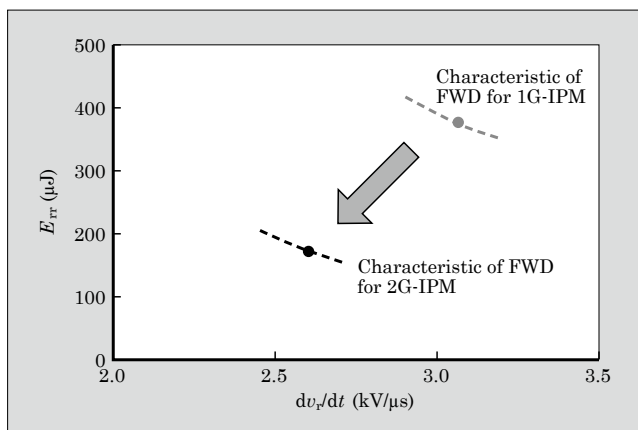


Fig.5 Trade-off relationship of dv_T/dt - E_{rr}

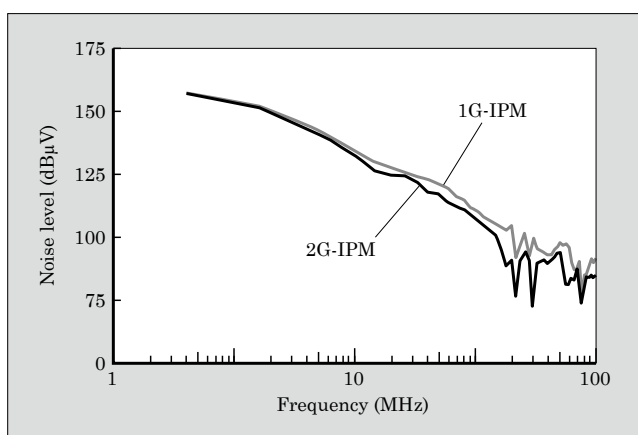


Fig.6 Result of FFT analysis of reverse recovery voltage waveform

tween dv_T/dt and E_{rr} , and the comparison of the FFT analysis of reverse recovery voltage waveforms between FWD chips for 1G-IPMs and those for 2G-IPMs respectively. The FWD for 2G-IPMs is based on the “X-Series FWD” technology. Furthermore, both of soft recovery waveforms and improvement of the trade-off characteristics have been realized by optimizing the anode diffusion profile and the lifetime control. Thus, 10-dB noise reduction by 15% decrease of the dv_T/dt and 55% reverse recovery loss reduction are expected compared with 1G-IPM.

3.2 Packaging

Figure 7 shows the cross section of the package structure. The package structure of newly developed 2G-IPMs is similar to that of 2G-IPMs in mass-production. This package structure has been realized by using the aluminum IMS (insulated metal substrate) and high adhesive strength with the molding resin. In the case of the 1G-IPMs in the actual operation, chip heat was transferred to the outer leads via wire, and there had been a problem that the outer leads reach high temperature. On the other hand, the temperature rise of the outer leads of 2G-IPMs is reduced with the structure in which the heat of the inter-

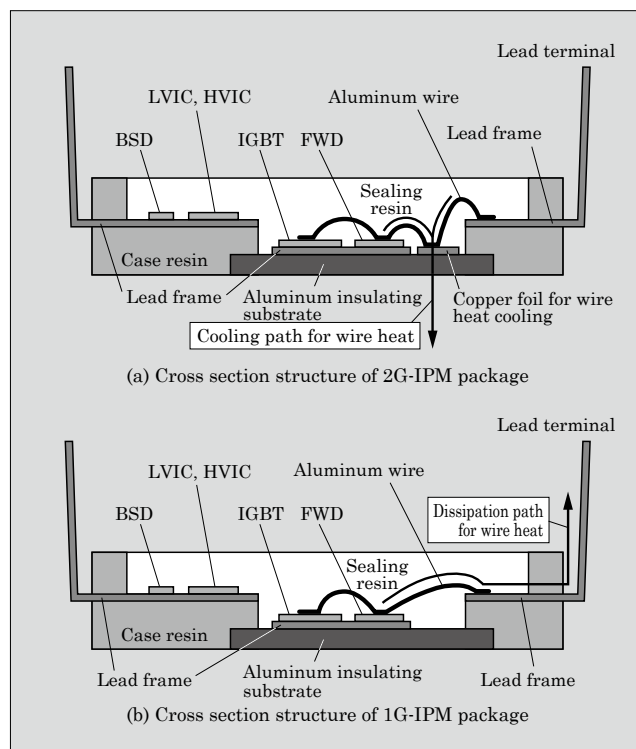


Fig.7 Cross section of package structure

nal wire is dissipated to the aluminum IMS.

Table 2 shows the results of reliability tests. To achieve the high reliability performance that is equivalent to that of the conventional types, the 2G-IPMs with rated values 650 V/50 A and 75 A are designed to suppress the heat generation due to the increase in the rated current and to reduce the internal stress of package caused by large package size.

- (1) Suppression of heat generation due to increase in rated current

The rated current of 2G-IPM is enhanced to 75 A from the 30 A of the conventional products. Therefore, the heat generated from the IGBT, FWD chip, aluminum wire and copper foil of aluminum IMS increases. To suppress the temperature rise similarly as with that of conventional types, the aluminum wire diameter and the thickness of the copper foil are increased. Thus, the newly developed 2G-IPM achieves the ΔT_{vj} power cycle capability that is equivalent to that of 2G-

Table 2 Result of reliability test (main items)

Test items	Test condition	Guaranteed value	Judgment
Thermal cycle test	Low temp.: -40°C High temp.: 125°C	100 cycle	No characteristics variation
ΔT_{vj} power cycle test	$\Delta T_{vj} = 100 \pm 5^{\circ}\text{C}$ $T_{vj} \leq 150^{\circ}\text{C}$ $T_C \leq 125^{\circ}\text{C}$ $I_C \geq 50\text{ A}$	15 kcycle	No characteristics variation
High temperature reverse bias test	$T_{vj} = 150^{\circ}\text{C}$ $V_{CC} = 20\text{ V}$ $V_{CE} = 510\text{ V}$	1,000 h	No characteristics variation

IPM in mass production.

(2) Optimization of assembly process with rated current increase

The internal residual stress after resin molding increases with enlarging the package size. In this case, there is the concern that molding resin is delaminated from chip during the reliability test with heat stress, such as the temperature cycling test, and that leads to the electrical characteristics deteriorating. Thus, the assembly process is optimized to reduce the residual stress inside the package and the stress caused by temperature change, realizing the reliability of newly developed 2G-IPM equivalent to 1G-IPM in mass production.

3.3 Protection function

Figure 8 shows the over-current protection circuit. The newly developed 2G-IPM adopts a current detecting method using a sense-IGBT and shunt resistor R_s . In addition, the overcurrent protection and short-circuit protection availability of 2G-IPM is same as 1G-IPM with external shunt resistor method shown in Fig. 8(b). The method of detecting current with the sense

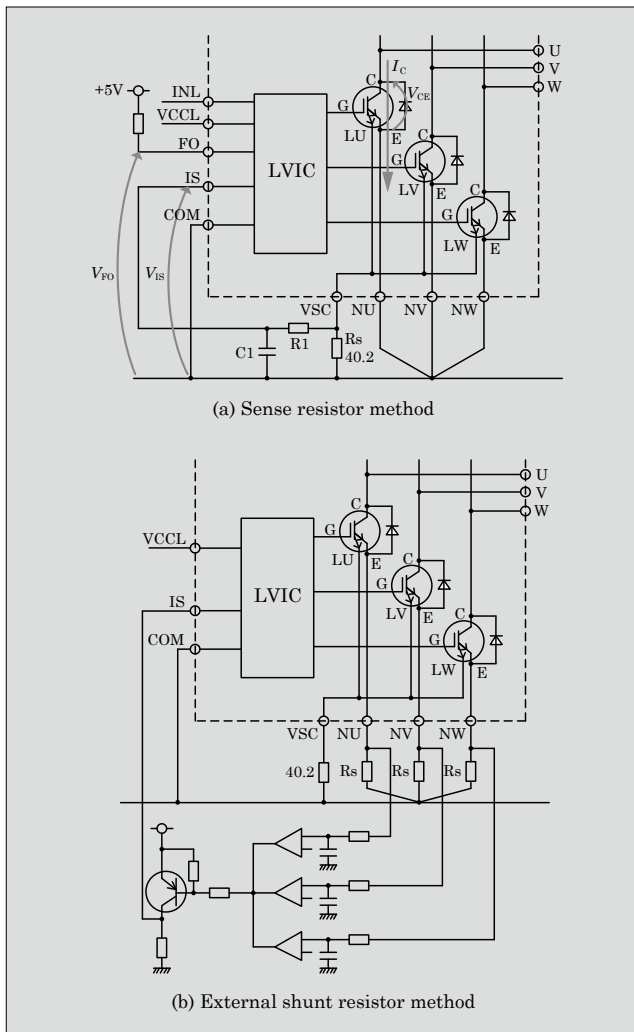


Fig.8 Over-current protection circuit

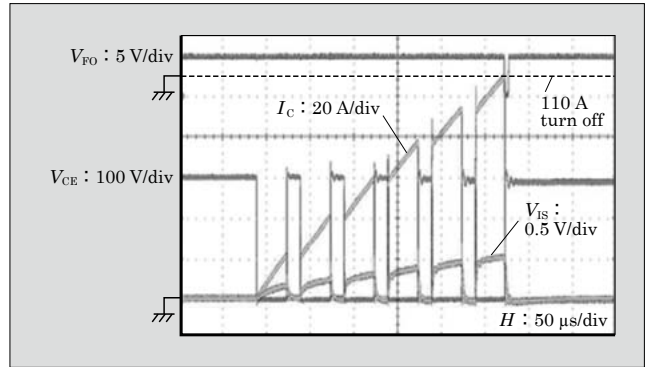


Fig.9 Waveform at over-current protection

IGBT and R_s can reduce the number of components of a filter circuit for current detecting, reducing costs of the total system and saving space of the print circuit board. Figure 9 shows the waveform at the time of over-current protection. As shown in Fig. 9, the alarm output signal V_{FO} is output at the threshold level of the current detection, and the low side IGBT cuts off.

4. Advantage for the Power Conversion System

Figure 10 shows the simulation result of the inverter loss assuming an minimum load of a package air conditioner (PAC) as 10 horsepower unit. The 2G-IPM is expected to exhibit loss of approximately 32% that of 1G-IPM with the same rated current as 75 A of 2G-IPM, improving the APF performance.

Figure 11 shows the simulation result of the inverter loss assuming the maximum load of the same model, and Fig. 12 shows the result of the temperature rise at this time. The 2G-IPM showed low power loss of about 27% that of 1G-IPM with same rated current. The loss reduction of 2G-IPM results in decreasing 20°C of temperature rise compared with 1G-IPM with same rated current. Further more, the rated maximum operating temperature range was increased by 25°C,

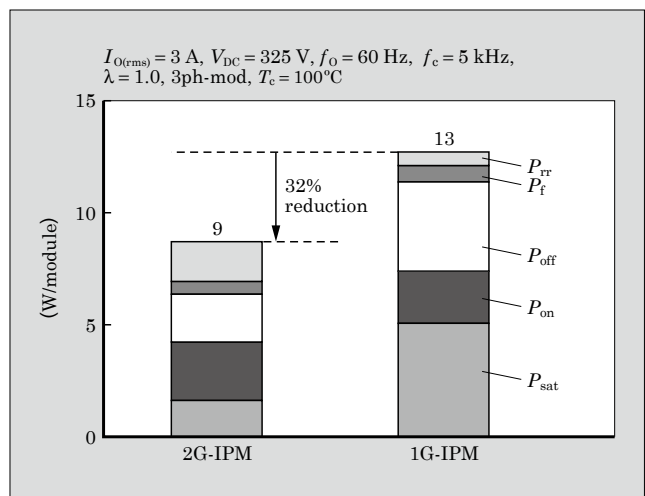


Fig.10 Calculation result of power dissipation [2G-IPM 650 V/50 A, PAC (10HP) medium load condition]

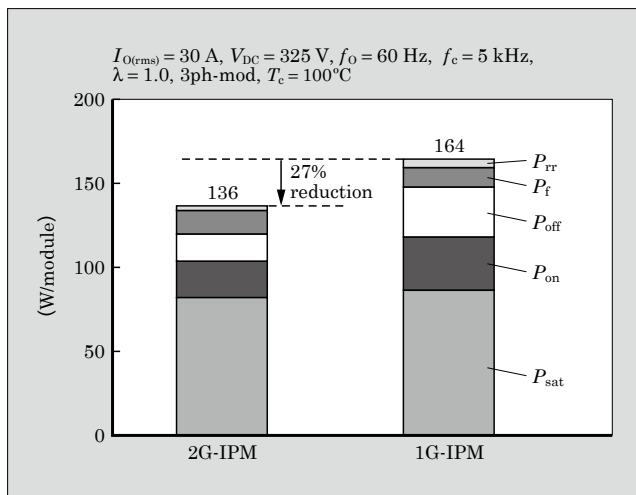


Fig.11 Calculation result of power dissipation [2G-IPM 650 V/50 A, PAC (10HP) maximum load condition]

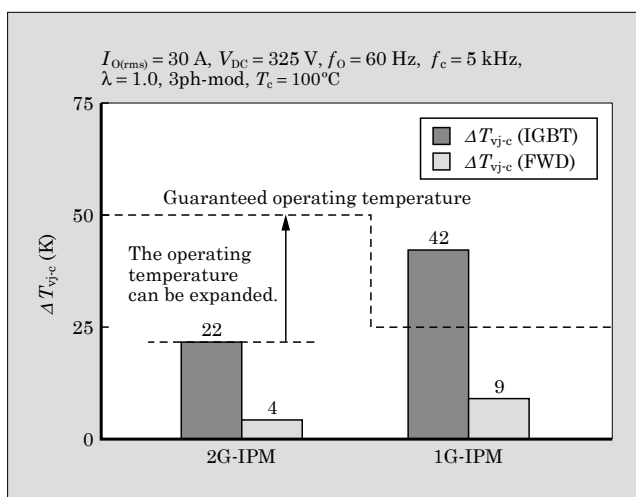


Fig.12 Calculation result of temperature rise [2G-IPM 650 V/50 A, PAC (10HP) maximum load condition]

and the output current can be expanded and equipment can be downsized.

5. Postscript

The series of the 2nd-generation IPM 650 V/50 A and 75 A has been described. This series is a part of the products that meet the requirements of motor drive inverter, servo amp and package air conditioner (PAC), which are expected to increase in demand of world wide. In addition, we are considering of expanding the line-up of 1,200-V series.

Fuji Electric will continuously offer superior products with advanced technologies and will realize many benefits such as downsizing, higher efficacy and reliable performance of power conversion systems.

References

- (1) Yamada, T. et al. "Novel Small Intelligent Power Module For RAC". proc. 2012 PCIM Asia.
- (2) Kawabata, J. et al. 7th-Generation "X Series" IGBT Module. FUJI ELECTRIC REVIEW. 2015, vol.61, no.4, p.237-241.
- (3) Araki, R. et al. 2nd-Generation Small IPM. FUJI ELECTRIC REVIEW. 2015, vol.61, no.4, p.242-246.
- (4) Ohashi, H. et al. "The 2nd Generation Small Intelligent Power Module for General-purpose Inverter". proc. 2016 PCIM Asia.

On-Chip Sensor Built-In IGBT Modules for Driving xEV Motors

NAKAYAMA, Tomoya* NAKANO, Hayato* YOSHIDA, Soichi*

ABSTRACT

In recent years, the switch to electric vehicles (xEV) has been increasing, and the xEVs are equipped with inverters for driving electric motors. Therefore, there has been growing demand for inverters and their component IGBT modules for xEVs. Fuji Electric has developed an IGBT module that integrates an on-chip sensor for driving motors of xEVs. The on-chip sensor is equipped with temperature and current sensors. The temperature sensor directly monitors the temperature of the IGBT chip to improve the permissible current of the module. The low-loss current sensor monitors large current and enables protective operation when there is an overcurrent caused by short circuit or other accidents.

1. Introduction

In recent years, in accordance with energy saving and CO₂ emission regulation, switching vehicles to electric vehicles (xEV), such as hybrid electric vehicles (HEV) and electric vehicles (EV), is accelerating even faster all over the world. The xEV is equipped with an inverter for driving an electric motor. Therefore, there is increasing demand for inverters and insulated gate bipolar transistors (IGBT) for xEVs, which are components of inverters.

The IGBT module for xEVs that Fuji Electric is

developing achieved a small module having a high current density by using reverse-conducting IGBTs (RC-IGBTs), on-chip sensors, and a structure in which a cooler is built in⁽¹⁾. In this article, the properties and characteristics of the IGBT module having a built-in on-chip sensor are described.

2. On-Chip Temperature Sensor

2.1 Characteristics

Figure 1 shows the circuit diagram of the IGBT module. In this circuit diagram, 2 IGBTs are config-

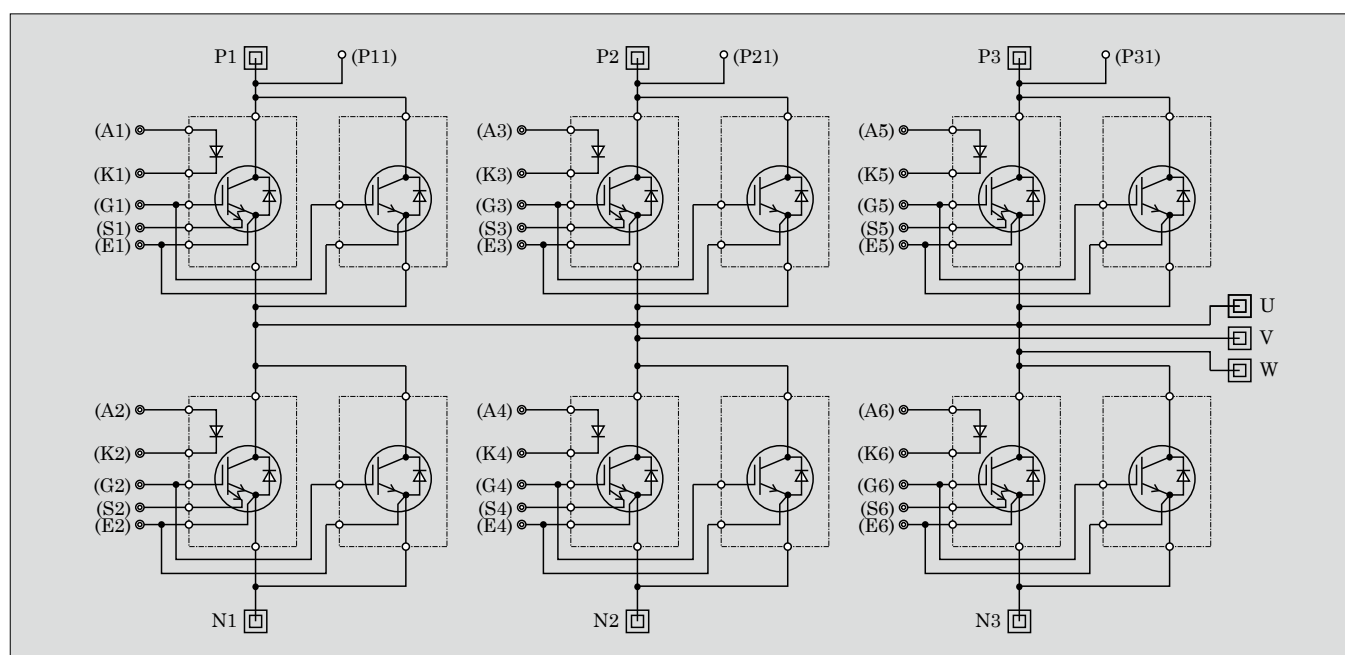


Fig.1 Circuit diagram of IGBT module

* Electronic Devices Business Group, Fuji Electric Co., Ltd.

ured in parallel in 3-phase upper and lower arms. The IGBTs in the 3-phase upper and lower arms are operated by switching, and convert the DC voltage of the battery into AC voltage to drive the motor. The temperature sensor diode (a diode between A and K terminals in Fig. 1) embedded in the IGBT chip monitors the chip temperature to protect from overheating. The conventional module had a structure for overheating protection in which a negative temperature coefficient (NTC) thermistor is mounted on the insulating substrate away from the chip in the module. However, the NTC thermistor cannot directly monitor the chip temperature. Therefore, the thermal design had to be created considering the variations of product characteristics, such as device characteristics and the thermal resistance of packages. Large safety margins had to be taken for this factor, and this had been a disadvantage for satisfying requirements (small, lightweight and large current) modules for automotive applications.

Using the on-chip temperature sensor can greatly reduce these safety margins. When the IGBT and the free wheeling diode (FWD) have different chip structures, only the temperature of the IGBT region can be monitored. However, the combination of the RC-IGBT and the temperature sensor allows the chip temperature to be monitored in a way that reflects both the IGBT region and the FWD region. This also protects against overheating when an unexpected reverse current is generated from the motor and the current flows into the power module (in this case, FWD).

2.2 Structure and characteristics

Figure 2 shows a schematic cross-sectional view of an RC-IGBT. This structure not only simply decreases the number of chips but also brings advantages like smaller element areas and thermal resistance reduction. Thus, smaller and more lightweight inverters are expected to be manufactured at low costs.

We have realized lower power dissipation of large capacity RC-IGBT chips, which had been technically difficult, and mass-producing high power RC-IGBTs with low power dissipation for vehicles and industrial

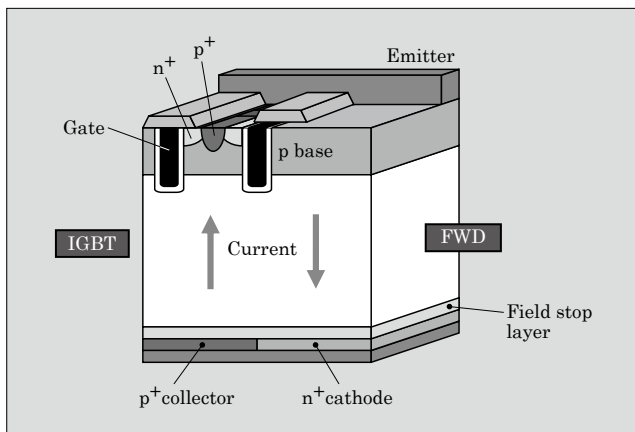


Fig.2 Schematic cross-sectional view of RC-IGBT

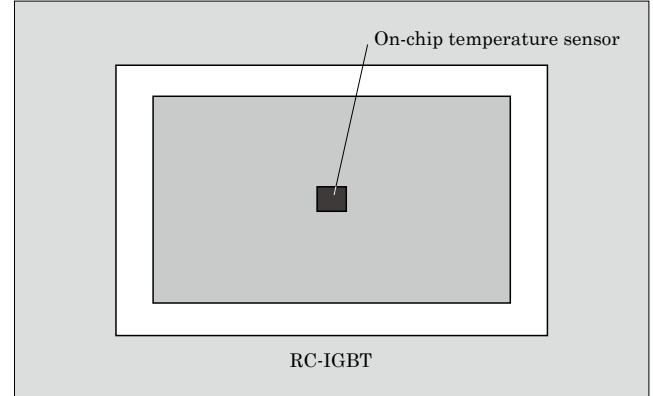


Fig.3 Planar schematic view of on-chip temperature sensor

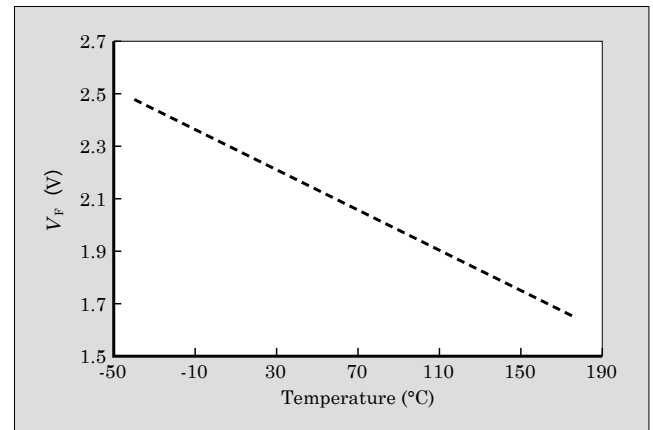


Fig.4 Temperature characteristics of on-chip temperature sensor

use.

Figure 3 shows a planar schematic view of an on-chip temperature sensor. An on-chip temperature sensor is a pn diode placed on the chip via an insulating oxide film. A sensor is positioned in the vicinity of the center of the RC-IGBT chip to monitor the maximum temperature of the chip.

Figure 4 shows the temperature characteristics of an on-chip temperature sensor. It shows the diode voltage at each temperature when a forward current of 1 mA flows through a temperature sensor diode. It shows good linearity from -40°C to 175°C .

2.3 Comparison with NTC thermistor

We verified how superior an on-chip temperature sensor is with respect to an NTC thermistor. Specifically, we calculated and compared the allowable current value of the IGBT module using an NTC thermistor with that using an on-chip temperature sensor under the conditions shown in Table 1.

The NTC thermistor was put on the insulating substrate, and the chip temperature was estimated from the measured temperature. Therefore, we needed to calculate the values considering the characteristic and dimension variations of the IGBT module components such as the chip and the package.

Table 1 Calculation condition of allowable current estimates

Item	Condition
Bus voltage V_{CE}	450 V
Output frequency	100 Hz
Switching frequency	10 kHz
Power factor	0.8
Modulation factor	1.0
Flow rate	8 L/min

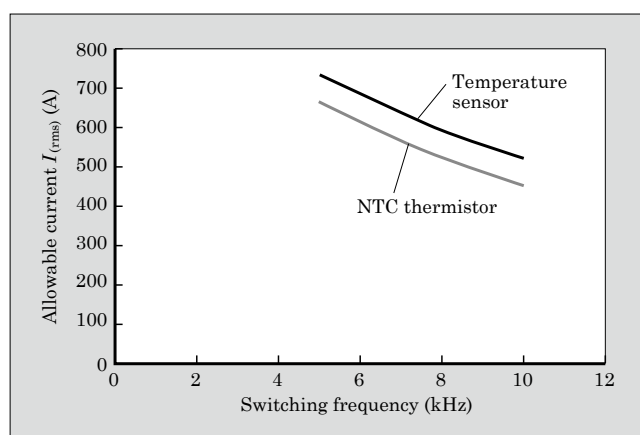


Fig.5 Relationship between switching frequency and allowable current

Figure 5 shows the result of comparing the allowable current $I_{(rms)}$ with respect to switching frequency between the on-chip sensor and the NTC thermistor. When the switching frequency was 8 kHz, the NTC thermistor showed $I_{(rms)}$ of 521 A, whereas the on-chip temperature sensor showed $I_{(rms)}$ of 589 A under the same condition. This estimated calculation shows that adopting an on-chip temperature sensor can increase the allowable current by about 13% compared with the case in which an NTC thermistor is used. This indicates that the same allowable current can be achieved with a 12% smaller chip. The size of the module itself can also be reduced by reducing the chip area; therefore, the on-chip temperature sensors are effective for making smaller and more lightweight modules.

2.4 Protection with respect to reverse current

As motors for xEVs are increasingly required to be more lightweight and provide higher output power, their operating voltage is increased so the cables can be made more lightweight. Figure 6 shows an xEV motor drive circuit. For example, the IGBT may turn off after detecting some trouble when the motor is rotating at high speed. At this time, if the counter electromotive force of the motor is larger than the battery voltage, a short-circuit current in a reverse direction flows from the motor to the IGBT module. The short-circuit current flows through the FWD, and the FWD needs to withstand the short-circuit current until the protection is applied⁽²⁾. To prevent module breakage, it is necessary to improve the short-circuit current

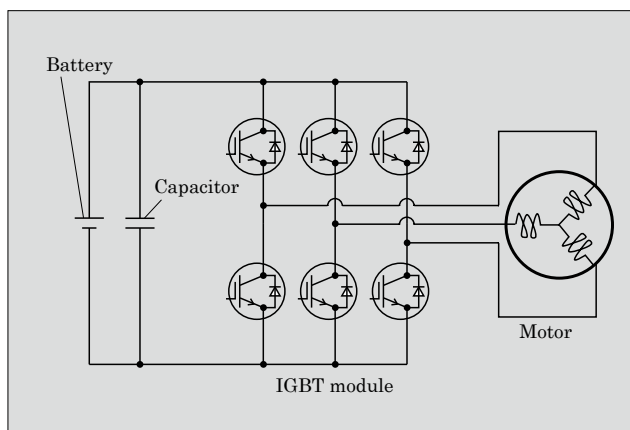


Fig.6 xEV motor drive circuit

capability of the FWD and at the same time immediately detect the failure and protect the module. When the IGBT and the FWD are different chips or when an on-chip temperature sensor is not embedded, the abnormality of the FWD cannot be directly detected. However, the combination of the RC-IGBT and the temperature sensor can detect abnormal heat generation of the FWD and apply protection.

3. On-Chip Current Sensor

An overcurrent like a short-circuit current may flow in the IGBT module. The IGBT chip may break in the worst case unless appropriate protection is performed. One way of giving protection would be to detect the current flowing through the IGBT with a shunt resistor connected inside or outside the module and apply overcurrent protection. The IGBT module for automotive applications of Fuji Electric can apply short-circuit protection by detecting the current with an extremely small sense IGBT placed inside the chip.

When short-circuit protection is applied to a large capacity module, the power dissipation of the shunt resistor becomes too significant to ignore because it detects the main current that flows in the IGBT. On the other hand, an on-chip current sensor detects, for example, a sense current of about a ten-thousandth of the main current. Thus, power dissipation can be greatly reduced.

Figure 7 shows an example of a circuit configuration using an on-chip current sensor. When overcurrent like short-circuit current flows to the IGBT, a part of the current is output from the sense IGBT. This current flows through an appropriate resistor connected to the outside, and thus, the value of the voltage generated across the resistor is read and the short-circuit protection operation can be started.

Figure 8 shows waveforms at the time of short-circuit protection. The waveforms shown in the figure correspond to voltage waveform V_{CE} (1), a main current waveform I_C (2), a gate voltage waveform V_{GE} (3) and a sense voltage waveform V_{SE} (4).

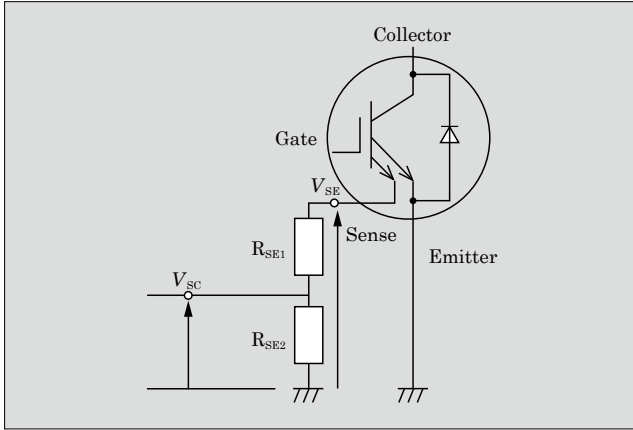


Fig.7 Circuit diagram of current sensor

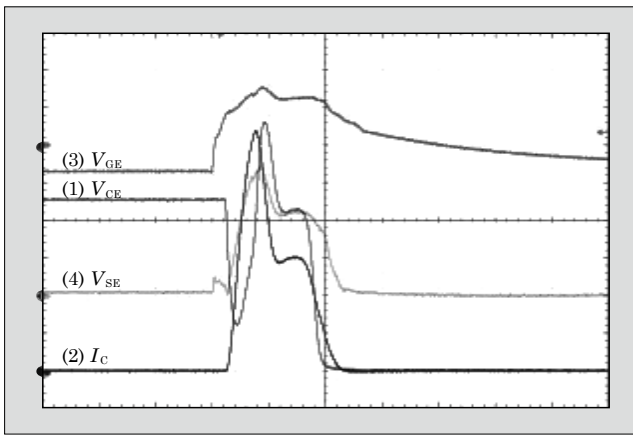


Fig.8 Waveforms at time of short-circuit protection

The waveform of V_{SE} is shown to be similar to that of I_C . Waveform V_{SE} can be used to apply protection when a certain threshold voltage is exceeded. In addition, like waveform V_{GE} , the surge voltage can be suppressed with a soft shutdown of the IGBT.

4. Postscript

An IGBT module having a built-in on-chip sensor for driving xEV motors has been described. A comparison of the temperature sensor and the NTC thermistor shows that the allowable current of the module can be improved by directly monitoring the IGBT chip temperature. Mounting the current sensor also makes it possible to monitor a large current with low power dissipation, enabling protection when an overcurrent like a short-circuit occurs.

There is an increasing demand for modules for xEVs, and we will continue contributing to global environment improvement by responding to the demand for electric vehicles.

References

- (1) Osawa, A. et al. "M660" High-Power IGBT Module for Automotive Applications. FUJI ELECTRIC REVIEW. 2017, vol.63, no.4, p.228-231.
- (2) Higuchi, K. et al. Improvement of I2t Capability for xEV Active Short Circuit Protection by Combination of RC-IGBT and Leadframe Technologies. IPEC, 2018.

3.3-kV All-SiC Module with Trench-Gate MOSFETs for Electric Distribution Equipment

KANAI, Naoyuki* HOYA, Masashi* TSUJI, Takashi*

ABSTRACT

Fuji Electric has participated in the project of the New Energy and Industrial Technology Development Organization (NEDO) and is developing electric distribution equipment and control systems to stabilize the power grid when the massive introduction of distributed energy sources, such as photovoltaic power generation. In this regard, we have developed a 3.3-kV All-SiC module equipped with SiC trench-gate MOSFETs for electric distribution equipment. The module reduces inverter loss by 60% and achieves higher power density compared with modules equipped with conventional SiC planar-gate MOSFETs.

1. Introduction

To cope with environmental problems such as global warming, emission of greenhouse gases such as CO_2 needs to be reduced. To realize this task, it is necessary to aggressively utilize renewable energy and save energy on power electronics. A power semiconductor plays an important role in power conversion of power electronics. Conventional mainstream silicon (Si) devices have been improved, but they are currently approaching the performance limit based on physical properties. Under such circumstances, a silicon carbide (SiC) device, which is a next-generation semiconductor realizing even greater reduction in power dissipation, is expected to contribute to size reduction and weight saving of power electronics.

Since September 2014, Fuji Electric is working on the “Demonstration Project for Constructing a Distributed Energy Next-Generation Electric Power Network” as a project of New Energy and Industrial Technology Development Organization (NEDO). We have been developing the next-generation voltage regulator (power distribution devices), such as a static var compensator (SVC) that utilizes a SiC power semiconductor, and control systems to expand the adoption of renewable energy like photovoltaic power generation and to maintain and improve Japan’s international competitiveness in the electric power equipment and systems industry.

2. All-SiC Module for Power Distribution Devices

In the “Demonstration Project for Constructing a Distributed Energy Next-Generation Electric Power Network” of NEDO, we are developing power distribu-

tion devices and control systems that deal with many technical challenges such as generation of surplus power, insufficient frequency trimming, and voltage increase in power distribution lines, which are caused when distributed energy such as photovoltaic power generation is largely adopted to distribution systems (see Fig. 1). Particularly in Japan, when the introduction amount of photovoltaic power generation of ordinary homes becomes larger than it is currently, there would create challenges such as power loss caused by reverse power flow at the time of voltage increase in 6.6-kV distribution systems and output suppression of

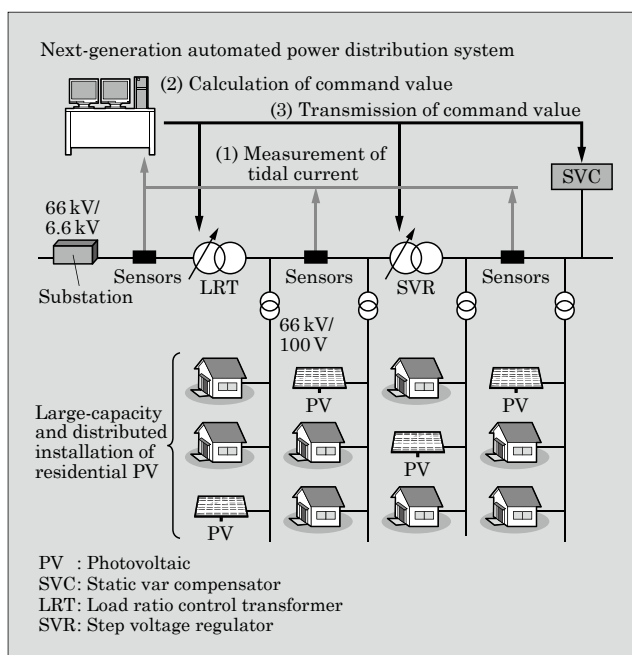


Fig.1 Outline of “Demonstration Project for Constructing a Distributed Energy Next-Generation Electric Power Network” of NEDO

* Electronic Devices Business Group, Fuji Electric Co., Ltd.

photovoltaic power generation. To solve this issue, it is necessary to adopt power distribution devices such as SVCs and step voltage regulators (SVRs) to regulate voltage of 6.6-kV power distribution systems. The power distribution devices to be adopted must be small and lightweight so that they can be mounted to existing electric poles (single poles) and must be self-cooling because water-cooling and forced air-cooling cannot be supported.

Si power semiconductors dissipate large amount of power and require large heat sink for releasing heat generated in the module. Therefore, it is difficult to develop small and lightweight power distribution devices, and they need to be installed to a frame provided on the dedicated adjacent 2 utility poles⁽¹⁾. Thus, the power distribution devices are not being adopted very much in terms of installation places and costs. By having an All-SiC power semiconductor module developed in the 2017 NEDO project, power distribution devices became small and lightweight, and they can now be installed on a single pole. High-frequency operation also became available, and it is expected that power distribution devices will be operated at the high-frequency (13 kHz or higher), which is higher than the audible frequency of humans, thus making possible to install in residential areas. In 2017, we developed an All-SiC 200-A 1-in-1 module with a withstand voltage of 3.3 kV for power distribution devices and a SVC equipped with this module⁽²⁾.

For further size reduction and weight saving of power distribution devices, we are developing modules with larger rated capacity. The package that is being developed is equipped with a SiC trench-gate metal-oxide-semiconductor field-effect transistor (MOSFET) having both low on-state resistance and high-speed switching characteristics. This article describes the structure and characteristics of the All-SiC 400-A 2-in-1 module with a withstand voltage of 3.3 kV that is being developed for power distribution devices (see Fig. 2).

Four 200-A 1-in-1 modules are necessary to make the same circuit configuration as the 400-A 2-in-1 module. Compared to this figure, the footprint size of the All-SiC 400-A 2-in-1 module is reduced by 45%.

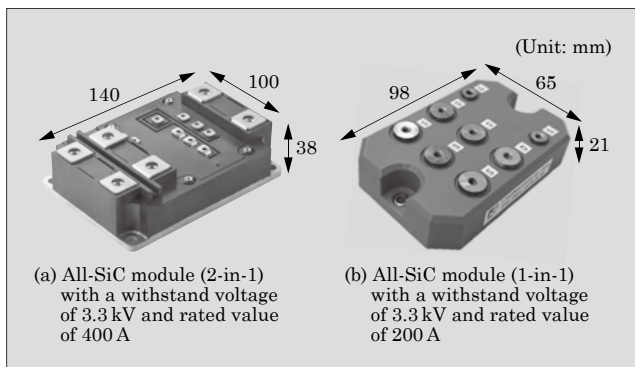


Fig.2 All-SiC module with withstand voltage of 3.3 kV

An All-SiC module is a combination of SiC-MOSFETs and SiC-Schottky barrier diode (SBD) chips. Since the on-state resistance per unit area becomes higher as the withstand voltage becomes higher, an insulated gate bipolar transistor (IGBT) is mainly used for a withstand voltage of 600 V or higher in the case of Si. The on-state resistance of IGBT modules is reduced by conductivity modulation in which positive holes serving as minority carriers are injected into the drift layer. However, accumulation of minority carriers generates tail current at the time of switching, causing large switching loss. On the other hand, SiC has lower drift layer resistance compared with Si devices because of a wide bandgap and can reduce the on-state resistance without conductivity modulation. Therefore, both high withstand voltage and low power dissipation can be achieved with a MOSFET.

The All-SiC 200-A 1-in-1 module developed in 2017 is equipped with SiC planar-gate MOSFETs. To reduce the on-state resistance per unit area of a SiC planar-gate MOSFET, miniaturization of the cell pitch is generally effective. However, excessive miniaturization increases the resistance of the junction field-effect transistor (JFET) and stops the decrease of the on-state resistance. The SiC trench-gate MOSFET can suppress the increase in JFET resistance components due to miniaturization, and thus, low on-state resistance can be achieved.

3. Module Structure

Figure 3 shows the comparison of schematic struc-

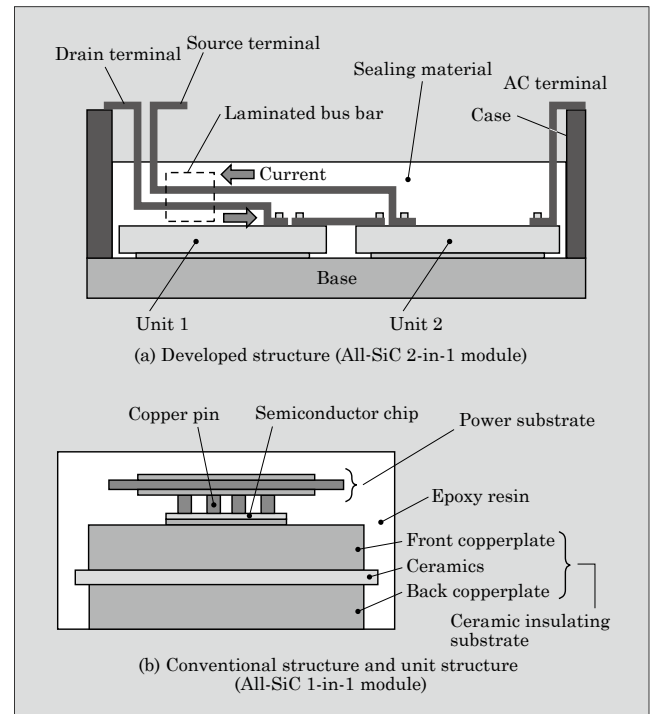


Fig.3 Comparison of schematic structures of cross sections of modules

tures of cross sections of modules. The All-SiC module with a withstand voltage of 3.3 kV follows the structure of the All-SiC module with a withstand voltage of 1.2 kV for power conditioning systems (PCS) that are being mass-produced^{(3),(4)}. The structure of the All-SiC modules is wired with copper pins formed on the power substrate. Thus, a large current can be supplied, enabling high-density mounting of SiC devices. For the insulating substrate equipped with a chip, a high-strength insulating substrate that is made of silicon nitride (Si_3N_4) and has a thick copperplate bonded is adopted to improve the resistance to residual stress of the epoxy resin sealing. Further, epoxy resin is used as the sealing material in the module to suppress deterioration of solder and insulation performance during high-temperature operation. Thus, high reliability is secured. However, increasing the capacity of this module structure caused a problem that the package becomes large because sufficient insulation distance needs to be secured.

Therefore, the developed module has a 2-in-1 circuit configuration that uses a bus bar and has plastic molded units allocated on the base. The module has a laminated structure in which units, a bus bar and the joint part thereof are further sealed with a sealing material. Thus, the capacity of the module has been increased with the insulating property secured without increasing the size of the unit. The module has same appearance as the large capacity power module "HPnC" (High Power next Core) to secure attachment compatibility with modules of other companies⁽⁶⁾. For the base material, a composite material of magnesium and silicon carbide (MgSiC) having a low coefficient of thermal expansion and excellent thermal conductivity is adopted to secure high reliability for power distribution devices.

The structure of a laminated bus bar, which is a wiring between units and terminals such as the drain terminal and the source terminal, has the characteristics described below. Thus, the insulation property is secured and the internal inductance of the module is reduced to 10 nH as with the HPnC.

Figure 4 shows the analysis result obtained by simulating the wiring inductance of the bus bar. Points for reducing the wiring inductance are to shorten the current pathways, increase the cross-sectional area of the current pathways, and utilize the mutual inductance. Among these, utilization of mutual inductance is important for package design. The influence of mutual inductance becomes larger as the interval between bus bars is narrower. The influence becomes significant when the interval reaches 3 mm or less. Regarding the developed module, the bus bar between the drain terminal or the source terminal and the unit is further sealed with a sealing material to narrow the interval while securing the insulation property. The directions of currents flowing through the bus bars are caused to face each other, thus realizing the module in-

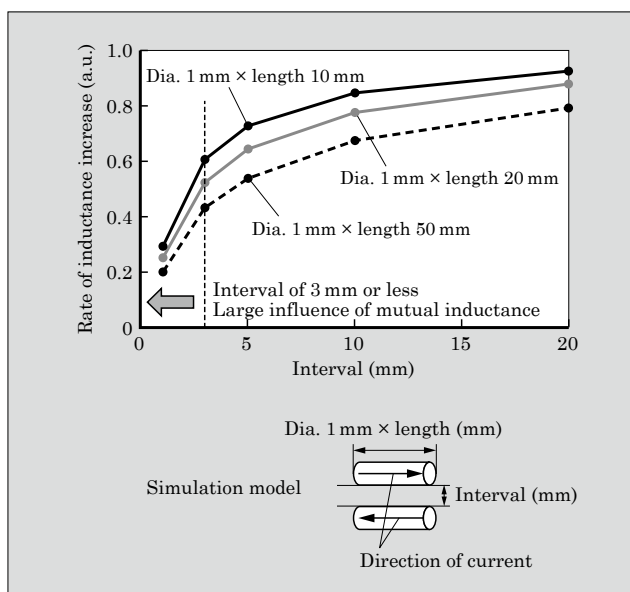


Fig.4 Wiring inductance (simulation)

ternal inductance that is equivalent to the inductance of the HPnC.

4. Characteristics

The rated current of the newly developed All-SiC 2-in-1 module with a withstand voltage of 3.3 kV is 400 A, and the module is equipped with SiC trench-gate MOSFETs. Therefore, the characteristics were compared with the characteristics of a 200-A 1-in-1 module equipped with SiC planar-gate MOSFET.

4.1 I - V characteristics during conduction

The loss generated at the time of module conduction (steady-state loss) is determined by the I - V characteristics. Figure 5 shows the I - V characteristics of an All-SiC 400-A 2-in-1 module and an All-SiC 200-A 1-in-1 module at $T_{vj} = 25^\circ\text{C}$ and $T_{vj} = 150^\circ\text{C}$. The drain voltage of the All-SiC 400-A 2-in-1 module equipped with SiC trench-gate MOSFETs remained equivalent even after the drain current is doubled

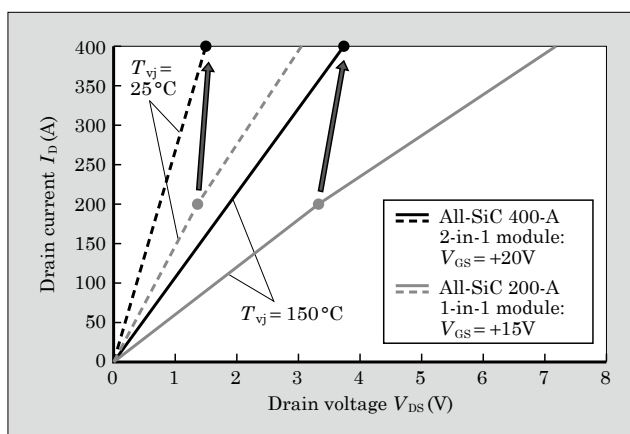


Fig.5 Comparison of I - V characteristics

at 25°C and 150°C when compared with the All-SiC 200-A 1-in-1 module equipped with SiC planar-gate MOSFETs. This is because the SiC trench-gate MOSFET has smaller on-state resistance than the SiC planar-gate MOSFET.

4.2 Switching characteristics

The switching loss can be divided into 3 different types: turn-on loss, turn-off loss, and reverse recovery loss. Figure 6 shows turn-on loss and Fig. 7 shows turn-off loss at $T_{vj} = 150^\circ\text{C}$. In addition, Fig. 8 shows total switching loss.

With respect to the All-SiC 200-A 1-in-1 module, the turn-on loss and turn-off loss of the All-SiC 400-A 2-in-1 module are reduced when the gate resistance is 4.7 Ω . This reduces the total switching loss by 20%. The SiC trench-gate MOSFET has faster switching characteristics compared with the SiC planar-gate MOSFET; therefore, the total switching loss is low even if the rated current is doubled.

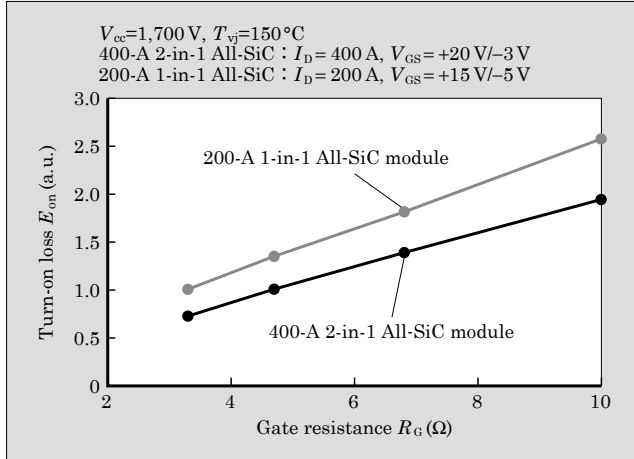


Fig.6 Turn-on loss

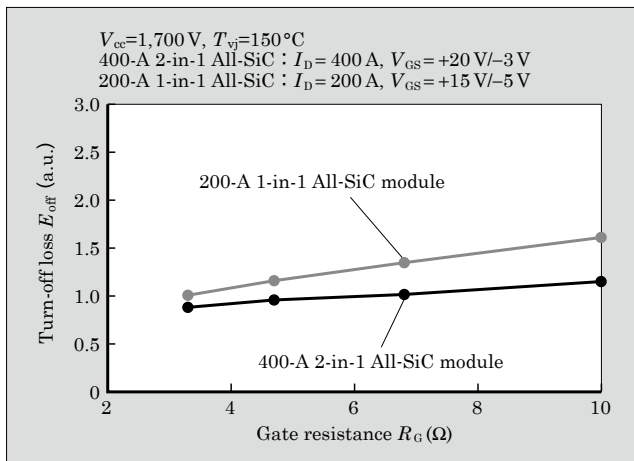


Fig.7 Turn-off loss

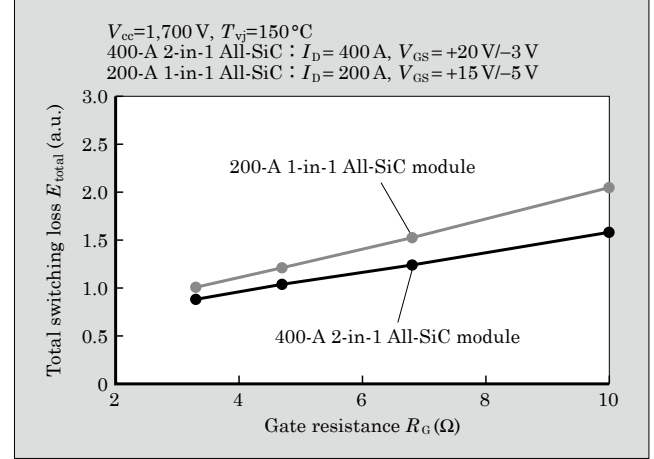


Fig.8 Total switching loss

4.3 Simulation of inverter generated loss

The inverter for the power distribution device SVC that is being developed is a 3-level inverter, and Fig. 9 shows its circuit configuration. Figure 10 shows simulation results of inverter loss of the All-SiC module equipped with SiC trench-gate MOSFET and All-SiC module equipped with SiC planar-gate MOSFETs under the operating condition of the 3-level inverter for a SVC. The loss of the 3-level inverter of the SVC depends more on switching loss than steady-state loss. Therefore, the All-SiC module equipped with SiC trench-gate MOSFETs and having low switching loss showed 60% lower inverter loss at a carrier frequency of 13 kHz with respect to the All-SiC module equipped with SiC planar-gate MOSFETs.

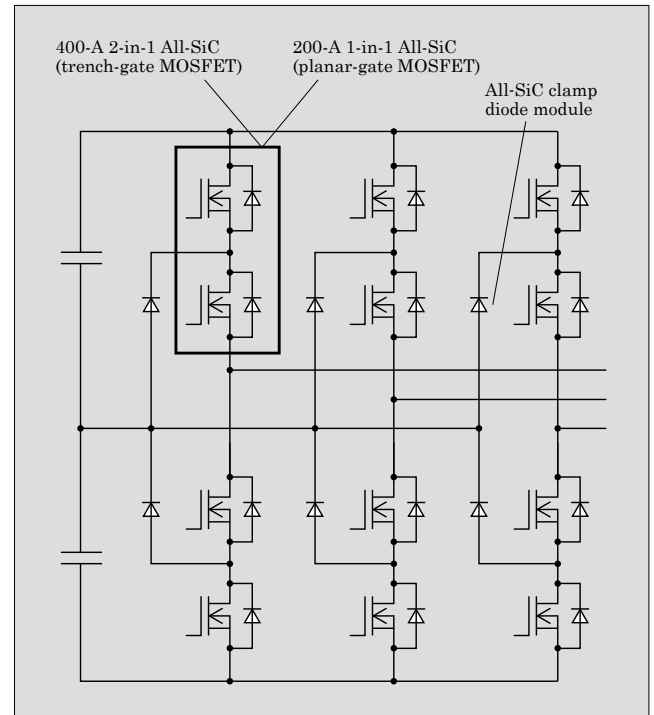


Fig.9 Circuit of 3-level inverter of SVC

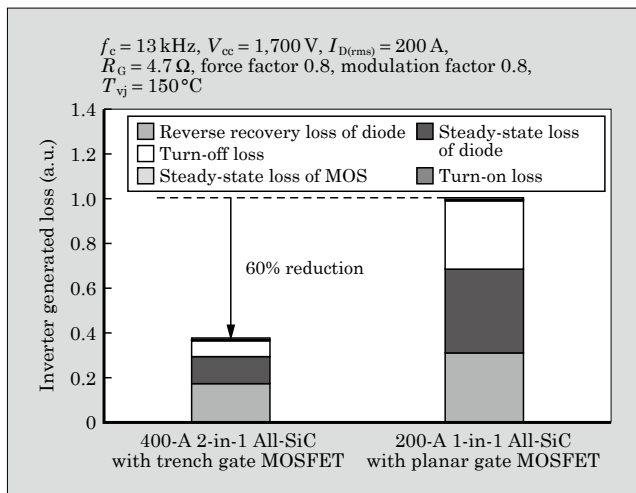


Fig.10 Simulation of inverter generated loss

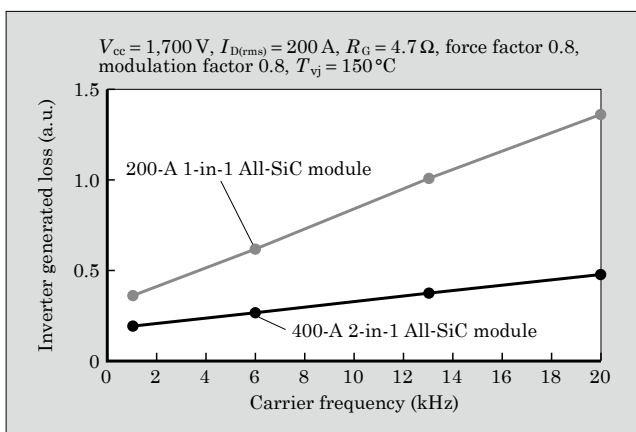


Fig.11 Carrier frequency dependence of inverter generated loss

Figure 11 shows the simulation results of carrier frequency dependence of a 3-level inverter loss. Under the operating condition of the 3-level inverter of a SVC, as the carrier frequency becomes higher, the difference in the generated loss becomes larger between the All-SiC module equipped with SiC trench-gate MOSFETs and the All-SiC module equipped with SiC planar-gate MOSFETs. The result shows that the All-SiC module equipped with SiC trench-gate MOSFETs is superior at a high frequency.

5. Postscript

The 3.3-kV All-SiC module equipped with trench-gate MOSFETs for power distribution devices has been described. The module follows the structure of the All-SiC module with a withstand voltage of 1.2 kV for power conditioners and has high reliability. The module also contributes to the development of small and lightweight power distribution devices SVC that can be self-cooled and mounted on a single pole utilizing features such as low power dissipation and high-frequency drive.

With respect to further size reduction and weight saving of power distribution devices, we will be accelerating the development of large capacity All-SiC modules and contribute to the development of power electronics technology and realization of the low-carbon society.

The results has been obtained from the “Demonstration Project for Constructing a Distributed Energy Next-Generation Electric Power Network” implemented by the New Energy and Industrial Technology Development Organization (NEDO). We would like to express our appreciation to all those involved in this project.

References

- (1) Kojima, T. et al. Distribution Static Var Compensators and Static Synchronous Compensators for Suppressing Voltage Fluctuation. FUJI ELECTRIC REVIEW. 2017, vol.63, no.1, p.36-40.
- (2) Taniguchi, K. et al. 3.3-kV All-SiC Modules for Electric Distribution Equipment. FUJI ELECTRIC REVIEW. 2017, vol.63, no.4, p.209-213.
- (3) Nashida, N. et al. All-SiC Module for Mega-Solar Power Conditioner. FUJI ELECTRIC REVIEW. 2014, vol.60, no.4, p.214-218.
- (4) Nakamura, H. et al. All-SiC Module Packaging Technology. FUJI ELECTRIC REVIEW. 2015, vol.61, no.4, p.224-227.
- (5) Sekino, Y. et al. “HPnC” High-Current SiC Hybrid Module. FUJI ELECTRIC REVIEW. 2017, vol.63, no.4, p.218-222.

SiC-MOSFET with High Threshold Voltage and Low On-Resistance Using Halo Structure

KOBAYASHI, Yusuke* OHSE, Naoyuki* KOJIMA, Takahito*

ABSTRACT

Fuji Electric has developed a trench gate MOSFET that uses silicon carbide (SiC) to reduce power dissipation of power semiconductor devices. Although shortening the MOSFET channel length can further reduce power dissipation, this makes it necessary to suppress the drop in the threshold voltage and breakdown voltage due to the short-channel effect. The simulations and prototype for a vertical trench gate SiC-MOSFET with a halo structure demonstrated the suppression of the short-channel effect. We were thereby able to reduce on-resistance while maintaining a high threshold voltage and breakdown voltage.

1. Introduction

Increasing demand for energy-saving products to realize a low-carbon society has led to the need to use energy-saving power semiconductor devices which are used in power electronics devices. Under these circumstances, it was discovered that vertical metal-oxide-semiconductor field-effect transistors (MOSFETs) using silicon carbide (SiC) offered reduced power loss over conventional vertical insulated gate bipolar transistors (IGBTs) using silicon (Si), making them a potentially ideal candidate for power semiconductor devices. Fuji Electric has already produced a prototype of a vertical SiC-MOSFET equipped compact, lightweight power conditioner (PCS⁽¹⁾) and begun commercializing⁽²⁾ PCS products for mega solar applications in its efforts to promote the development of energy-saving power electronics devices. However, even greater power loss reductions than those offered by SiC-MOSFET are necessary to deliver further energy savings, and reducing on-resistance $R_{on} \cdot A$ during conduction, the dominant of loss factors, is key to achieving this. This paper describes a vertical SiC-MOSFET which simultaneously achieves low on-resistance and suppresses short-channel effects using a halo structure.

2. MOSFET Low On-Resistance and Short-Channel Effects

Fuji Electric has achieved^{(3),(4)} the world's highest level of low on-resistance through the adoption of

trench gate structure (see Fig. 1) high channel density and high channel mobility. Furthermore, we have simultaneously reduced the electrical field applied to the gate oxide film with buried p-layers and realized high

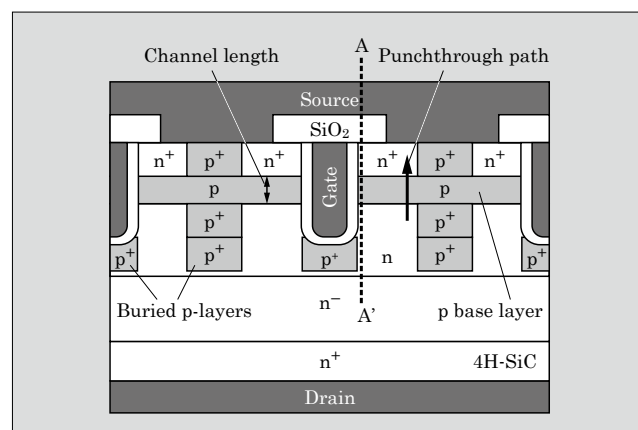


Fig.1 Cross-sectional structure of trench gate MOSFET

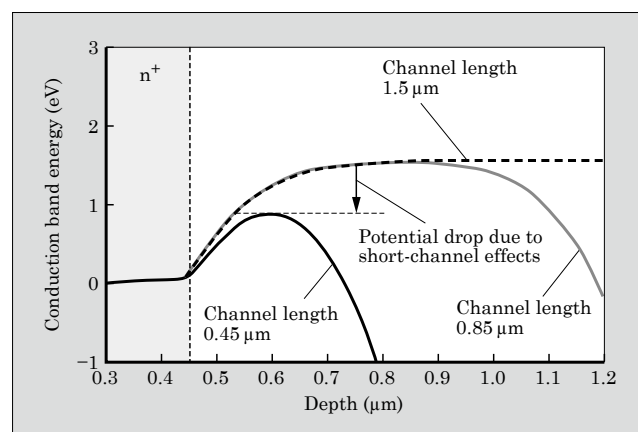


Fig.2 Channel length dependency of channel section (A-A') conduction band energy

* The Advanced Power Electronics Research Center, the National Institute of Advanced Industrial Science and Technology (seconded from Fuji Electric)

* Electronic Devices Business Group, Fuji Electric Co., Ltd.

reliability. In the 1.2-kV breakdown voltage class, channel resistance makes up the greatest proportion of the on-resistance components, even with a trench gate structure. Reducing channel resistance is therefore effective in reducing on-resistance. It is believed that one method of reducing channel resistance is to shorten the channel length L_{ch} . By shortening the channel length, however, a depletion layer penetrates both ends of the channel, causing a drop in conduction band energy levels as shown in Fig. 2. As a result, noise immunity deteriorates due to the drop in threshold voltage^{*1}, and breakdown voltage drops due to p base layer punchthrough. The problem which arises by shortening the channel length in this way is known as “short-channel effects”⁽⁵⁾⁻⁽⁷⁾.

3. Halo Structure

Research into short-channel effects as one of the issues involved in the miniaturization of horizontal silicon MOSFET has been ongoing since the mid-twentieth century, and a halo structure is known to be a suppression technology^{(8),(9)}.

Figure 3 shows a halo structure for horizontal MOSFET and a formation method involving tilt angle ion implantation.

A halo structure prevents penetration of the depletion layer from both ends of the channel by forming a p layer with higher concentration than that of the channel near the channel to suppress short-channel effects [see Fig. 3(a)]. Note that as there is no change in the carrier concentration of the channel layer directly

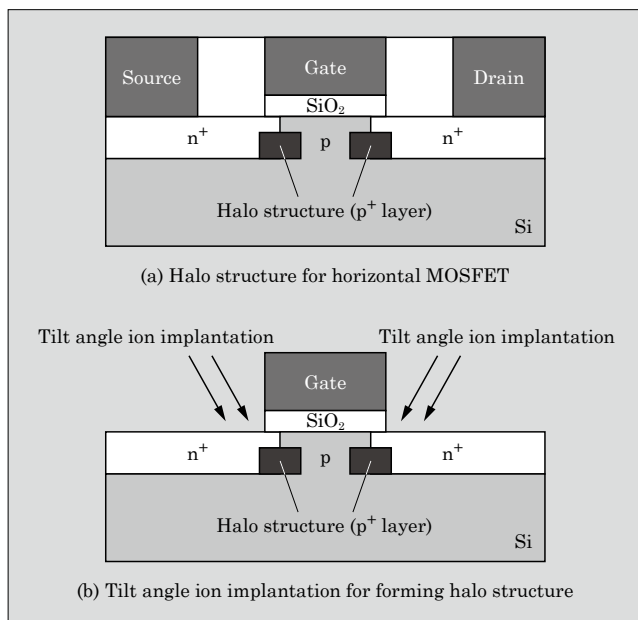


Fig.3 Halo structure for horizontal MOSFET and tilt angle ion implantation for forming halo structure

*1: Threshold voltage: Voltage value between gate and source necessary to turn on MOSFET

beneath the MOSFET, there is no deterioration in channel mobility, or increase in on-resistance. A halo structure suppresses variations in distance from the channel ends and channel surface. To prevent any impact on device characteristics, tilt angle ion implantation is performed, and a halo structure is formed with cell alignment using a polysilicon gate for the shadow mask in the case of silicon-based horizontal MOSFETs [see Fig. 3(b)].

If applying a halo structure to vertical SiC trench gate MOSFETs, on the other hand, it is necessary to form a channel on the trench side wall. Furthermore, taking the thermal history of the process into consideration, it is necessary to form the halo structure prior to forming the polysilicon gate. It is therefore not possible to use the existing halo structure formation process as is. Accordingly, we devised a device structure in which a halo structure is formed on the source side only [see Fig. 4(a)]. To be more specific, we used the angle of the gate trench as a shadow mask, and performed tilt angle ion implantation on the trench side wall [see Fig. 4(b)]. The distance from the channel surface is determined by the tilt angle ion implantation energy, and the distance from the channel ends is determined by the tilt angle ion implantation angle, allowing formation by self-alignment with respect to the trench shape.

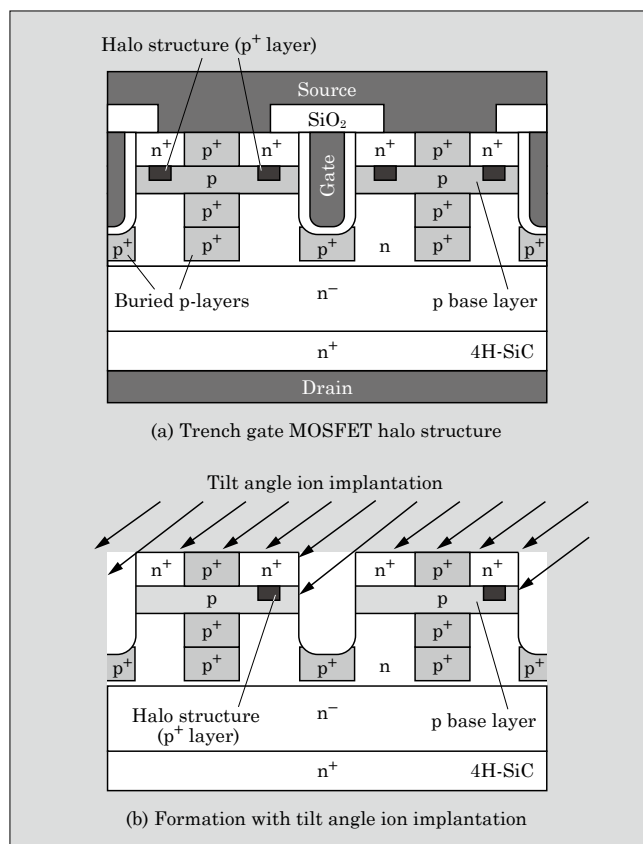


Fig.4 Trench gate MOSFET halo structure and formation with tilt angle ion implantation

4. Prototype Results

We carried out a simulation, and produced a prototype of a 1.2-kV breakdown voltage class vertical trench gate MOSFET with halo structure. Thereafter, we produced a prototype of a 4-inch wafer using a TPEC*2 manufacturing line. The threshold voltage channel length dependency is shown in Fig. 5. Without a halo structure, we find that there is a sharp drop in threshold voltage due to an increase in short-channel effects as the channel length shortens. By applying a halo structure, on the other hand, we find that we are able to suppress the drop in threshold voltage due to short-channel effects.

Due to the high power supply voltage of several hundreds of voltage or higher, a high threshold voltage is required even with high drain voltage. Figure 6 shows threshold voltage drain voltage dependency. By applying a halo structure, we are able to suppress a phenomenon known as drain-induced-barrier-lowering (DIBL), one of the short-channel effects in which threshold voltage drops further when drain volt-

age is increased.

Figure 7 shows the breakdown voltage when p base concentration is changed. Breakdown voltage drops when p base layer punchthrough, one of the short-channel effects, occurs. When the p base concentration is low, the depletion layer inside the channel tends to expand easily, enhancing the short-channel effects. Consequently, breakdown voltage drops rapidly when the p base concentration is lowered without applying a halo structure. With a halo structure, on the other hand, breakdown voltage is maintained even when the p base concentration is lowered, allowing the drop in breakdown voltage caused by punchthrough to be suppressed.

The relationship between on-resistance for each structure and threshold voltage is shown in Fig. 8. Device characteristics of low on-resistance and high threshold voltage are preferable, and therefore the lower right direction in the diagram is the direction of improved trade-off. Shortening the channel length allows the on-resistance to be reduced as a result of the drop in channel resistance, however, without a halo structure, the threshold voltage also drops simultane-

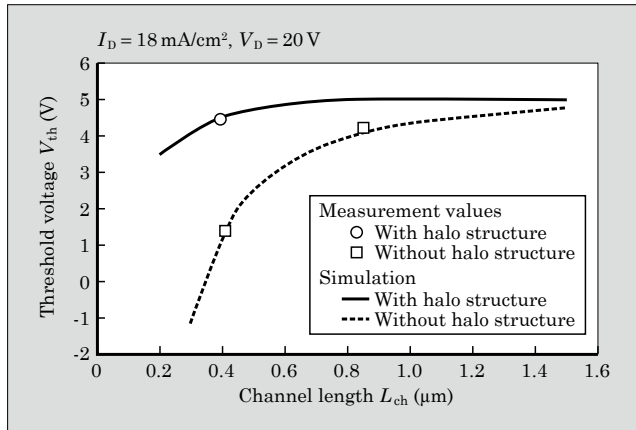


Fig.5 Threshold voltage when channel length changed

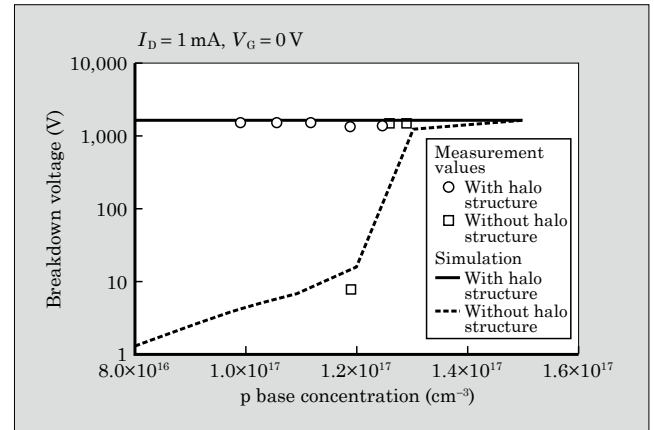


Fig.7 Breakdown voltage when p base concentration changed

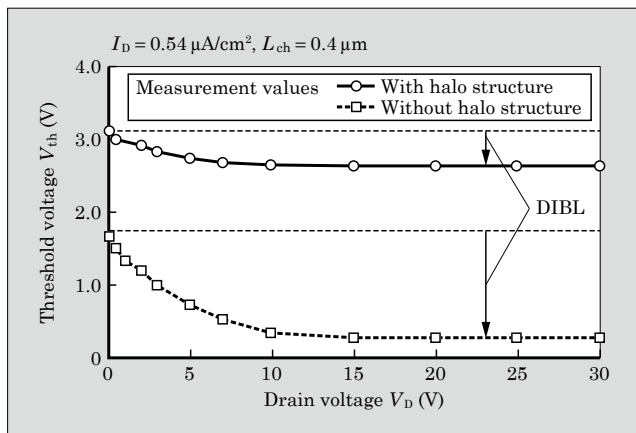


Fig.6 Threshold voltage when drain voltage changed

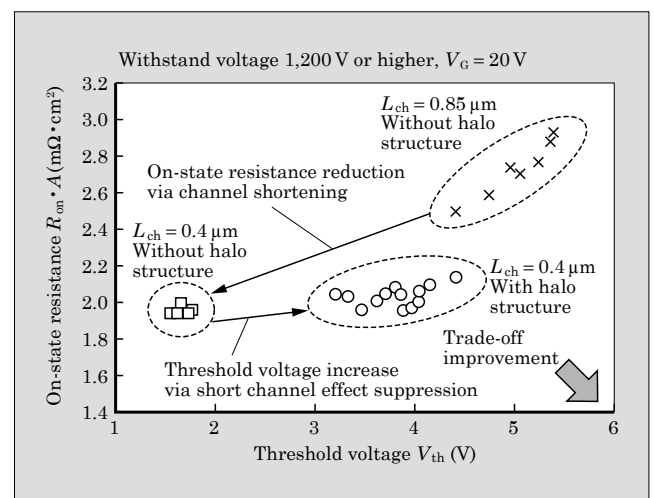


Fig.8 Relationship between on-resistance and threshold voltage

*2: TPEC: Joint research body Tsukuba Power Electronics Constellation

ously. With a halo structure, on the other hand, even by shortening the channel length, the application of a halo structure simultaneously realizes a drop in on-resistance and high threshold voltage without any drop in threshold voltage, providing evidence of improved trade-off.

Figure 9 shows the internal allocation of each on-resistance element estimated from actual measurement and simulation. Without a halo structure, channel resistance contributes most, and is dominant. With a halo structure, a drop in on-resistance is achieved for elements with shortened channel length due to a drop in channel resistance. Note that the contribution ratio of the channel resistance becomes smaller than that of the drift layer and substrate resistance.

Figure 10 shows the relationship between short-circuit breaking time t_{sc} and on-resistance when the cell pitch of each structure is changed. Generally

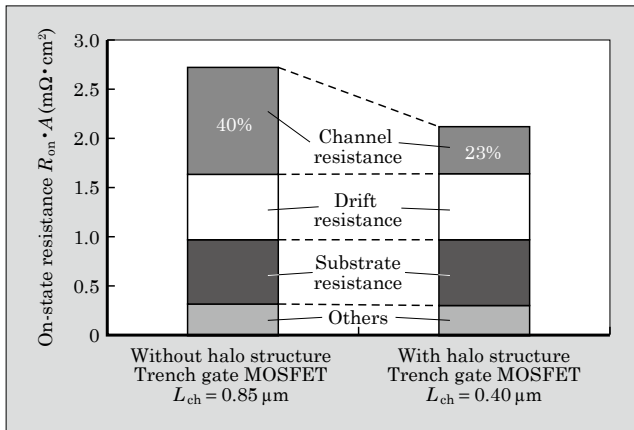


Fig.9 On-resistance of each structure and its components

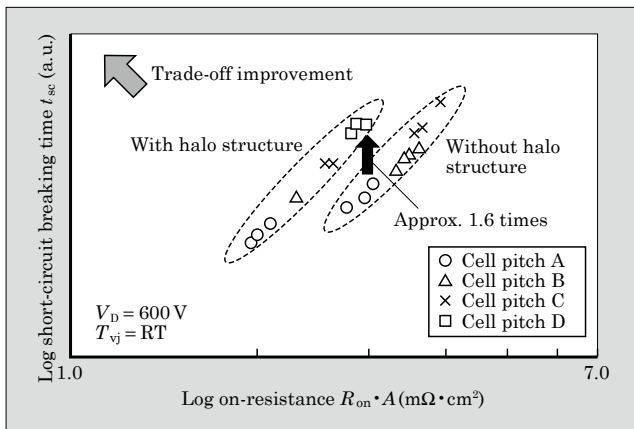


Fig.10 Relationship between short circuit capacity and on-resistance

speaking, the longer the t_{sc} and lower the channel resistance, both relationships exhibit a trade-off even for SiC-MOSFET in the same way as that for Si-MOSFET. By using a halo structure, we find that t_{sc} is approximately 1.6 times longer even with the same on-resistance, and that the trade-off has improved.

5. Postscript

We described SiC-MOSFET, which achieved both high threshold voltage and low on-resistance using a halo structure. With a breakdown voltage of 1.2 kV, we produced a prototype of an SiC-MOSFET with halo structure and confirmed an improvement effect with the halo structure. To contribute to the realization of a low-carbon society, we will continue to pursue further reductions in SiC-MOSFET on-resistance and improvements in reliability.

This paper has been implemented under a joint research project of Tsukuba Power Electronics Constellations (TPEC). We would like to express our gratitude to all those concerned.

References

- (1) Matsumoto, Y. et al. Power Electronics Equipment Applying SiC Devices. FUJI ELECTRIC REVIEW. 2015, vol.58, no.4, p.212-216.
- (2) Oshima, M. et al. Mega Solar PCS Incorporating All-SiC Module "PVI1000 AJ-3/1000". FUJI ELECTRIC REVIEW. 2015, vol.61, no.1, p.11-16.
- (3) Harada, S. et al. "1200 V SiC IE-UMOSFET with Low On-resistance and High Threshold Voltage", Materials Science Forum, 2017, vol. 897, p.497-500.
- (4) Nakazawa, M. et al. All-SiC Modules Equipped with SiC Trench Gate MOSFETs. FUJI ELECTRIC REVIEW. 2017, vol.63, no.4, p.204-208.
- (5) Noborio, M. et al. "Experimental and theoretical investigations on short-channel effects in 4H-SiC MOSFETs". IEEE transactions on Electron Devices. 2005, vol.52, no.9, p.1954-1962.
- (6) Kobayashi, Y. et al. Simulation Based Prediction of SiC Trench MOSFET Characteristics. FUJI ELECTRIC REVIEW. 2016, vol.62, no.1, p.12-16.
- (7) Kobayashi, Y. et al. "Low on-resistance SiC trench MOSFET with suppressed short channel effect by halo implantation" ICSCRM, FR.D2.1, 2017.
- (8) C. F. Codella; Ogura, S. "Halo doping effects in submicron DI-LDD device design", IEDM, 1985.
- (9) Y. Taur, E. J. Nowak. "CMOS devices below 0.1μm: how high will performance go?". IEDM, 1997.

Estimation of Power Losses, Temperatures and Power Cycle Lifetime for IGBT Modules by Using IGBT Simulator

TAKAKU, Taku* YUKAWA, Fumio* IKENOUCHI, Shun*

ABSTRACT

Fuji Electric has released its IGBT simulator free of charge on the website. It simulates the power dissipation and the junction temperature of Fuji Electric IGBT modules that are incorporated into power electronics systems, such as inverters. It supports 3-level circuits and many of the widely used pulse width modulation methods and provides the calculation of the dependence of the power loss on the junction temperature, allowing users to run more realistic simulations. Providing the power loss and the temperature rise transitions of IGBT modules helps users select modules and estimate their lifetime at the initial stages of design.

1. Introduction

In recent years, the continuous size reduction and densification of power electronics equipment has been accompanied by a wider utilization of insulated gate bipolar transistors (IGBT) in applications that are characterized by frequent and repeated load changes due to acceleration and deceleration, such as in the case of electric vehicles. Thermal fatigue due to repeated changes in the junction temperature T_{vj} of semiconductor elements is a problem related to the lifetime and reliability of the equipment. Therefore, it is necessary to adopt a design that sufficiently takes into consideration the power loss and temperature rise that occur in complex operation patterns. Fuji Electric has released an IGBT simulator⁽¹⁾ that is available free of charge to calculate the power losses and temperatures that occurs in IGBT modules. We have recently released Ver. 6 on our website*¹ as a simulator that enables more realistic calculation of characteristics such as the temperature dependence of power loss.

2. Overview of IGBT Simulator Ver. 6

Figure 1 shows the operation screen of IGBT Simulator Ver. 6. The simulator is compatible with Windows 7*² and higher. Compared with Ver. 5 of the simulator, Ver. 6 includes the following functionality:

- Supports 3-level circuits
- Includes 3-phase inverter PWM methods
- Enables calculation of the T_{vj} dependence of power loss.

*1: <https://www.fujielectric.com/products/semiconductor/model/igbt/simulation/>

* Electronic Devices Business Group, Fuji Electric Co., Ltd.

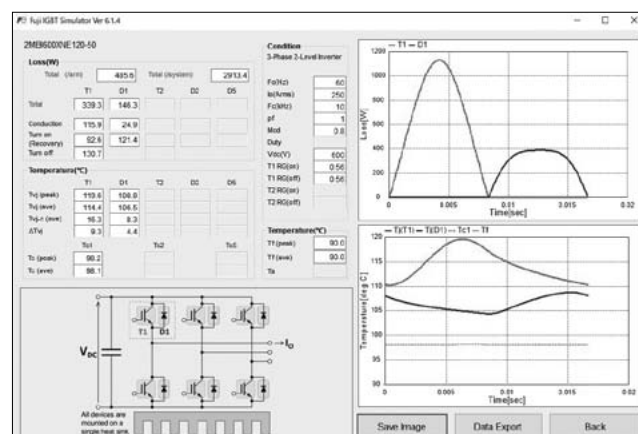


Fig.1 IGBT Simulator Ver. 6 operation screen

3. Calculation of IGBT Module Power Loss

3.1 Support for 3-level circuits

The IGBT Simulator supports 3-phase 2-level inverter circuits and boost and buck chopper circuits as conventionally done. In addition, it supports 2 kinds of 3-level circuits that are increasingly used in photovoltaic power generation, wind power generation and uninterruptible power systems (UPSs) (see Fig. 2).

3.2 Addition of 3-phase inverter PWM methods

In addition to previously supported sinusoidal pulse width modulation (PWM) and 2-phase modulation PWM (discontinuous PWM 1), it supports the following 3 widely used modulation methods:

- Space vector PWM
- 3rd harmonic injection PWM

*2: Windows 7 is a trademark or registered trademark of Microsoft Corporation

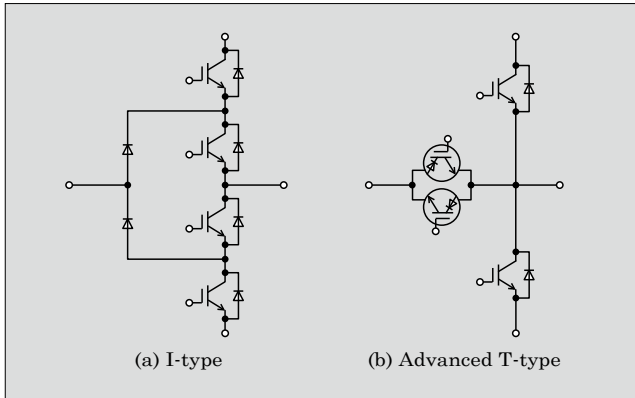


Fig.2 Newly supported 3-level circuits

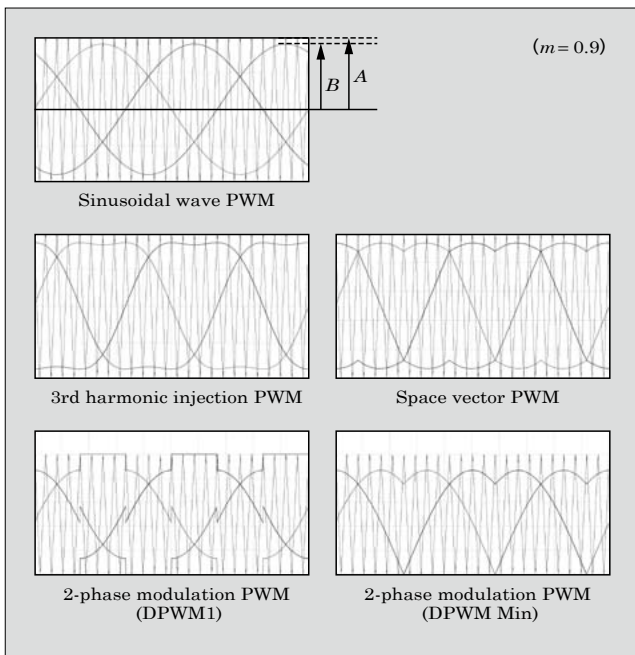


Fig.3 Control signal and triangular wave carrier signal waveforms for each modulation method

(c) 2-phase modulation PWM (discontinuous PWM Min)

Figure 3 shows the control signal and triangular wave carrier signal waveforms for each modulation method. In Ver.6, simulations can be performed by changing the control rate (modulation rate) m . m is defined as B/A , that is, the ratio of the amplitude A of a triangular carrier signal to the amplitude B of a control signal in the sinusoidal wave PWM as shown in the figure.

3.3 Power losses and temperature calculation flowchart

Figure 4 shows the calculation flowchart for the IGBT simulator. Power losses of an IGBT and a free wheeling diode (FWD), which constitute an inverter, are categorized into conduction loss (steady-state loss) generated during energization and switching loss generated during switching. Conduction losses are calculated on the basis of the output characteristics of the

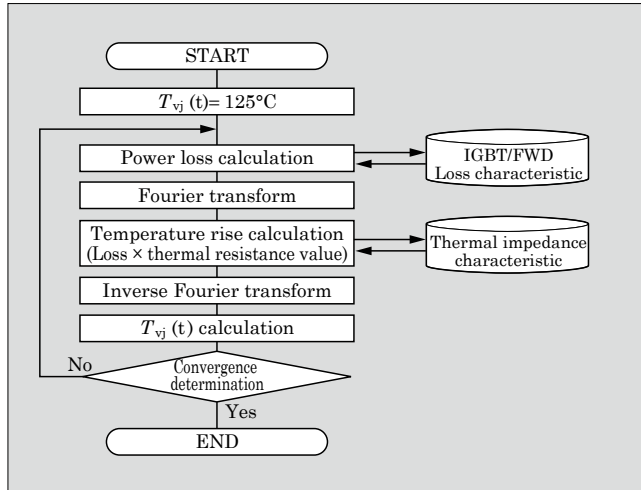


Fig.4 Calculation flowchart

IGBT and FWD, while switching losses are calculated based on current and gate resistance characteristics. For more details on how power loss is calculated, please refer to the reference material⁽¹⁾. In the IGBT simulator, the characteristic curve data at each temperature is stored as database content for each module, and is thereafter used in calculations.

4. Calculation of IGBT Module Temperature

4.1 Thermal resistance model

Figure 5 shows the one-dimensional thermal circuit model of a 3-phase inverter in the simulator. It consists of junction-to-case thermal impedance $Z_{th(j-c)}$, case-to-fin thermal impedance $Z_{th(c-s)}$, and heat sink-to-ambient thermal resistance $Z_{th(s-a)}$. In this model, the case temperature T_c and the heat sink temperature T_s are defined as temperatures directly below the chip. The ambient temperature T_a is treated as a constant.

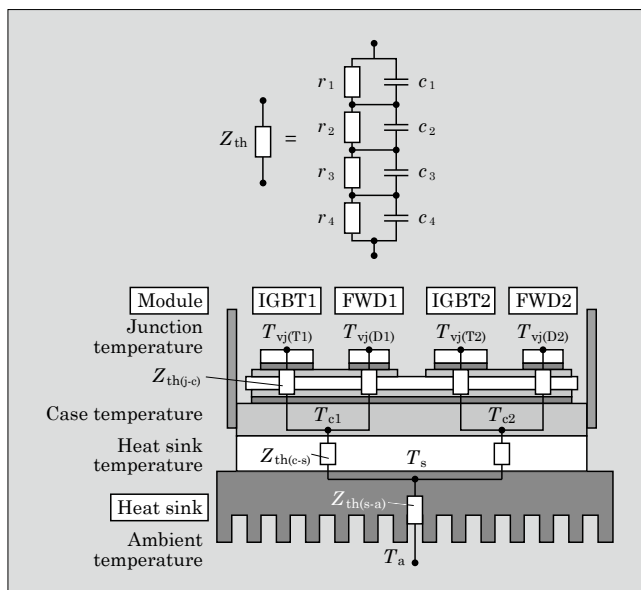


Fig.5 Inverter thermal circuit model

To calculate the transient temperature rise, each thermal impedance curve is expressed as a 4th-order Foster Network circuit represented by Equation 1, in which 4 parallel circuits of components R and C are connected in series. In the circuit, r_n and c_n are values calculated by the least squares method using the characteristic curve data for transient thermal impedance on the data sheet. As shown in Fig. 4, these values are registered in the database for each module of the simulator.

$$Z_{th}(t) = \sum_{n=1}^4 r_n \left\{ 1 - \exp\left(-\frac{t}{r_n c_n}\right) \right\} \dots\dots\dots (1)$$

Z_{th} : Thermal impedance
 r_n : Resistance component in the Foster Network
 c_n : Capacitance component in the Foster Network
 t : Time

4.2 Calculation of temperature rise

To calculate the junction-to-case temperature rise T_{vj-c} of an IGBT and FWD, loss waveform $P_{loss}(t)$ generated by the IGBT is Fourier transformed, the obtained Fourier coefficient is multiplied by transient thermal resistance value, and is then inverse Fourier transformed. First, $P_{loss}(t)$ is expanded in a Fourier series, and Fourier series a_0 , a_m , b_m for each frequency component is obtained as expressed in Equation 1.

$$P_{loss}(t) = a_0 + \sum_{m=1}^g \{ a_m \cos(m\omega t) + b_m \sin(m\omega t) \} \dots\dots\dots (2)$$

$P_{loss}(t)$: Loss waveform
 ω : Output angular frequency of the inverter
 g : Arbitrary integer

Next, Fourier series c_m , d_m of the temperature rise waveform are obtained by the product of the determined Fourier coefficient and junction-to-case thermal impedance $Z_{th(j-c)}$.

$$c_m = \sum_{n=1}^4 \frac{(a_m - m\omega \tau_n b_m)}{1 + (m\omega \tau_n)^2} r_n \dots\dots\dots (3)$$

$$d_m = \sum_{n=1}^4 \frac{(m\omega \tau_n a_m + b_m)}{1 + (m\omega \tau_n)^2} r_n \dots\dots\dots (4)$$

The $T_{vj-c}(t)$ waveform is obtained by applying an inverse Fourier transform to these series.

$$\begin{aligned} T_{vj-c}(t) &= T_0 + \sum_{m=0}^g \{ c_m \cos(m\omega t) + d_m \sin(m\omega t) \} \\ &= P_{loss(ave)} \sum_{n=1}^4 r_n + \sum_{m=0}^g \{ c_m \cos(m\omega t) + d_m \sin(m\omega t) \} \dots\dots\dots (5) \end{aligned}$$

$T_{vj-c}(t)$: Junction-to-case temperature
 T_0 : Average value of temperature rise

Using the heat sink-to-ambient temperature T_{s-a}

and the case-to-heat sink temperature T_{c-s} , which is obtained by the same method as that used for the junction-to-case temperature $T_{vj-c}(t)$, Equation 6 gives the waveforms of the heat sink temperature T_s , case temperature T_c , and junction temperature T_{vj} .

$$\begin{aligned} T_s(t) &= T_a + T_{(s-a)}(t) \\ T_c(t) &= T_s(t) + T_{(c-s)}(t) \\ T_{vj(IGBT)}(t) &= T_c(t) + T_{vj-c(IGBT)}(t) \\ T_{vj(FWD)}(t) &= T_c(t) + T_{vj-c(FWD)}(t) \dots\dots\dots (6) \end{aligned}$$

$T_{(c-s)}$: Case-to-heat sink temperature
 $T_{(s-a)}$: Heat sink-to-ambient temperature
 T_s : Heat sink temperature
 T_c : Case temperature
 $T_{vj(IGBT)}$: IGBT chip junction temperature
 $T_{vj(FWD)}$: FWD chip junction temperature

4.3 Calculation in consideration of the T_{vj} dependence of power loss

In IGBT simulators Ver.5 and before, power losses are calculated with a constant junction temperature T_{vj} of 125°C. However, in order to facilitate more realistic calculations, Ver. 6 comes equipped with a new calculation function that takes into consideration the T_{vj} dependence of power losses.

In the IGBT simulator, loss and temperature cannot be calculated simultaneously because the temperature is calculated after obtaining the power losses for the entire period of the calculation as shown in Fig. 4. Therefore, the T_{vj} dependence of power losses is calculated as below.

As an initial value, calculate power losses are from assuming junction temperature $T_{vj}(t) = 125^\circ\text{C}$ for the entire period of the applicable calculation. Next, calculate the junction temperature $T_{vj}(t)$ from each of the values of thermal impedance. After this, recalculate power loss based on the $T_{vj}(t)$ obtained as described above. Finally, obtain the convergence value by repeatedly calculating loss and temperature in this manner.

Figure 6 shows the differences between the number

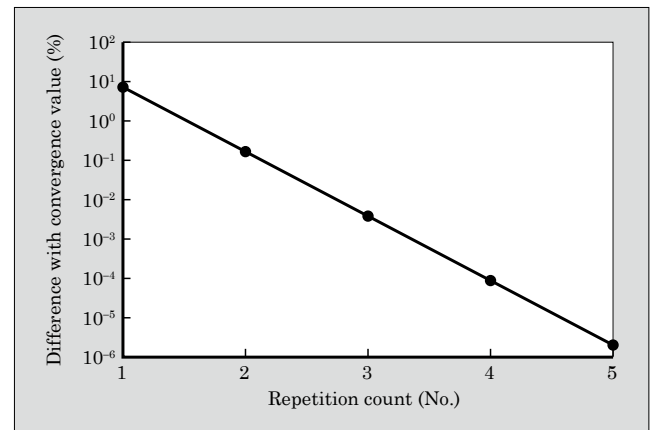


Fig.6 Difference between the number of recalculations and the convergence values

of recalculations of loss and temperature and the convergence value. The calculated IGBT loss for a single recalculation (assuming $T_{vj} = 125^{\circ}\text{C}$) has a margin of error of 7% with respect to the convergence value. On the other hand, when the number of recalculations is increased to 3, the difference with the convergence value is less than 0.01%, thereby providing a practical value that can be used without concern.

5. Comparison with Commercially Available Simulator

In order to verify if IGBT Simulator Ver. 6 correctly calculates loss while taking into consideration T_{vj} dependence, we compared its results with those of the commercially available circuit simulator PLECS^{(2)*3}.

PLECS is an electrical circuit simulation software for power electronics systems. Switching devices are modeled as ideal switches. In addition, PLECS can determine the loss generated in a circuit's switching element by inputting the loss characteristics of the switching element. Temperature simulation is also possible by incorporating a one-dimensional thermal resistance model.

Table 1 shows the simulation conditions, and Table 2 and Fig. 7 shows a comparison of the simulation results. All of the results coincide extremely well,

Table 1 Simulation conditions

Item	Condition
IGBT module	2MBI600XNE120-50
Circuit and control method	3-phase inverter Sinusoidal modulated PWM
AC output frequency	50 Hz
AC output current	300 A
DC bus voltage	600 V
Switching frequency	8 kHz
Power factor	0.9
Modulation rate	0.9
Gate resistance	0.56 Ω
Case temperature	90°C

Table 2 Comparison of simulation results

Item	IGBT Simulator Ver. 6 (Fuji Electric product)	PLECS Ver.4.1
IGBT conduction loss (W)	147.6	147.5
IGBT switching loss (W)	103	103.1
FWD conduction loss (W)	30.9	30.9
FWD switching loss (W)	49.9	49.5
IGBT junction temperature (°C)	106.5	106.6
FWD junction temperature (°C)	96.3	96.6

*3: PLECS is a trademark or registered trademark of Plexim GmbH

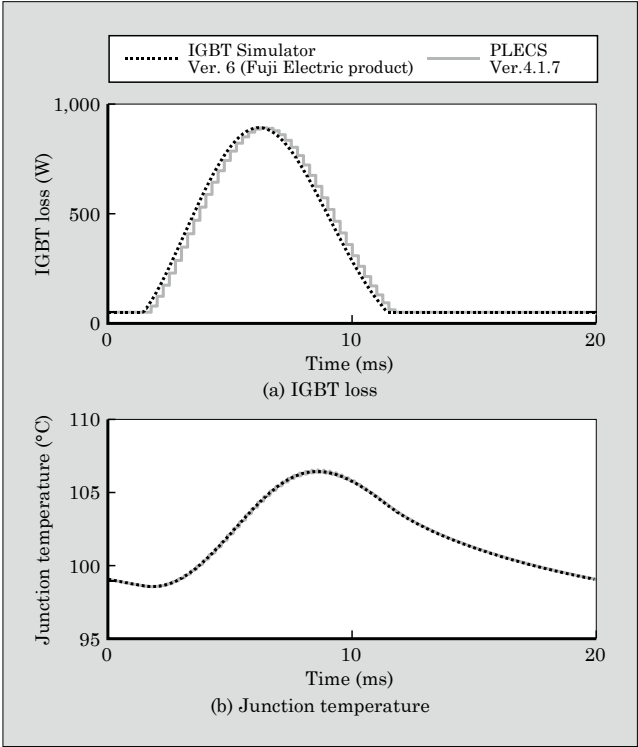


Fig.7 Comparison of IGBT loss and temperature calculation results

thereby verifying the validity of the calculation.

6. Estimation of the Power Cycle Lifetime

6.1 IGBT module power cycle lifetime

In servo drive systems and applications such as elevators and electric vehicles equipped with power converters that use IGBT modules, frequent and repeated acceleration and deceleration can fluctuate the junction temperature during speed changes, low frequency operation and motor lock mode, which in turn can cause failure in the IGBT module⁽³⁾. Figure 8 shows an example of the ΔT_{vj} power cycle curve of an IGBT module, and Fig. 9, an example of a load cycle calculated by the IGBT simulator. The temperature waveform plot-

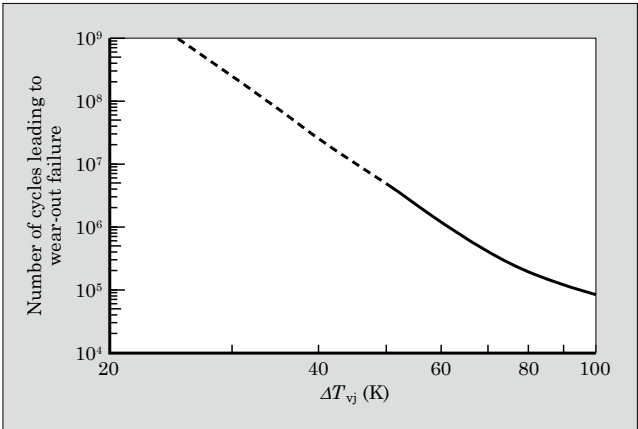


Fig.8 Example of IGBT module ΔT_{vj} power cycle curve

ted with solid line shows the maximum temperature for the inverter output period, whereas that with the dashed line shows the average temperature for the output period. For details, please refer to the manual⁽⁴⁾ of the IGBT simulator.

Figure 8 shows the number of cycles (lifetime) leading to failure when a constant temperature change ΔT_{vj} is repeatedly applied to an IGBT module. However, since the actual load changes during the specified operation cycle of the specified period as shown in Fig. 9, the lifetime of the IGBT module cannot simply be estimated by using the ΔT_{vj} power cycle curve.

In general, module breakdown due to the ΔT_{vj} power cycle corresponds to wear-out failure^{*4}. If there are multiple temperature fluctuations in a specified operating cycle, the power cycle lifetime can be estimated on the basis of the linear cumulative damage rule (Miner's rule).

Multiple temperature fluctuations occurring during a specified operation cycle are expressed as ΔT_{vj1} , ΔT_{vj2} , ΔT_{vj3} , ..., ΔT_{vji} . Next, the number of repetitions until breakdown occurred at each temperature fluctuation is obtained from Fig. 8 and expressed as N_1 , N_2 , N_3 , ..., N_i . If the number of times ΔT_{vj1} , ΔT_{vj2} , ΔT_{vj3} , ..., ΔT_{vji} occurs during the specified operation cycle is n_1 , n_2 , n_3 , ..., n_i , the fatigue damage ratio D per operation cycle can be expressed by Equation 7.

$$D = \frac{n_1}{N_1} + \frac{n_2}{N_2} + \frac{n_3}{N_3} + \dots + \frac{n_i}{N_i} \dots\dots\dots (7)$$

n_i : Number of ΔT_{vji} occurrences during a single operation cycle

N_i : Number of power cycles until ΔT_{vji} fatigue damage occurs

D : Fatigue damage ratio per operation cycle

Module failure occurs if the cumulative fatigue

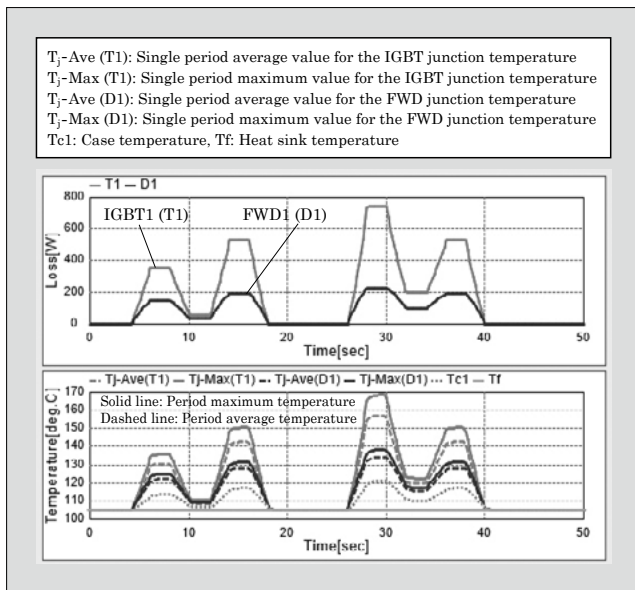


Fig.9 Example of load cycle calculation via IGBT simulator

damage ratio $N_{\text{cycle}} \times D$ is more than 1 when the operation cycle is repeated N_{cycle} . The number of operation cycles until module failure is determined by Equation 8.

$$N_{\text{cycle}} = 1/D \dots\dots\dots (8)$$

N_{cycle} : Number of operation cycles until module failure

6.2 Power cycle count via rainflow-counting method

The peak counting method, the range pair counting method and other methods are proposed for predicting the lifetime in wear-out failure. The rainflow counting is one of the major methods.

As an example shown in Fig. 10, the T_{vj} profile during an operation cycle that is repeated every 60 seconds was obtained via the IGBT simulator. Then, the number of occurrences n_i for multiple ΔT_{vj} obtained by using the rainflow-counting method from the T_{vj} profile is shown in Table 3.

N_i is the power cycle lifetime at each ΔT_{vj} obtained from Fig. 8. On the basis of these values, $N_{\text{cycle}} = 1.9 \times 10^6$ cycles can be obtained by using Equation 8 to calculate the number of cycles until the module is failed for the 60-second cycle, and from this, the IGBT module lifetime can be estimated to be 10.9 years when

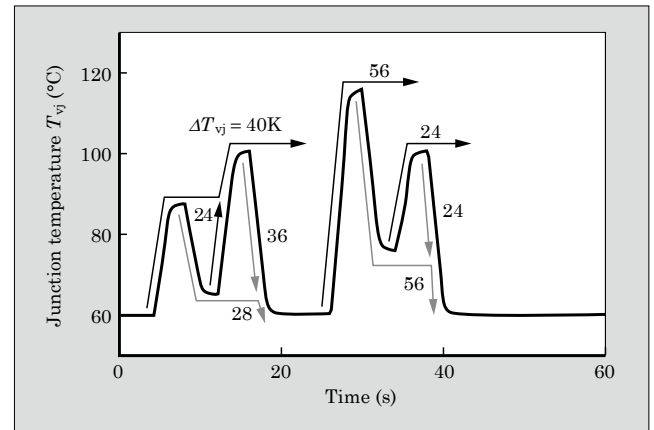


Fig.10 Power cycle count via rainflow-counting method

Table 3 Power cycle count calculated via rainflow-counting method

ΔT_{vj} (K)	Occurrences n_i	N_i	n_i/N_i
23 to 25	1.5	1.27×10^9	1.2×10^{-9}
27 to 29	0.5	4.19×10^8	1.2×10^{-9}
35 to 37	0.5	5.90×10^7	8.5×10^{-9}
39 to 41	0.5	2.56×10^7	2.0×10^{-8}
55 to 57	1.0	2.02×10^6	5.0×10^{-7}

*4: Wear-out failure: the failure rate curve can be separated into the 3 periods: initialization failure, accidental failure and wear-out failure. Wear-out failure causes the failure rate to increase over time due to wear and fatigue.

operated 8 hours a day with $N_{\text{cycle}} \times 60 \text{ seconds} = 1.1 \times 10^8 \text{ seconds}$.

7. Postscript

In this paper, we described the estimation of power loss, temperature and lifetime of IGBT modules using our simulator. In addition to supporting 3-level circuits and many of the widely used PWM methods, it enables calculation of power loss depended on junction temperature in order to provide a more realistic simulation. Furthermore, we also explained how to estimate power cycle lifetime from simulation results in applications characterized by complex output fluctuations such as those of electric vehicles.

The described simulator, though in simple manner, helps users understand movements in the power loss and temperature rise of IGBT modules in a user-

friendly manner. We recommend that this simulator be used during the initial stages of design to aid users in selecting modules and estimating lifetime.

References

- (1) Takaku, T. et al. Power Loss and Temperature Simulator for IGBT Module. FUJI ELECTRIC Journal. 2008, vol.81, no.6, p.438-442. (Japanese).
- (2) Plexim. <https://www.plexim.com/>, (accessed 2018-09-20).
- (3) Morozumi, A. et al. Reliability of Power Cycling for IGBT Power Semiconductor Modules. IEEE Transactions On Industry Applications. 2003, vol.39, no.3, p.665-671.
- (4) Fuji IGBT Simulator. <https://www.fujielectric.com/products/semiconductor/model/igbt/simulation/index.html>, (accessed 2018-09-20).



“FA1B00 Series” 4th-Generation Critical Conduction Mode, Power Factor Correction Control ICs

ENDO, Yuta* YAGUCHI, Yukihiro* HIASA, Nobuyuki*

ABSTRACT

Fuji Electric has developed the “FA1B00 Series” 4th-generation critical conduction mode, power factor correction control ICs to meet the market demand for power supplies with low power consumption and low cost. We have newly developed an input current trapezoidal wave control method to suppress output voltage ripple while reducing power source harmonic current. This method facilitates the miniaturization of the output capacitor of a PFC circuit. Furthermore, by inheriting the light-load bottom-skip function and standby mode burst function from the previous model, the “FA1B00 Series” helps reduce the power consumption and cost of power supplies.

1. Introduction

The use of switching power supplies has become widespread due to the smaller size and weight of electronic devices such as televisions. Harmonic current in switching power supplies can lead to operational failure, decrease power factor of equipment and distribution facilities, and increase apparent power. Therefore, the international standard IEC 61000-3-2 classifies electrical and electronic devices in classes A to D, as shown in Table 1, and establishes regulatory values with respect to power source harmonic current.

To solve problems related to power source harmonic current and power factor, power filter correction (PFC) circuits using an active filter are often utilized, and it is against this backdrop that Fuji Electric has commercialized ICs for controlling PFC circuits.

In recent years, there has been increasing demand for size and price reduction of electronic devices such as televisions, and this in turn has increased the need for small and low-cost switching power supplies for these products.

In addition, energy savings in electrical products in general has become increasingly important to reduce environmental burdens worldwide. PFC circuits also need to be reduced in standby power and improved in

efficiency at light loads.

In response to these demands, Fuji Electric has developed the “FA1B00 Series” 4th-generation critical mode PFC control IC line-up as the successor to the “FA1A00 Series” 3rd-generation critical mode PFC control IC line-up for counteracting harmonic current. The “FA1B00 Series” satisfies power source harmonic current regulations, contributes to miniaturization of the PFC circuit output capacitor and enables highly efficient power control during light loads and standby.

2. Overview of the “FA1B00 Series”

Figure 1 shows the external appearance for the recently developed FA1B00 Series, and Table 2 shows a comparison of major features.

The FA1B00 Series has lined up the “FA1B21N” as an IC modified to control the suppression of PFC output voltage ripple on the basis of the “FA1B20N,” which integrates communication and burst functions with the conventional FA1A00 Series to reduce the standby power. By using ceramic capacitors and film capacitors for the output capacitors, volume has been reduced to one-tenth of that of conventional electrolytic capacitors, thereby contributing to smaller size and

Table 1 Classification of power source harmonic current regulations (IEC 61000-3-2)

Classification	Typical equipment
Class A	Major home appliances, Audio equipment
Class B	Portable power tools, Arc welding machines
Class C	Lighting equipment
Class D	PCs, TVs

* Electronic Devices Business Group, Fuji Electric Co., Ltd.

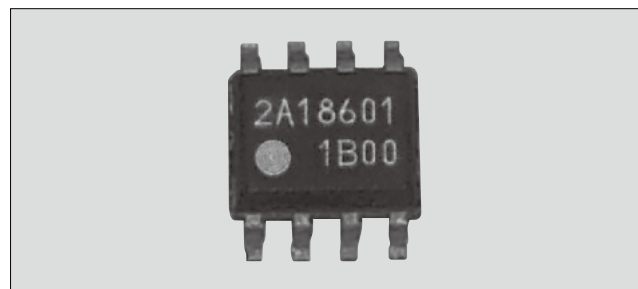


Fig.1 “FA1B00 Series”

Table 2 Comparison of main “FA1B00 Series” features

Item	FA1B00N	FA1B20N	FA1B21N
Turn-on timing detection	ZCD winding	Inductor current	Inductor current
Pulse width control	Voltage mode	Voltage mode	Current mode
Light load switching operation	Limiting Max. frequency	Bottom skip	Bottom skip
Communication capability with LLC	No	Yes	Yes
Current detection polarity	Plus	Minus	Minus
PFC output over-voltage protection	Single	Double	Double
Main applications	LED lighting, etc.	General purpose use	Flat screen TVs

longer lifespan of devices. However, this has resulted in decreased capacitor capacitance and therefore has the disadvantage of a greatly deviating input voltage specification for the converter connected to the rear stage of the PFC circuit. In order to compensate for this disadvantage, the IC suppresses output voltage ripple to achieve size reduction and a longer service life for the device.

Furthermore, the “FA1B00N” has been designed for applications that improves power factor at light loads by utilizing a zero current detection (ZCD) winding for inductor current zero-cross detection in order to determine metal-oxide-semiconductor field-effect transistor (MOSFET) turn-on timing. Figure 2 shows the block diagram for the “FA1B21N.”

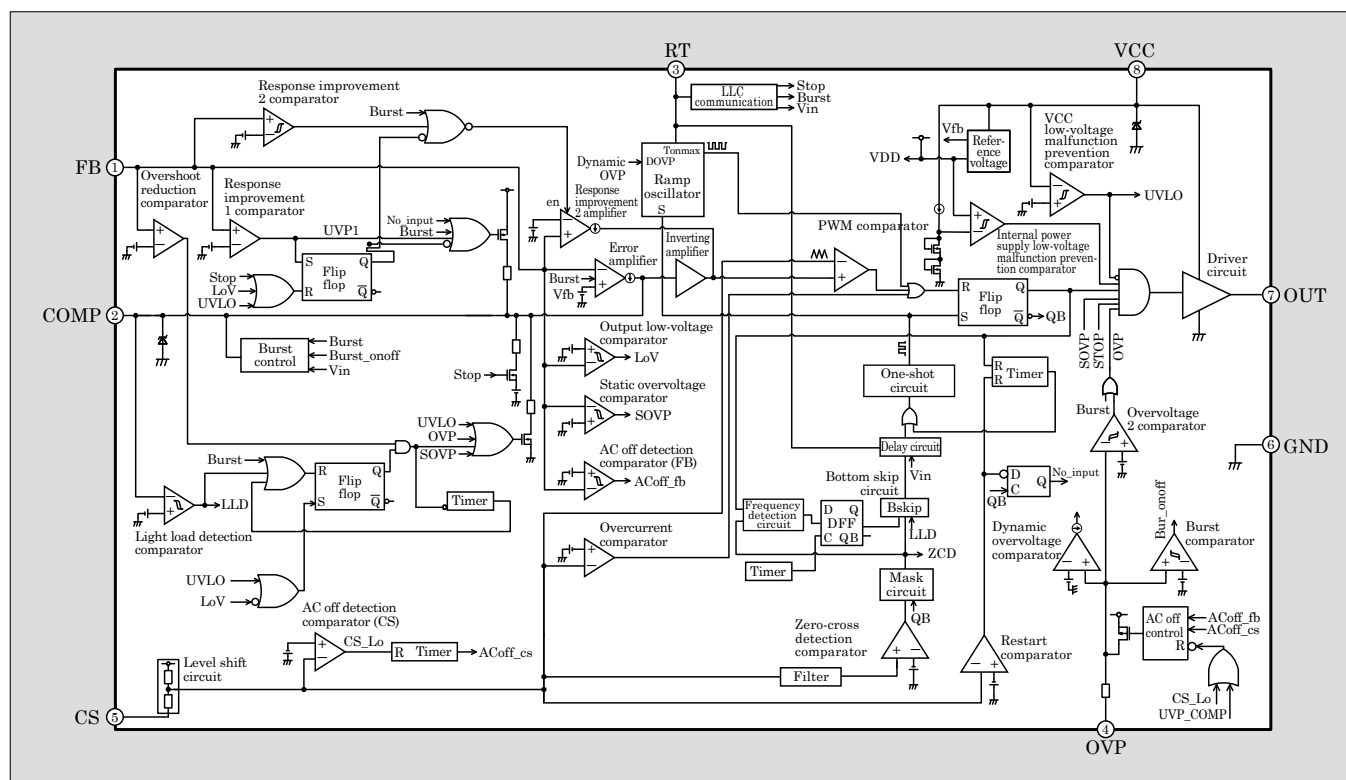


Fig.2 “FA1B21N” block diagram

3. Features

3.1 PFC output capacitor miniaturization

Figure 3 shows the conceptual block diagram for the PFC circuit.

In general, capacitors in this circuit need to have a large capacitance and high withstand voltage to accommodate an output voltage of 400 V (450 V for electrolytic capacitors). However, this has required enlarging a capacitor (C2), which is used for smoothening PFC output voltage, and this in turn has created the problem of a larger footprint in the PFC circuit portion of the power supply board.

When capacitor capacitance is reduced to achieve space and cost savings for the board, PFC output voltage ripple increases during steady-state operation. Moreover, when dynamic conditions such as commercial AC input fluctuation or load fluctuation occur, a high output voltage is generated near a phase compo-

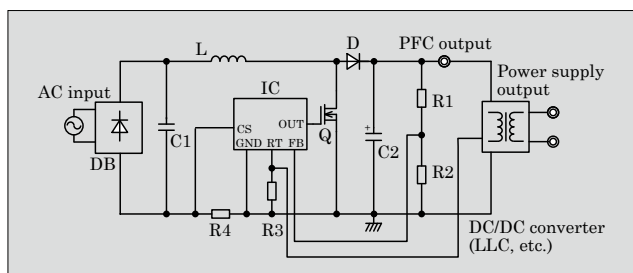


Fig.3 PFC circuit conceptual block diagram

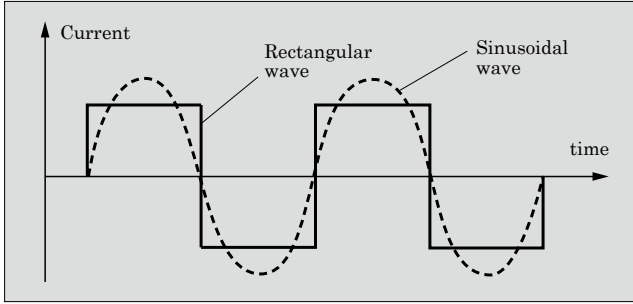


Fig.4 Schematic diagram of input current waveform

ment of 90 degrees in response to the input voltage, and this can lead to power element or electrolytic capacitor breakdown due to the overvoltage. On the other hand, near 0 degrees, a large output voltage drop below the minimum input voltage of the DC/DC converter connected to the rear stage of the PFC circuit may occur, thereby potentially leading to power supply operation stoppage or system reset for the equipment.

Therefore, we newly developed and applied an input current trapezoidal wave control method as a new control method that both suppresses output voltage ripple and reduces power source harmonic current.

Equation 1 shows the theoretical equation of output voltage ripple for the conventional method using a sinusoidal input current, Equation 2 shows that for the new method using an input current approximated to a rectangular wave, and Fig. 4 shows the waveform schematic diagram.

$$\Delta V_{PP0} = \frac{P_o}{2\pi f_{ac} V_o C} \dots \dots \dots (1)$$

$$\Delta V_{PP1} = (\sqrt{\pi^2 - 4} + 2 \arcsin\left(\frac{2}{\pi}\right) - \pi) \Delta V_{PP0} \\ = 0.661 \Delta V_{PP0} \dots \dots \dots (2)$$

ΔV_{PP} : Output voltage ripple (peak to peak)
 P_o : Output power
 f_{ac} : AC input frequency
 V_o : Output voltage
 C : PFC output capacitor capacitance

It can be seen from Equation 1 and Equation 2 that the output voltage ripple of the rectangular wave decreases to 66.1% with respect to that of the sinusoidal wave. In this respect, it is expected that the new trapezoidal waveform control method will be able to reduce output voltage ripple in the same manner as rectangular waves while also achieving lower power source harmonic current than rectangular waves.

3.2 High efficiency at light loads (bottom skip function)

Switching frequency increases at light loads in critical current operation PFC circuits that turn on the MOSFET after the inductor current becomes zero. As a result, MOSFET switching loss increases, resulting in the problem of degraded efficiency.

The conventional 3rd-generation FA1A00 Series

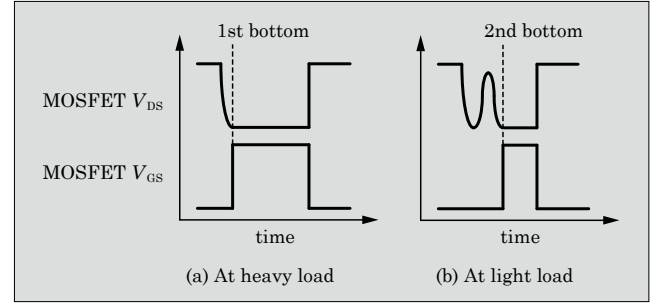


Fig.5 Bottom skip operation

incorporated a bottom skip function to improve efficiency at light loads⁽¹⁾. The FA1B20N and FA1B21N of the 4th-generation FA1B00 Series also make use of this function.

Figure 5 shows the switching operation of heavy loads (no bottom-skip operation) and light loads (with bottom-skip operation).

When bottom-skip operation is not performed, the mechanism for increasing operation frequency at light loads is as follows:

- Load is lightened.
- IC transitions to control the shortening of the MOSFET ON period.
- Since the ON period is short, the OFF period until the first bottom occurs in the MOSFET V_{DS} is also shortened after entering the OFF state.
- Frequency increases because both the ON period and OFF period become shorter.

On the other hand, when bottom-skip operation is performed, the mechanism for suppressing operation frequency at light loads is as follows:

- Load is lightened.
- IC transitions to control the shortening of the MOSFET ON period.
- Since the ON period is short, the OFF period until the first bottom occurs in the MOSFET V_{DS} is also shortened after entering the OFF state. When the sum of the ON period and the OFF period is less than a certain constant, the bottom skip function delays the turn ON timing of the MOSFET from the first bottom to the second bottom.
- The OFF period is longer than when the function is not implemented, therefore, the frequency increase is suppressed.

By suppressing the increase in frequency, switching loss is reduced, and this improves efficiency at light loads. In addition, the MOSFET will generate less heat, and this can contribute to power supply cost reduction because the size of the heat sink for dissipating heat can be reduced.

3.3 High efficiency in standby mode (burst function)

In standby mode in which the load is lighter than normal light loads, PFC circuit switching loss occupies a large percentage of total loss. Therefore, the

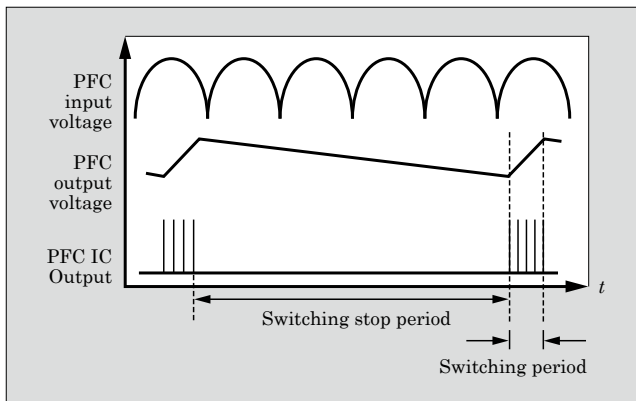


Fig.6 Burst operation

power supplied to the PFC control IC is generally cut off and switching is stopped to reduce standby power. However, PFC output voltage becomes largely dependent on the input voltage. As a result, the standby efficiency of the rear stage LLC converter deteriorates. Furthermore, external circuit components are required to cut off the power supply, which increases the space and cost of the power supply board.

In order to solve this problem, Fuji Electric has developed and produces the “FA1A60N” as a product that uses a function (burst function) to improve efficiency while maintaining the operation of the PFC control IC in standby mode. The FA1A60N identifies the standby mode by means of the communication signal input in the RT terminal from the LLC converter control IC FA6B20N⁽²⁾.

In the FA1B00 Series, the polarity of the signal input of the communication function is changed to reduce the number of external components required for the communication function.

During light or heavy loads, error amplification is performed inside the IC on the basis of the voltage of the dividing resistors (R1, R2) responsible for monitoring the output voltage input to the FB terminal as shown in Fig. 3, with the output pulse width of the OUT terminal controlled to maintain PFC output voltage at a constant value.

In standby mode, the burst function is used to stop switching when the output voltage exceeds a certain range and restart switching when it falls below a certain range as shown in Fig. 6. This control mechanism improves efficiency in standby mode.

3.4 Two turn-on timing detection methods

In order to correspond to 2 methods for detecting the turn-on timing of the MOSFET, the FA1B00 Series employs an inductor current detection method for FA1B20N and FA1B21N and a ZCD winding detection method for FA1B00N, as shown in Fig. 7.

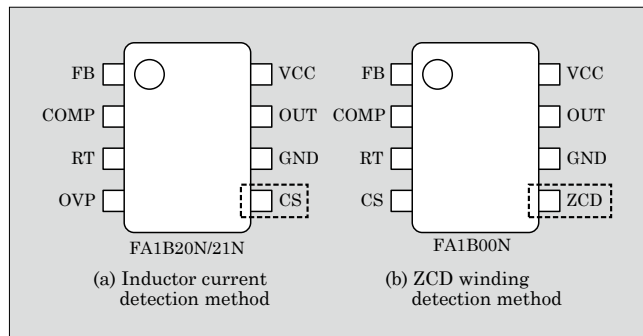


Fig.7 Terminal arrangement corresponding to 2 detection methods

4. Effect of Application on Power Supplies

Figure 8 shows an evaluation-use application circuit (inductor current detection method) equipped with an FA1B00 Series product.

Figure 9 shows the power supply operation waveforms for the different control methods. Figure 9(a) shows the waveform at the implementation of the new control method (input current: trapezoidal wave) using an FA1B21N and output capacitor with a rating of 15 μ F, which is approximately one-tenth of that of the conventional method. Figure 9(a) shows the waveform at the implementation of the conventional control method (input current: sinusoidal wave) using an FA1A20N and output capacitor with a rating of 165 μ F. In the FA1B21N, we confirmed that changing the control method to the input current trapezoidal wave control method was able to deliver the same level of stable operation as the conventional method with no switching operation instability or input current disturbance. The measurements for the evaluation results described below were conditioned upon an input voltage of 100 V AC and load power of 200 W.

Furthermore, as shown in Fig. 10, we confirmed that the output voltage ripple in the new method was 70% of that of the conventional method over the entire input voltage range. In addition, the basic characteristics shown in Table 3 did not differ with respect to efficiency or power factor, and the power source harmonic current characteristic shown in Fig. 11 was also satisfactory, securing a margin of 30% or more with respect to the Class D regulation values. This shows that the input current trapezoidal waveform control method is an effective means of size reduction of PFC output capacitors.

For example, if power supply specifications are satisfied even at a ripple voltage of 1.4 times that of the conventional method, the capacitance of the output capacitor will be halved, thereby enabling space and cost savings for the power supply board.

Moreover, with respect to the bottom-skip function and burst function inherited from previous models, we confirmed light load efficiency and the standby power

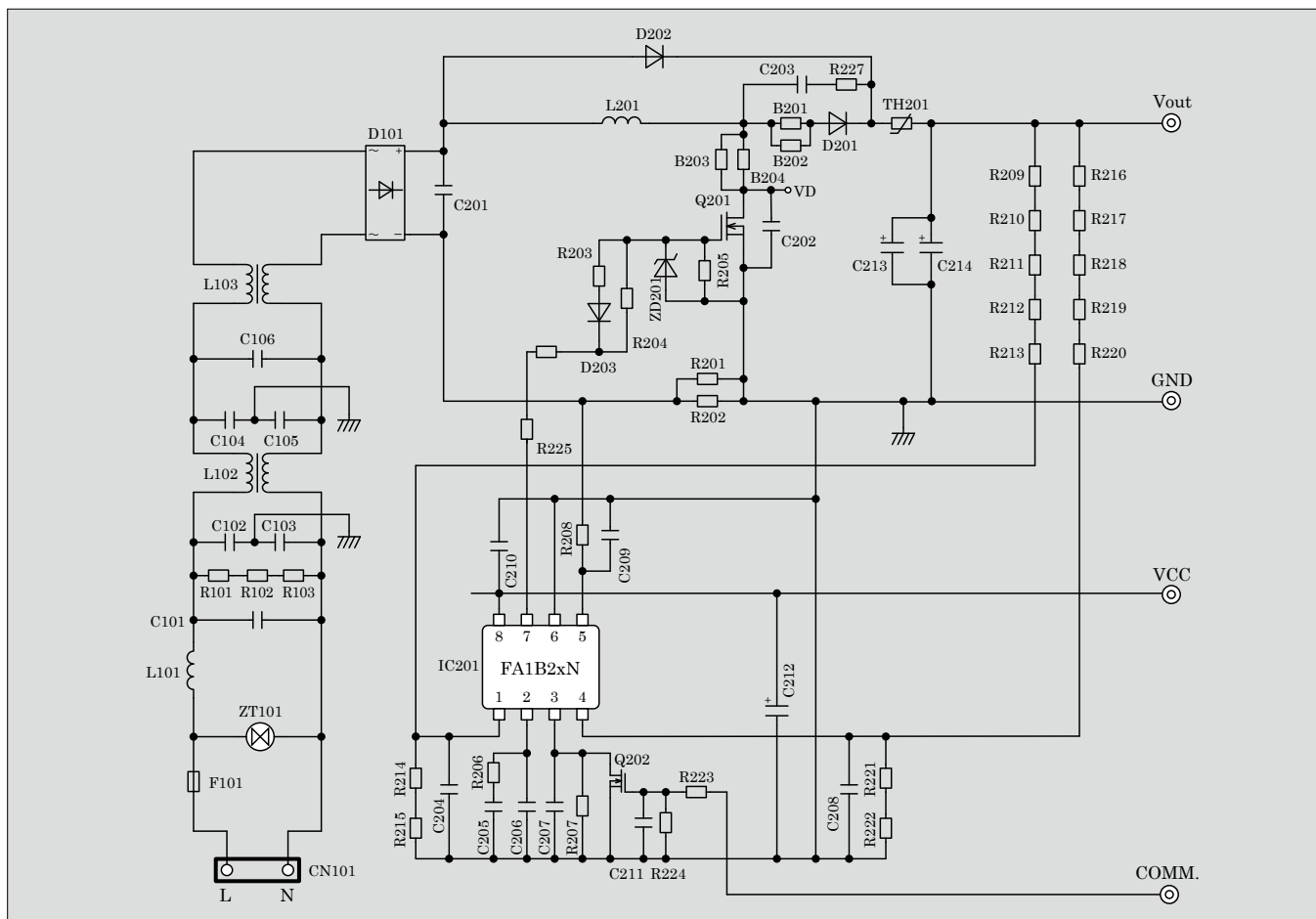


Fig.8 Evaluation-use application circuit (input: 90 to 264 V AC; output: 400 V/200 W)

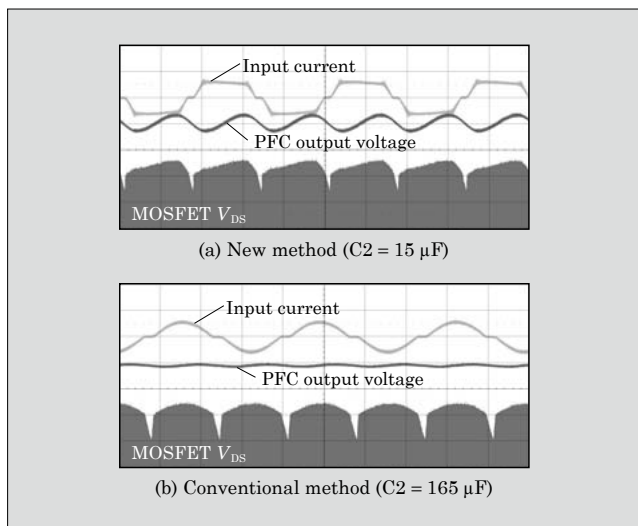


Fig.9 Input current waveforms during power supply operation

characteristic using a power supply equipped with a FA1B20N and verified that high-efficiency characteristics were the same as previous models. Figure 12 shows the standby power characteristic.

Please note that these power supply characteristics are the result of applying the FA1B20N, which uses inductor current to detect turn-on timing. We have

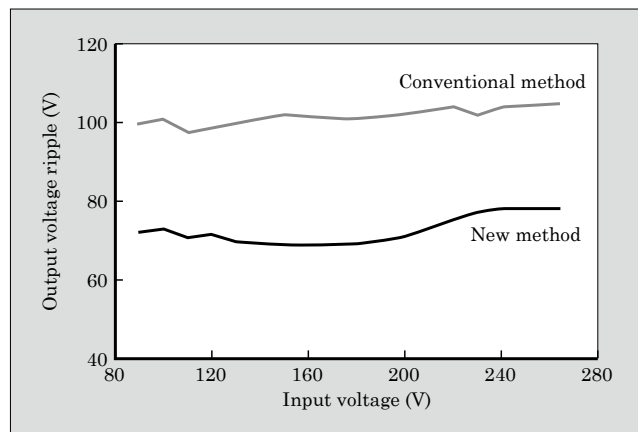


Fig.10 Comparison of output voltage ripple (C2 = 15 μF)

Table 3 Comparison of basic characteristics for control methods

Method	Efficiency (%)		Power factor (–)	
	100 V AC	230 V AC	100 V AC	230 V AC
New method	86.6	90.3	0.978	0.940
Conventional method	86.6	89.6	0.986	0.940

also confirmed adequate power supply characteristics for the FA1B00N, which uses a ZCD winding to make detection.

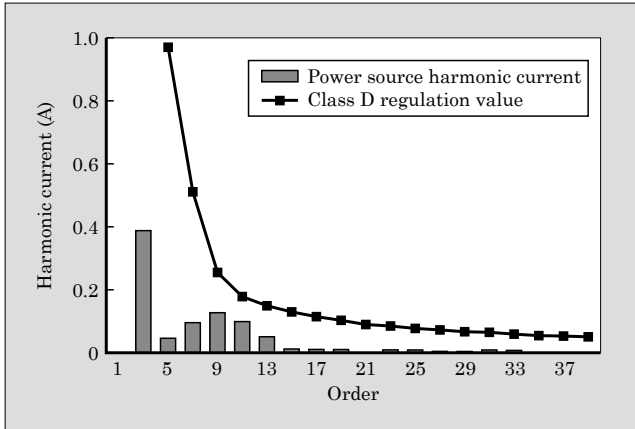


Fig.11 Power source harmonic current characteristic (C2 = 15 μ F)

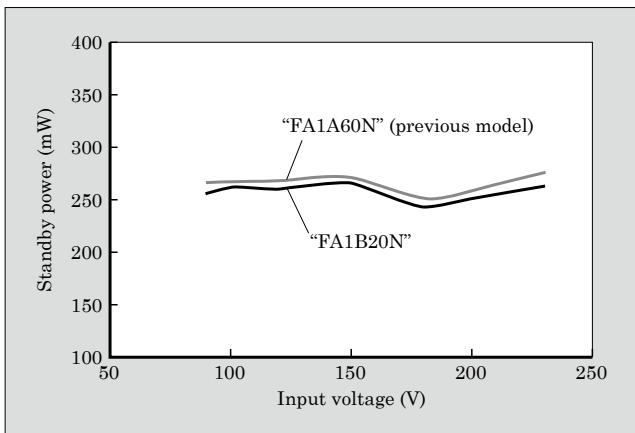


Fig.12 Standby power characteristic (load: 125 mW)

The FA1B20N and FA1B21N are suitable for power supplies that are required to improve efficiency at light loads or lower the cost by the reduction of the amount of auxiliary windings responsible for detecting inductor current. The FA1B00N is suitable for a power supplies that are required to improve power factor at light loads or further reduce the switching loss of power elements by detecting turn-on timing with high precision with a inductor auxiliary winding. In this way, adequate product can be selected according to the detection method of the turn-on timing.

5. Postscript

In this paper, we described the “FA1B00 Series” 4th-generation critical mode PFC control ICs. Critical mode PFC control ICs are required to achieve high power factor and high efficiency power supply characteristics, while facilitating cost reductions.

In the future, we plan to continue developing product series equipped with features that meet the various requirements of the market, as well as products that further optimize control and functionality.

References

- (1) Sugawara, T. et al. 3rd-Gen. Critical Mode PFC Control IC “FA1 A00 Series”. FUJI ELECTRIC REVIEW. 2014, vol.60, no.4, p.233-237.
- (2) Sonobe, K. et al. Critical Mode PFC Control IC “FA1 A60N” and LLC Current Resonant Control IC “FA6B20N” for High-Efficiency Power Supplies. FUJI ELECTRIC REVIEW. 2016, vol.62, no.4, p.269-274.

“XS Series” 650-V Discrete IGBTs

HARA, Yukihiro* KATO, Yoshiharu* TAMURA, Takahiro*

ABSTRACT

Fuji Electric has developed and launched the “XS Series” 650-V discrete IGBTs as a product line-up for UPSs and photovoltaic power generation PCSs that operate at a switching frequency of approximately 20 kHz. These devices are improved in a trade-off between conduction loss and switching loss. The series has a rating of 650 V/30 to 75 A, and its conduction loss and switching loss are lower than previous products by 20% or more. When Incorporated in a UPS, the device showed higher efficiency than previous products for all load ranges, increasing by up to 0.12 points. It also showed that the rise in device case temperature becomes smaller.

1. Introduction

Recently, utilization of the Internet of Things (IoT), big data and artificial intelligence (AI) is progressing and data usage is globally on the rise. In this situation, servers and data centers that handle data have high demands for energy saving and efficiency improvement is progressing for uninterruptible power systems (UPSs) intended for these types of equipment requiring high-quality power.

Meanwhile, the spread of renewable energy including photovoltaic and wind power generation has led to more energy decentralization, which has increased demand for power conversion. With power conditioning systems (PCSs), which convert direct-current power generated by photovoltaic systems into alternating-current power, device efficiency has been improving as with UPSs.

To improve efficiency of UPSs and PCSs, there is very high demand for switching devices with a lower loss.

Fuji Electric has developed and launched the “XS Series” 650-V discrete insulated gate bipolar transistors (IGBTs) as a product line that improves the on-state voltage and switching loss trade-off characteristic so as to improve the efficiency of UPSs and PCSs. This paper outlines the product series and describes the effect of its application.

2. Outline of “XS Series”

Figure 1 shows major applications of discrete IGBTs. The 650-V XS Series that Fuji Electric has developed targets UPSs and PCSs that operate at a switching frequency of approximately 20 kHz. IGBT

and free wheeling diode (FWD) chips with a rated current of 30 to 75 A are mounted in the TO-247, a standard package for discrete products, as shown in Fig. 2. Table 1 shows the major maximum ratings and electrical characteristics of the XS Series. It provides wide-ranging options according to the equipment power supply capacity.

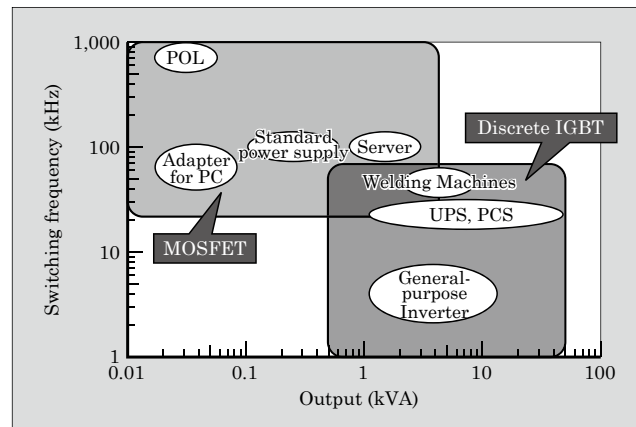


Fig.1 Major applications of discrete IGBTs

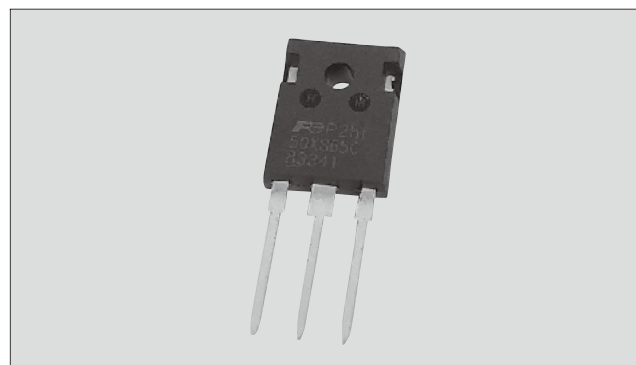


Fig.2 “XS Series” (TO-247 package)

* Electronic Devices Business Group, Fuji Electric Co., Ltd.

Table 1 Major maximum ratings and electrical characteristics of “XS Series”

Model	Built-in FWD	Package	Maximum rating				Electrical characteristic			
			IGBT			FWD	IGBT		FWD	
			V_{CES}	I_C $T_{vj}=100\text{ }^{\circ}\text{C}$	I_{CP}	I_F $T_{vj}=100\text{ }^{\circ}\text{C}$	$V_{CE(sat)}$ $T_{vj}=25\text{ }^{\circ}\text{C}$ (typ.)	$V_{CE(sat)}$ $T_{vj}=125\text{ }^{\circ}\text{C}$ (typ.)	V_F $T_{vj}=25\text{ }^{\circ}\text{C}$ (typ.)	V_F $T_{vj}=125\text{ }^{\circ}\text{C}$ (typ.)
			(V)	(A)	(A)	(A)	(V)	(V)	(V)	(V)
FGW50XS65D	Provided	TO-247	650	50	200	30	1.35	1.50	1.70	1.78
FGW75XS65D	Provided	TO-247	650	75	300	30	1.35	1.50	1.70	1.78
FGW30XS65C	Provided	TO-247	650	30	120	30	1.35	1.50	1.70	1.78
FGW40XS65C	Provided	TO-247	650	40	160	40	1.35	1.50	1.70	1.78
FGW50XS65C	Provided	TO-247	650	50	200	50	1.35	1.50	1.70	1.78
FGW75XS65C	Provided	TO-247	650	75	300	75	1.35	1.50	1.70	1.78
FGZ75XS65C	Provided	TO-247-4	650	75	300	75	1.35	1.50	1.70	1.78
FGW30XS65	None	TO-247	650	30	120	—	1.35	1.50	—	—
FGW40XS65	None	TO-247	650	40	160	—	1.35	1.50	—	—
FGW50XS65	None	TO-247	650	50	200	—	1.35	1.50	—	—
FGW75XS65	None	TO-247	650	75	300	—	1.35	1.50	—	—

3. Issues with Discrete IGBTs

For UPSs and PCSs with a few kilovolt ampere or larger capacity, 3-level inverters are generally adopted for improving the power conversion efficiency of the inverter unit. Figure 3 shows circuit diagrams of the I-type and T-type 3-level inverters.

UPS and PCSs often have discrete IGBTs operating at a switching frequency of approximately 20 kHz. Figure 4 shows breakdowns of the loss of discrete IGBTs in T1 and T2 of the I-type and AC switches (T3 and T4) of the T-type, for which products rated at 650 V are used. With the I-type, T1 requires a reduction in all of the conduction loss P_{sat} , turn-on loss P_{on} and turn-off loss P_{off} and T2 requires a reduction in P_{sat} . With the T-type, a reduction in the IGBT and FWD conduction loss $P_{sat} + P_f$ and the FWD recovery loss of P_{rr} is important.

To improve device efficiency, minimizing this power loss in inverter circuits is important and the XS Series has its focus on reducing the conduction loss and switching loss of both IGBTs and FWDs.

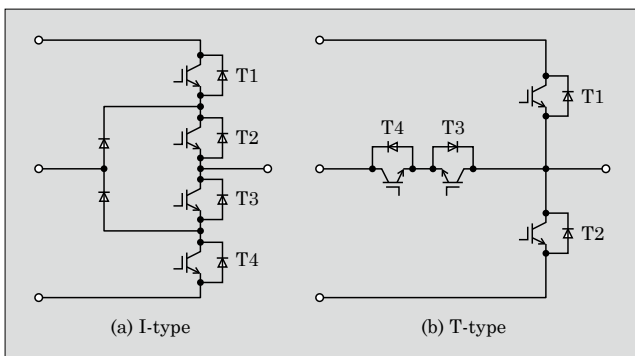


Fig.3 3-level inverter circuit diagrams

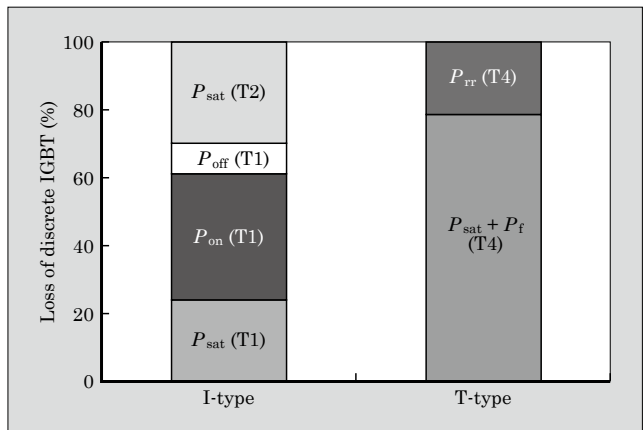


Fig.4 Result of device loss analysis ($f_c=20\text{ kHz}$)

4. Features of “XS Series”

The 650-V XS Series is based on the IGBT and FWD chip technologies of the 7th-generation “X Series” and has the optimum design for discrete products used at a switching frequency of approximately 20 kHz.

4.1 IGBT chip

Figure 5 shows a cross-sectional structure of the IGBT chips. The “High-Speed W Series,” a conventional product line, uses the 6th-generation “V Series” IGBT for modules as the basis and is designed with the focus on high-speed switching characteristics. It achieves this by adopting a surface structure with the parasitic capacitance significantly reduced, optimizing the field stop (FS) layer, controlling the hole injection into the collector layer and thinning the Si substrate⁽¹⁾. With the XS Series, in comparison, on the basis of the 7th-generation X Series IGBT technology that has improved the trade-off characteristic of $V_{CE(sat)}-E_{off}$ from the 6th generation, we have adopted design measures

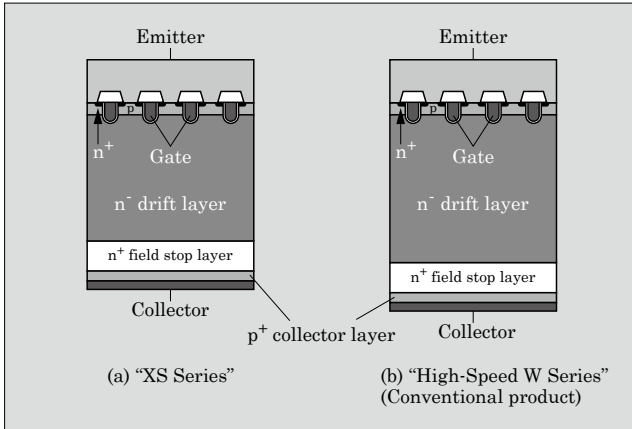


Fig.5 IGBT chip cross-sectional structure

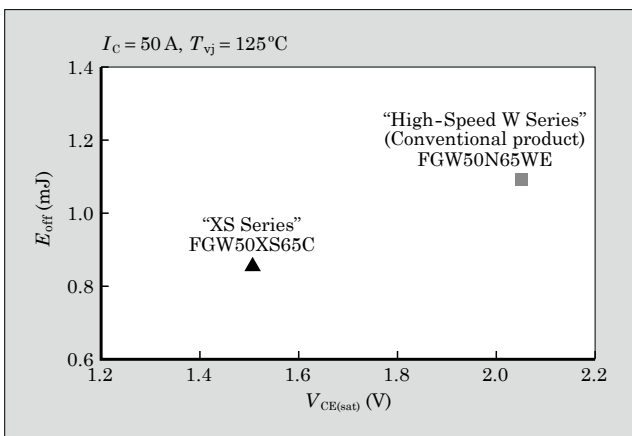


Fig.6 Trade-off characteristic (IGBTs)

to improve the trade-off characteristic of $V_{CE(sat)}$ - E_{off} . They include adopting a surface structure that is optimum for discrete IGBTs for UPSs and PCSs, optimizing the FS layer, controlling hole injection into the collector layer and thinning the Si substrate. This has achieved a significant improvement in the trade-off characteristic from that of the conventional products with a 0.5-V reduction in $V_{CE(sat)}$ and, at the same time, an approximately 20% reduction in E_{off} , as shown in Fig. 6.

4.2 FWD chip

Figure 7 shows a cross-sectional structure of the FWD chips. The FWD is based on the 7th-generation X Series FWD, which has the most advanced V_F - E_{rr} trade-off characteristic, with the Si substrate thinned and the amount of lifetime killers optimized. In addition to improving the trade-off characteristic of V_F - E_{rr} in this way, we have given the focus on the low V_F characteristic for optimization to suit UPS and PCS applications and successfully reduced V_F by approximately 0.3 V from that of the High-Speed W Series, which is shown in Fig. 8.

4.3 Package

The industry standard TO-247 package has been

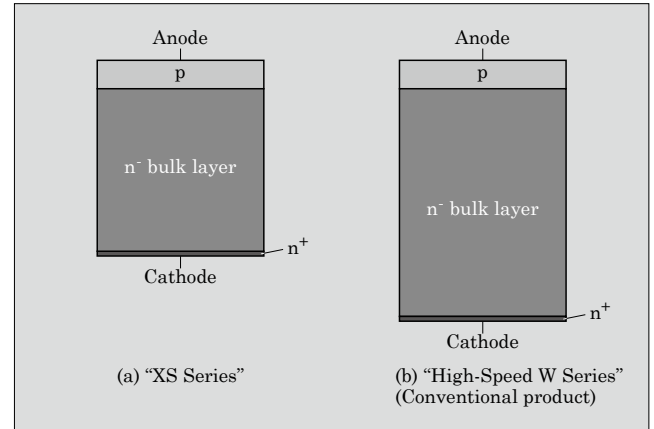


Fig.7 FWD chip cross-sectional structure

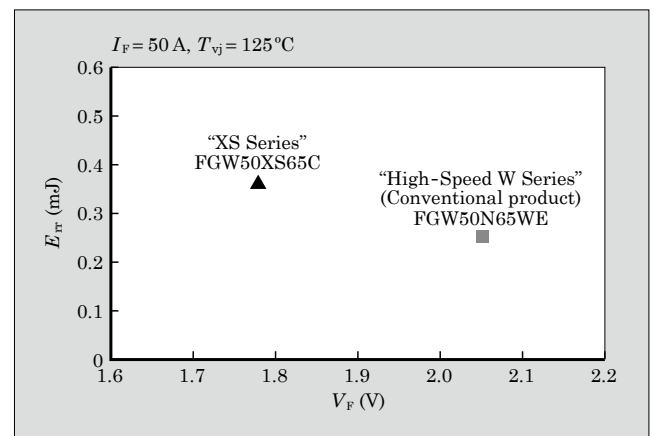


Fig.8 Trade-off characteristic (FWDs)

adopted. For connection between the chip and lead frame, lead-free solder is used, which conforms to the RoHS Directive*1 (EU2011/65/EU).

For products with a 75-A rating, a larger current rating, we also offer a line-up that uses the TO-247-4 package with a sub-emitter terminal added. Reducing the wiring inductance of the gate-emitter loop by lowering the emitter common inductance improves the gate response, which significantly reduces the switching loss in large-current operation.

5. Effect of Application of "XS Series"

5.1 Result of device loss simulation

Figure 9 shows the result of calculating the generated loss of the discrete IGBT of the I-type 3-level inverter. As compared with the High-Speed W Series, the XS Series has less loss in T1 and T2 by improving the $V_{CE(sat)}$ and E_{off} trade-off characteristic.

Figure 10 shows the result of calculating the generated loss of the IGBT and FWD in the AC switch (T4) of the T-type 3-level inverter. As compared with

*1: RoHS Directive: A European Union (EU) directive on the restriction of the use of certain hazardous substances in electrical and electronic equipment

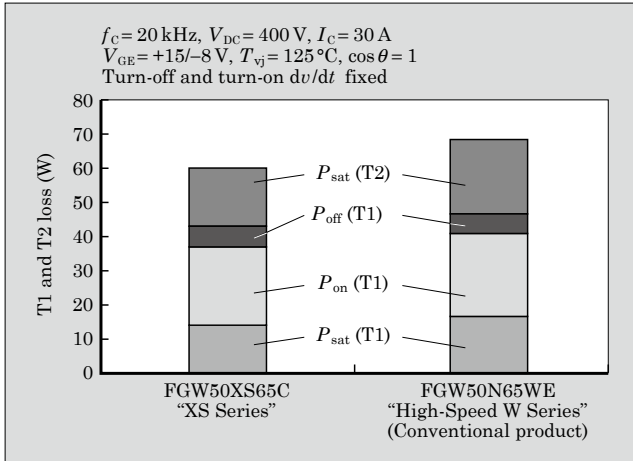


Fig.9 Device loss (3-level I-type)

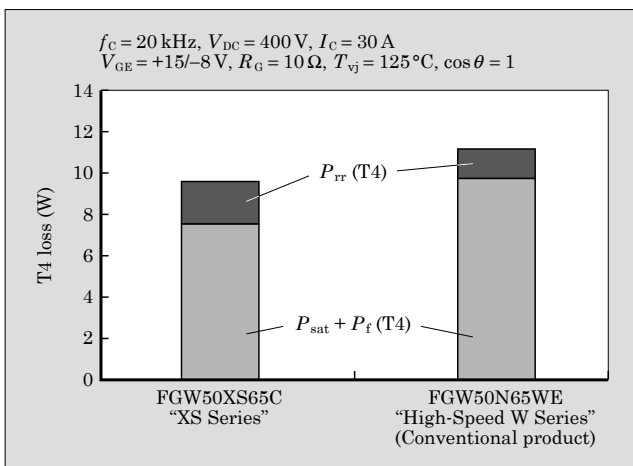


Fig.10 Device loss (3-level T-type)

the High-Speed W Series, the XS Series has been confirmed to have lower loss with the T-type as well achieved by reducing the IGBT $V_{CE(sat)}$ and FWD V_F .

5.2 Result of UPS evaluation

Figure 11 shows the result of measuring the effi-

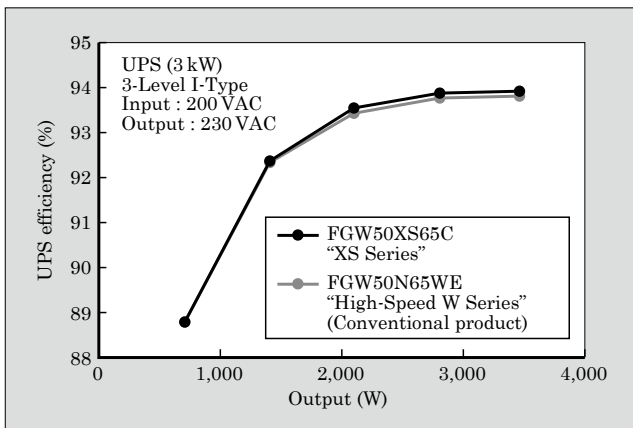


Fig.11 Comparison of UPS efficiency

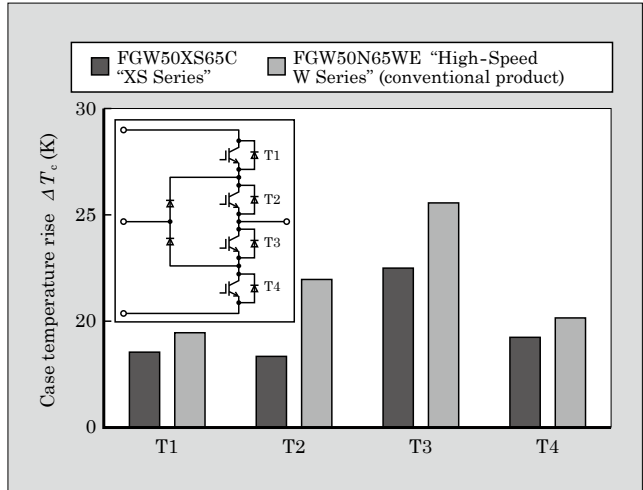


Fig.12 Comparison of IGBT case temperature rise

ciency with the XS Series applied to a UPS that uses the I-type 3-level inverter. The output capacity of the UPS used for the evaluation is 3 kW and the switching frequency of the IGBT is 24 kHz.

The XS Series offers higher efficiency than the High-Speed W Series, a conventional product, in all load ranges, increasing by up to 0.12 points. It has also been confirmed that the rise in device case temperature is smaller with the XS Series than with the High-Speed W Series in all of T1 to T4, as shown in Fig. 12.

6. Postscript

This paper has described the "XS Series" 650-V discrete IGBTs. We have developed this product mainly for UPSs and PCSs but it can also be widely applied to the PFC circuit of switching power supplies and industrial devices. We also plan to develop 1,200-V rated products of the "XS Series" discrete IGBTs intended for the main switches of T-type 3-level inverters used for UPSs and PCSs and 2-level inverters.

Fuji Electric intends to continue to contribute to energy saving and improvement of power conversion efficiency by working on further loss reduction of devices and offering products that meet the market needs.

References

- (1) Hara, Y. et al. High-Speed Discrete IGBT "High-Speed W-Series". FUJI ELECTRIC REVIEW. 2015, vol.61, no.4, p.280-284.

6.5th-Generation Automotive High Pressure Sensors

SATO, Eisuke* UENO, Fumiya* UZAWA, Ryohei*

ABSTRACT

To respond to environmental regulations and fuel consumption improvement in recent years, high-precision control technology is being applied to internal combustion engines, namely gasoline and diesel engines, and high-density mounting is being adopted to achieve downsizing. As a result, automotive high-pressure sensors are required to achieve high precision and a high guaranteed operating temperature. To meet these needs, Fuji Electric has developed a 6.5th-generation high-pressure sensor for automotive applications. The product is characterized by its integration of a metal based package that ensures a high breakdown voltage with the sensor chip that guarantees operation and precision even under high temperature and pressure. The sensor has achieved miniaturization and guarantees operation at 150 °C using miniaturization technology and revised circuit layout.

1. Introduction

Today's automobiles not only need ensure safety and comfort, but are also increasingly required to reduce environmental burdens according to laws that regulate the emission of air pollutants and CO₂. In order to meet these regulations, there has been rapid development of control systems for electric-powered vehicles such as hybrid electric vehicles (HEV), electric vehicles (EV) and fuel cell vehicles (FCV). At the same time, conventional internal combustion engines are undergoing developments to reduce environmental burdens through high-precision control technology.

Automotive pressure sensors include low-pressure sensors with a measuring range of less than 1 MPa and high-pressure sensors with a range of more than 1 MPa. Low-pressure sensors are being increasingly used for systems that seek to improve fuel efficiency in internal combustion engines, such as gasoline and diesel engines, by precisely controlling intake volumes and fuel mixture ratios, as well as for systems that endeavor to clean exhaust emissions by recirculating gas after combustion in order to reduce the emission of air pollutants. High-pressure sensors are designed to improve fuel efficiency and safety and are used in the hydraulic pressure control units of automobile engines, transmissions, power steering and brakes.

Fuji Electric started mass production of automotive pressure sensors in 1984. Since then, our sensors have been utilized in automobiles throughout the world by improving detection accuracy and achieving a high level of reliability capable of withstanding harsh automotive environments. Starting in 2005, we were able to improve detection accuracy with our 5th-generation digital trimming type pressure sensors

that utilized a complementary metal oxide semiconductor (CMOS) process. Furthermore, in 2010 we started mass production of 6th-generation pressure sensors designed for miniaturization and enhanced noise resistance⁽¹⁾.

In this paper, we introduce our 6.5th-generation automotive high-pressure sensor capable of ensuring precision in the high-temperature environments that have accompanied engine downsizing. This product has refined the conventional 5th-generation automotive high-pressure sensor for engine oil pressure.

2 Overview of Pressure Sensors

2.1 Application of automotive pressure sensors

Figure 1 shows the applications of automotive low-pressure sensors, and Fig. 2, those of high-pressure sensors. The electronic fuel injection systems for improving fuel efficiency in automobiles make use of manifold absolute pressure (MAP) sensors for measuring intake pressure, as well as temperature manifold absolute pressure (TMAP) sensors that implement temperature detection. In addition, many other types of pressure sensors for improving fuel efficiency are also used, such as barometric sensors for assisting highland correction in prevention of fuel efficiency degradation during high-altitude travel, pressure sensors for detecting intake air filter box clogging, and sensors used with turbo engines for detecting supercharging pressure.

Furthermore, there are also pressure sensors for detecting diesel particulate filter (DPF) clogging and sensors for exhaust gas recirculation (EGR) in systems that reuse exhaust gases, both of which were designed to satisfy enhanced emissions regulations typified by Japan's exhaust gas regulations or Europe's Euro 6 regulations.

* Electronic Devices Business Group, Fuji Electric Co., Ltd.

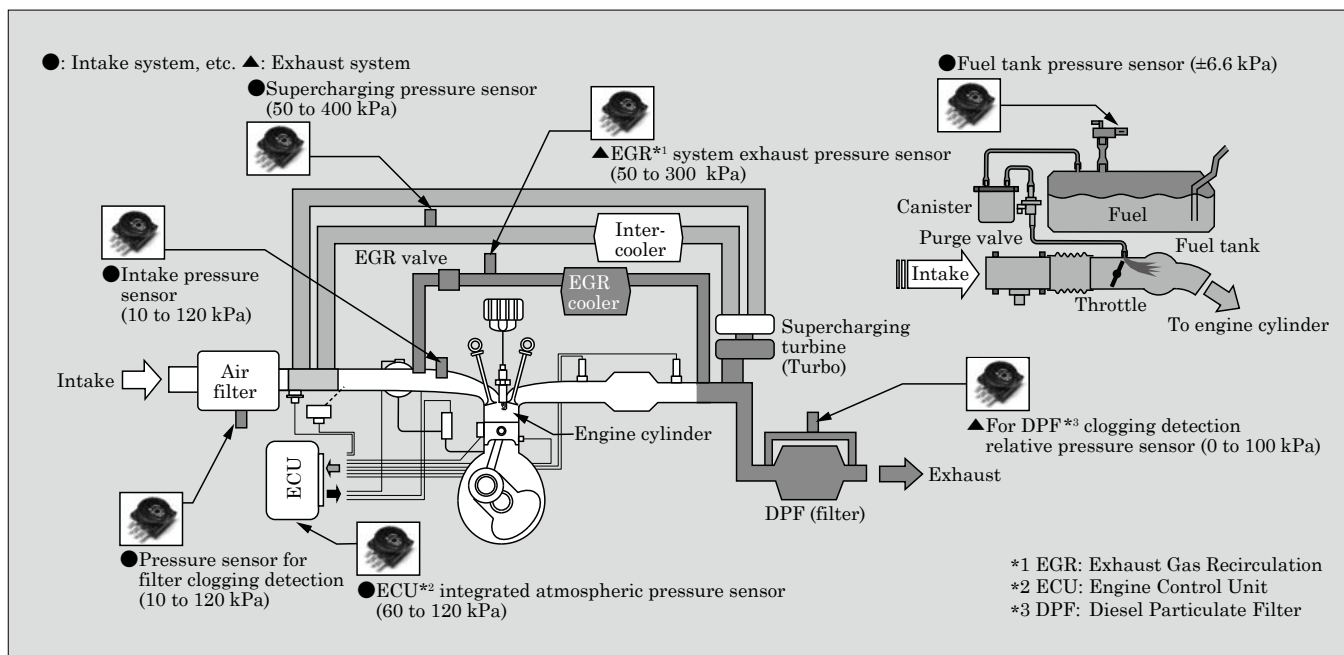


Fig.1 Automotive low-pressure sensor applications

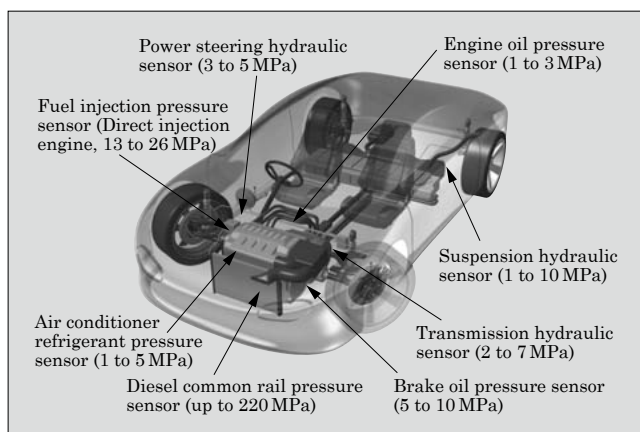


Fig.2 Automotive high-pressure sensor applications

Moreover, there are also fuel tank pressure sensors to detect fuel leakage used in Europe and the United States as pressure sensors required to meet safety regulations.

For high-pressure detection applications, the demand is increasing for fuel pressure sensors that can be mounted on diesel engines and direct-injection engines because automobile makers have become increasingly using downsized engines to improve fuel efficiency. In addition, transmissions have also advanced in compactness, lightweight, and function for high fuel efficiency, and they use multiple pressure sensors. Pressure sensors are also increasingly used for hydraulic systems, such as for measuring engine oil pressure (1 to 3 MPa). In this way, the demand for high-pressure sensors has thus been rapidly expanding.

2.2 Installation environments of automotive pressure sensors

In recent years, high-density mounting has been increasingly utilized as engines are downsized to achieve better fuel efficiency for automobiles. As a result, pressure sensors are required to ensure high-precision high-temperature operation and electromagnetic compatibility (EMC), that is, having durability in electromagnetic noise generated by other electronic devices. Furthermore, depending on their application, they also need to have high-pressure resistance, corrosion resistance and electrification characteristics.

3 Overview of 6.5th-Generation Automotive High-Pressure Sensors

Our 6.5-generation automotive high-pressure sensors have the structure shown in Fig. 3 in order to ac-

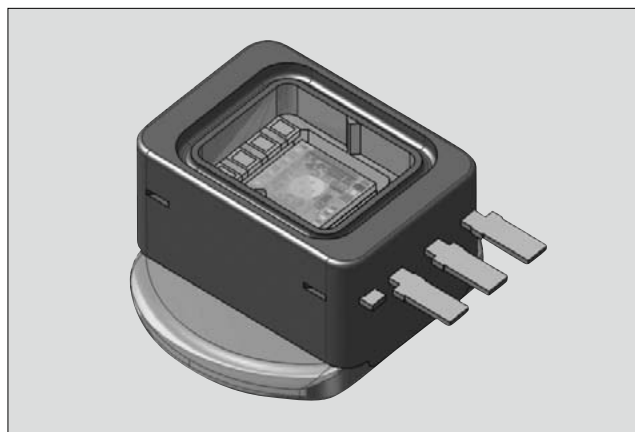


Fig.3 Automotive high-pressure sensor

commodate use in high-pressure and high-temperature environments.

In particular, these sensors have the feature of integrating a package that utilizes a metal base and ensures high pressure resistance with a sensor chip that guarantees operation and accuracy even when high temperatures and high pressures are applied.

3.1 High pressure resistant package with metal base

The package for low-pressure pressure sensors is characterized by integrally molding the lead frame for electrically connecting the sensor chip with a poly-phenylene sulfide (PPS) resin. However, the pressure resistant strength of the PPS resin itself is insufficient when applied with a high pressure. In order to solve this problem with respect to automotive high-pressure sensors, a metal base is used for the section where pressure is applied in order to improve pressure resistance of the entire sensor structure. Figure 4 shows the high-pressure sensor structure and mounting state schematically. The drawing shows the parts subjected to pressure when pressure is applied (area A_0 , A_s) and

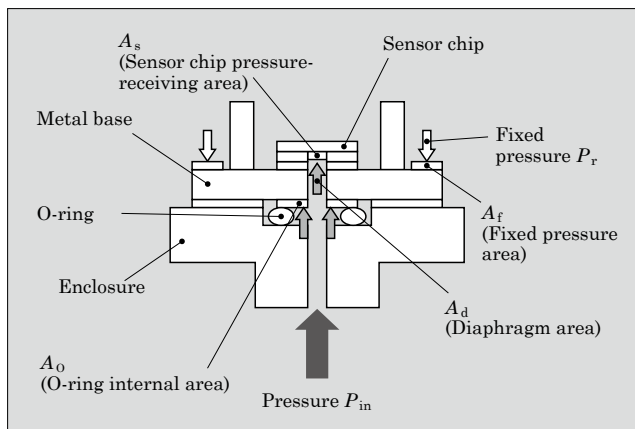


Fig.4 Schematic diagram of the high-pressure sensor and its mounted state

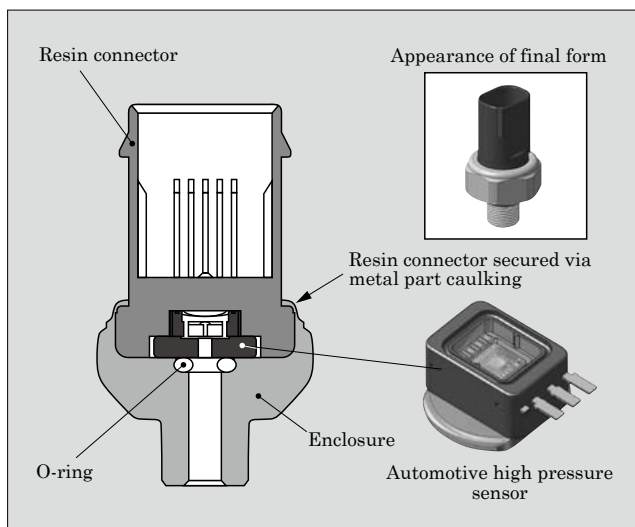


Fig.5 High-pressure sensor mounting example

the part with the counteracting reactive force (area A_f). Figure 5 shows an example of mounting the high-pressure sensor. The enclosure shown here represents the side to which the high-pressure sensor is mounted. The high-pressure sensor is secured by the enclosure and a fixture inserted from the top. Airtightness is ensured by an O-ring inserted between the enclosure and the high-pressure sensor.

Since the high-pressure sensor is secured with the help of the reactive force from the fixture, the relationship between the applied pressure and fixed load can be expressed by the following equation.

(1) Applied pressure and fixed load

$$F = P_{in} \cdot (A_0 + A_s) = P_r \cdot A_f \dots \dots \dots (1)$$

F : Fixed load

P_{in} : Applied pressure

A_0 : O-ring internal area

A_s : Sensor chip pressure-receiving area

P_r : Fixed pressure

A_f : Fixed pressure area

By rearranging Equation 1, fixed pressure can be expressed as $P_r = P_{in} \cdot (A_0 + A_s) / A_f$. However, in the actual structure, $(A_0 + A_s) / A_f$ is extremely small, and this means that fixed pressure P_r can be reduced and the size of the high-pressure sensor miniaturized, thereby contributing to the miniaturization of the entire structure.

In addition, the mechanical strength required for each member (adhesive between sensor chip and metal base, and the metal base itself) when the applied pressure P_{in} is generated can be expressed by the following equation that takes into consideration respective stress balances.

(2) Structural design for the applied pressure

$$P_{in} \cdot (A_d + A_s) < \sigma_m \cdot A_f \dots \dots \dots (2)$$

P_{in} : Pressure

A_d : Diaphragm area

A_s : Sensor chip adhesive area

σ_m : Metal base elastic limit stress

A_f : Fixed pressure area

$$P_{in} \cdot A_d < \sigma_s \cdot A_s \dots \dots \dots (3)$$

P_{in} : Pressure

A_d : Diaphragm area

σ_s : Bonded member breaking stress (i.e., the adhesive)

A_s : Sensor chip adhesive area

Since the temperature environment for automobiles ranges widely from -40 to $+150^\circ\text{C}$, it is necessary to employ a design that takes into consideration the stress generated by differences in the thermal expansion coefficients of each member. In particular, the selection of the adhesive and metal base materials is important with regard to the stress generated between the sensor chip and the metal base.

We created an FEM analysis model during the

package design stage for the high-pressure sensor. In particular, we analyzed the deformation and stress distribution when applying pressure P_{in} , as well as the thermal stress deformation and stress distribution at the time of temperature change. Figure 6 shows the FEM analysis model diagram, and Fig. 7, the FEM analysis results. The material and structural dimensions of each member were determined on the basis of the results of this calculation.

3.2 Sensor chip for high-temperature operation

Fuji Electric has developed pressure sensor chips that incorporate high-precision technology on the basis of the principle “All in one chip” that combines all features such as pressure detection, characteristic compensation, signal processing, protection circuit, failure diagnosis and EMC protection.

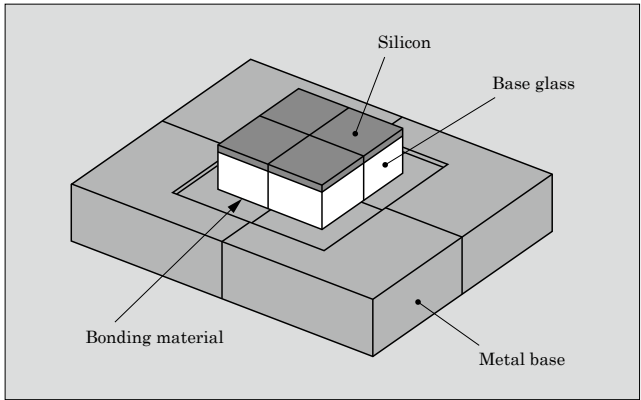


Fig.6 FEM analysis model diagram

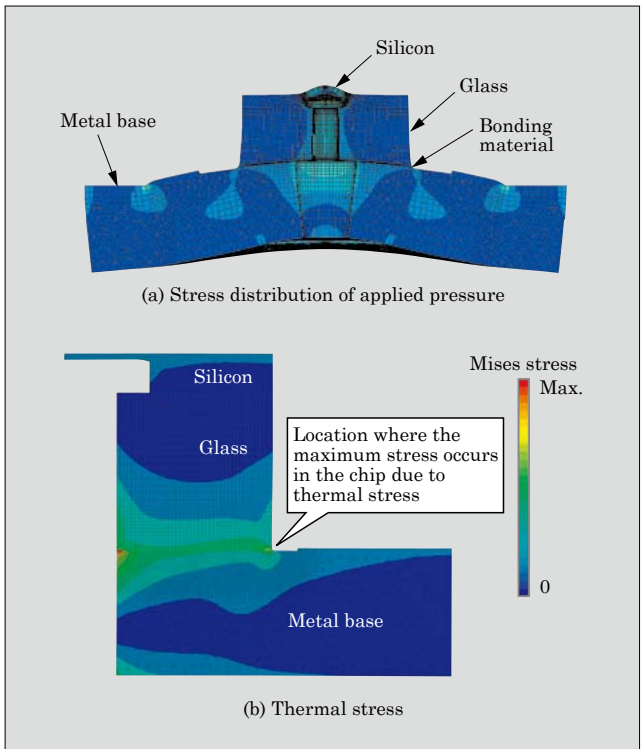


Fig.7 FEM analysis results

The basic operation of the pressure sensor chip is shown below. The diaphragm, which is formed by processing a portion of silicon into a thin film using Fuji Electric’s proprietary etching technology, will deform in response to applied pressure. At such a time, there are changes in each of the resistance values of the 4 piezoelectric resistors, which are composed of the diffusion wiring arranged on the diaphragm. The balance of the Wheatstone bridge circuit composed of the piezoelectric resistors is lost, resulting in a potential difference in the output. By amplifying and outputting this potential difference, the applied pressure is converted into an electrical signal. Figure 8 shows an overview of the pressure sensor chip.

In order to reduce the size of conventionally mass-produced 5th-generation automotive high-pressure sensors and increase the guaranteed operating temperature to 150°C, we have recently developed a chip for 6.5th-generation automotive high-pressure sensors. Figure 9 shows the external appearance of the chip for the 6.5th-generation pressure sensor and 5th-generation pressure sensor.

The chip uses the technologies of CP processing and circuit miniaturizing developed for the 6th-

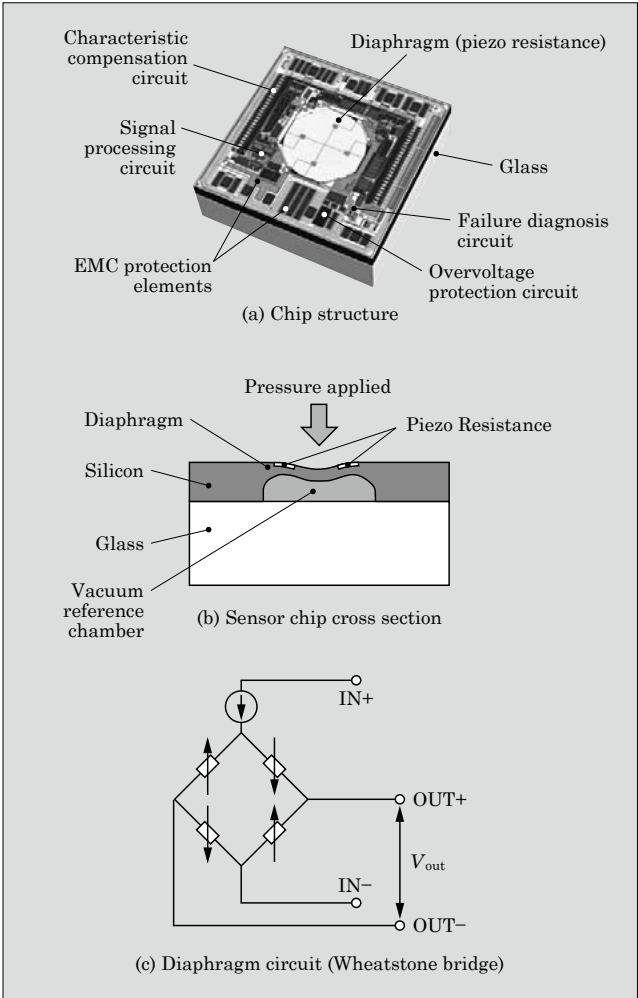


Fig.8 Overview of the pressure sensor chip

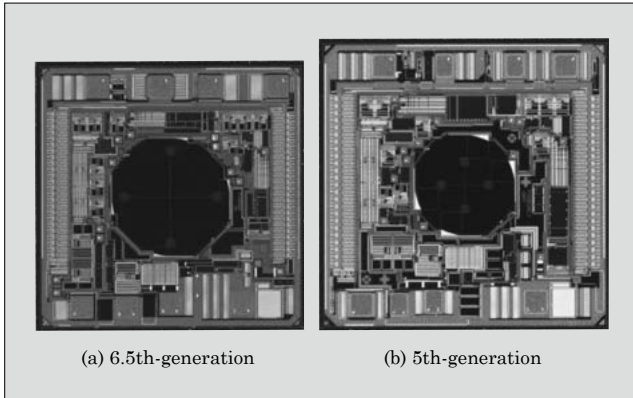


Fig.9 Pressure sensor chip appearance

generation pressure sensors. As a result, it is 14% smaller than the 5th-generation chip (area ratio). Furthermore, the linearity of the output characteristic is improved by optimizing the diaphragm diameter and thickness and the gauge resistors position. Moreover, by optimizing the temperature characteristics of each circuit block shown in Fig. 10, characteristic degradation in the high-temperature operating region is suppressed and accuracy was ensured at 150°C (see Fig. 11).

Figure 12 shows the pressure-output characteristic diagram for the product. By setting the output of the sensor to the diagnostic voltage region when the wire harness is disconnected, it becomes possible for the higher-level system to detect failures. On the other

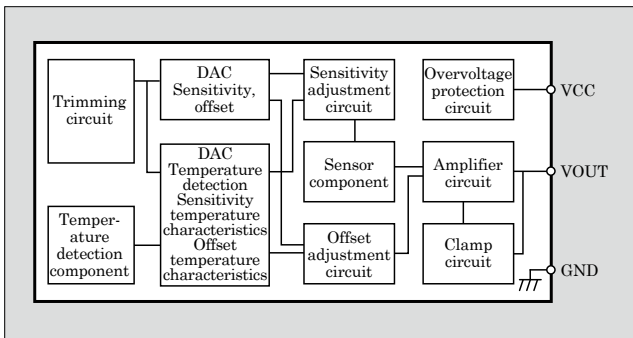


Fig.10 Circuit block diagram for the 6.5th-generation automotive pressure sensor

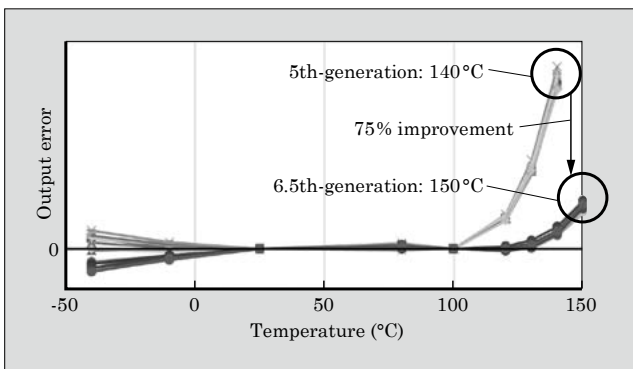


Fig.11 Output error temperature characteristic

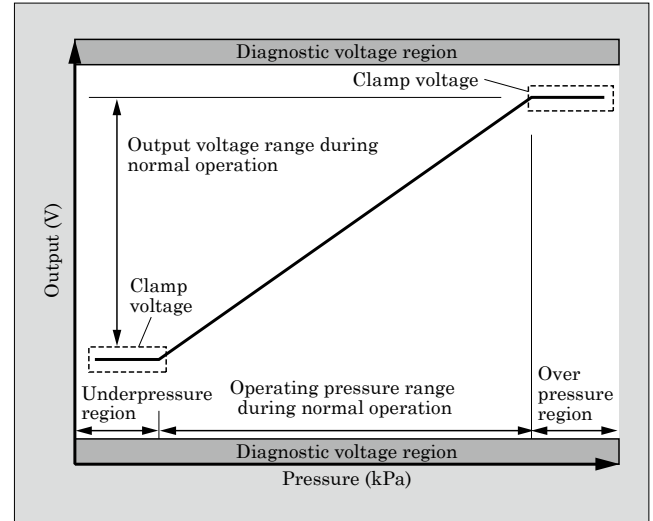


Fig.12 Pressure-output characteristic diagram for the 6.5th-generation automotive pressure sensor

hand, when too much or too little pressure is applied, the output may reach the diagnostic voltage region and lead to erroneous detection. However, this product is able to prevent erroneous detection because it comes with an output voltage clamping circuit and is able to reliably dissociate the diagnostic voltage region and normal output voltage range⁽²⁾.

Table 1 shows the specifications for the 6.5th-generation automotive high-pressure sensor.

Table 1 Specifications of the 6.5th-generation automotive high-pressure sensor

Item	Specifications
Product size (resin section)	W7.5 × H10.0 × D5.6 (mm)
Operating temperature range	-40 to +150 °C
Operating pressure range (engine oil pressure)	0 to 1 MPa
Rated pressure	Pressure range × 3
Power supply voltage	5 ± 0.25 V
Output voltage (at power supply voltage of 5 V)	0.5 to 4.5 V
Sink/source capability	Sink 1 mA, source 0.1 mA
Clamp function	Clamp voltage 0.35 V/4.65 V (typ.)
Pressure direction	Pressurized from back
ESD (external interface terminal)	
MM (0 Ω, 200 pF)	±1 kV or higher
HBM (1.5 Ω, 100 pF)	±8 kV or higher
Transient voltage surge	ISO 7637 (2011) standard Pulse1, 2, 3a, 3b Clears LEVEL-III
Impulse	±1 kV or higher
Latch-up (current injection method)	±500 mA or higher
Overvoltage (VCC-GND)	16.5 V (max.)
Reverse connection (VCC-GND)	0.3 A (max.)

4. Postscript

In this paper, we introduced our 6.5th-generation automotive high-pressure sensor. In the future, we plan to further expand its application range to include other types of high-pressure applications (up to 4 MPa) in addition to engine oil pressure applications. As product development expands throughout the world, it is expected that pressure sensors will be increasingly required to meet harsh demands regarding enhanced product performance from the standpoint of better

fuel efficiency and compliance with environmental and safety regulations. In this regard, we will continue to work hard to develop the products needed by the market in order to meet the requirements of the market.

References

- (1) Nishikawa, M. et al. 6th Generation Small Pressure Sensor. FUJI ELECTRIC REVIEW. 2011, vol.57, no.3, p.103-107.
- (2) Uzawa, R. et al. 6.5th-Generation Automotive Pressure Sensors. FUJI ELECTRIC REVIEW. 2017, vol.63, no.4, p.232-236.



“UPS7000HX Series” and “UPS6000DX Series,” Using Lithium Ion Batteries

YASUMOTO, Koji* KITANO, Akihiro* GOTO, Mizuho*

ABSTRACT

There has been increasing demand for large-capacity uninterruptible power systems (UPSs) for data centers and other facilities that require a stable supply of power. Fuji Electric has developed a large-capacity UPS system that uses lithium-ion batteries (LIBs). The system employs highly reliable LIBs manufacturing by Samsung SDI and comes equipped with a battery management system that ensures the safe operation. The LIBs, having a life expectancy of 15 years, will be used without replacement during the entire life of the UPS main body. The installation space of the LIB is only 53% that of a lead-acid battery, achieving space saving.

1. Introduction

The development of the information age has brought about increased demand for large-capacity uninterruptible power systems (UPS) that provide a stable supply of power. The data center field in Japan is expected to further grow because of the need for new types of data processing, such as cognitive computing^{*1}, AI and the Internet of Things (IoT), in addition to expanded use of cloud services. In such circumstances, UPS systems are required to operate stably and efficiently and need to be installed in smaller spaces.

Lead storage batteries have been conventionally used as the backup power supply of UPS systems. These lead storage batteries are low-cost and have high reliability. However, they have the disadvantages of being heavy and large and having a low energy density. Lithium ion batteries (LIB), which are superior to lead storage batteries, provide high energy density, high voltage, and small size, and they are used in many industrial products. The application of LIBs has been expanded mostly to mobile devices, and they are also being rapidly used for electric vehicles and power storage facilities. However, LIBs are not being used for large-capacity UPS systems that much. This is because UPS systems are installed in the electric room of buildings. An LIB uses electrolytes having fire risks

like petroleum. Facilities that store or handle a large amount of LIBs need to take certain measures as dangerous facilities in accordance with the Fire Services Act.

Fuji Electric has employed Samsung SDI's LIB that can be expected to save space on large capacity UPSs such as the “UPS7000HX Series” and “UPS6000DX Series.”

2. Outline of UPS

2.1 Specifications of the UPSs and LIB

Figure 1 shows the appearance of the “UPS7000 HX-T3,” which uses lithium ion batteries, and the LIB unit (one rack), and Table 1 shows the specifications of the “UPS7000HX-T3” and “UPS6000DX-T3.”⁽¹⁾ Table 2 shows the specifications of the LIB unit, and Fig. 2 shows the connection diagram of the UPS system and the LIB unit. One rack of the LIB unit has one series

*1: Cognitive computing: A system that causes computers to not only process instructions given from humans but also thinks and learns like humans to present materials that help human decision-making.

* Power Electronics Systems Business Group, Fuji Electric Co., Ltd.

* Samsung SDI Japan Co., Ltd.

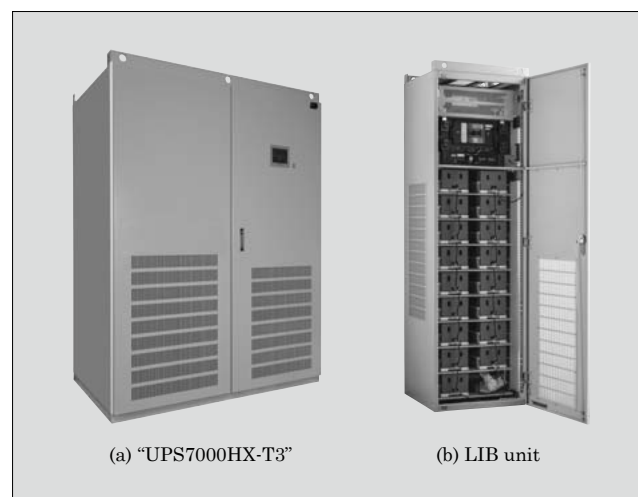


Fig.1 Appearance of “UPS7000HX-T3” and LIB unit

Table 1 Specifications of “UPS7000HX-T3” and “UPS6000DX-T3”

Item		UPS7000HX-T3	UPS6000DX-T3
AC input	Circuit system	UPS double conversion	
	Rated voltage	415/420 V (440 V)	200/210 V
	Input power factor	0.99 (delay) or more	
	Rated frequency	50/60 Hz	
	Harmonic current (total)	5% or below	
Bypass input	Rated voltage	415/420 V (440 V)	200/208/210 V (220/230/380/400/415/420/440 V)
	Voltage range	±10%	
	Rated frequency	50/60 Hz	
Inverter output	Rated output apparent power	500 kVA	100/150/200/250/300 kVA
	Rated output active power	500 kW	100/150/200/250/300 kW
	Rated power factor	1.0	
	Rated voltage	415/420 V (440 V)	200/208/210 V (220/230/380/400/415/420/440 V)
	Voltage distortion factor (100% linear load)	2% or below	
	Voltage distortion factor (100% rectifier load)	5% or below	
	Voltage accuracy	Within ±1%	
	Transient voltage fluctuation	3% or below (at 100% sudden load change)	4% or below (at 100% sudden load change)
		2% or below (at 10% sudden input voltage change)	
		2% or below (at AC input blackout and restoration)	1% or below (at AC input blackout and restoration)
		5% or below (when switched from bypass to UPS)	
	Settling time	50 ms	
	Overload capacity	125% × 10 min, 150% × 1 min	
	Frequency accuracy	±0.01% (at internal oscillation)	
	External synchronous frequency range	50/60 Hz ± 5%	

circuit having a predetermined voltage and capacity. Components are installed in the order of a conductor for parallel connections, switchgear, a switching-mode power supply (SMPS) assembly, and battery modules from the upper shelf. The battery management system (BMS) monitoring these components consists of a system BMS, a rack BMS and module BMSs.

The switchgear includes a protection circuit and a rack BMS. The rack BMS collects all the information related to the rack and monitors the state of all the

Table 2 Specifications of LIB unit per rack

Item	UPS7000HX Series	UPS6000DX Series
Rated cell capacity (1-hour rate)	67 Ah	
Rated cell voltage	3.8 V	
Rated module capacity	2036.8 Wh	
Rated rack capacity	34.6 kWh	24.4 kWh
Number of modules	17 modules	12 modules
Rated rack voltage	516.8 V	364.8 V
Final voltage of rack	435.2 V	307.2 V
Rated discharge current of rack	450 A	
Maximum discharge current of rack*	600 A	
Charge voltage of rack	571.2 V	403.2 V
Charge current of rack	22.3 A	
Temperature	23 ± 5 °C	
Dimensions	W700 × D700 × H2,350 (mm)	W700 × D700 × H1,900 (mm)
Weight	700 kg	600 kg
Electrolyte amount	38.76 L	27.36 L

*Amount of current the battery can produce in 1 second at the time of overload.

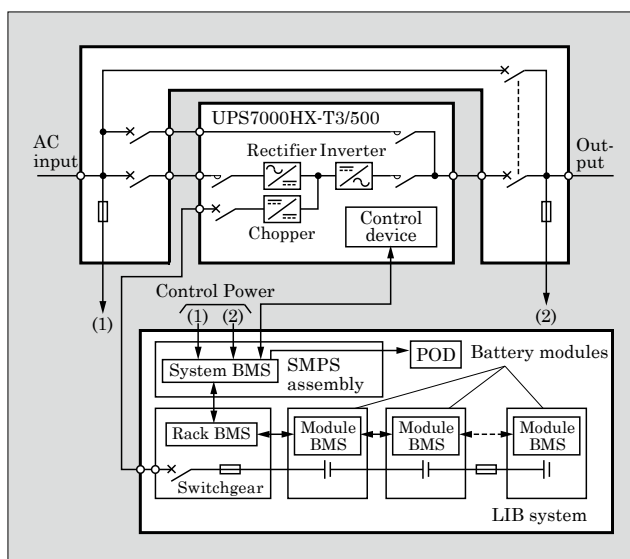


Fig.2 Connection diagram of “UPS7000HX-T3” and LIB unit

modules in the rack. In addition, when an abnormality occurs, it protects the battery system and transmits the rack information to the system BMS, which monitors the rack parallel system.

The SMPS assembly includes a control power supply and a system BMS. The system BMS collects all the information of the rack BMS in the parallel system and transmits the data to the outside via MODBUS*2 communication. The surface of the LIB unit has a liquid crystal display (POD), and the state inside the rack can be monitored. The data can also be stored in an

*2: MODBUS: Trademark or registered trademark of Schneider Automation, Inc.

SD card and used as analysis data.

The battery module has 8 battery cells connected in series. It also has a module BMS inside to monitor the state of the modules. The system measures the cell voltage and the cell temperature and transmits the data to the rack BMS.

The connections between devices, including main circuits and protection circuits, can be performed at the front side, therefore provide good maintainability. The short-circuit protection fuses are in the secondary side of the MCCB (wiring breaker) in the switchgear and in the module section. The control power supply is duplicated and supplied from the input and output of the UPS. The interface with the UPS is only the failure signal of the contact, and the state can be monitored from outside through MODBUS communication.

The rated cell capacity is 67 Ah (1-hour rate), and the rated cell voltage is 3.8 V. The UPS7000HX-T3 includes 17 modules, and the UPS6000DX-T3 includes 12 modules. The rated discharge current per rack is 450 A, and the maximum discharge current is 600 A per second at the time of overload.

The number of racks necessary for the LIB unit is determined by the backup time of the design lifespan (It does not guarantee the life), UPS capacity, load power factor and DC/AC efficiency with the following conditions as standard: an design lifespan of 15 years, ambient temperature of 25 °C, and discharge condition of a 5% discharge 24 times a year and 100% discharge 2 times a year. Regarding the momentary voltage drop in power systems, it has been reported that the annual average number of momentary voltage drops per substation is 2.8 times. In addition, the duration of momentary voltage drops tends to be 6 cycles or below. This result shows the discharge condition has a sufficient margin.

2.2 Safety of LIB

LIBs have risks of fire and bursts caused by an internal temperature increase due to overcharging or short circuits, and an occurrence need to be prevented. Therefore, measures for preventing accidents are taken for each layer of the LIB cell, the LIB module and the LIB system.

The LIB cell has a structure for preventing short circuits between the anode and the cathode and a safety mechanism regarding temperature increases. In addition, the LIB module has a structure that suppresses temperature increase of cells and uses incombustible materials. The LIB system is also protected in 4 stages: at the UPS, the BMS, the rack fuse and the cell. Figure 3 shows the safety protection of the LIB system. To protect the battery system, the UPS monitors charging overvoltage and undervoltage and trips the MCCB when detecting them.

Table 3 shows the battery system protection function of the LIB unit. There are major failures that release the MCCB and disconnect the Lib system from

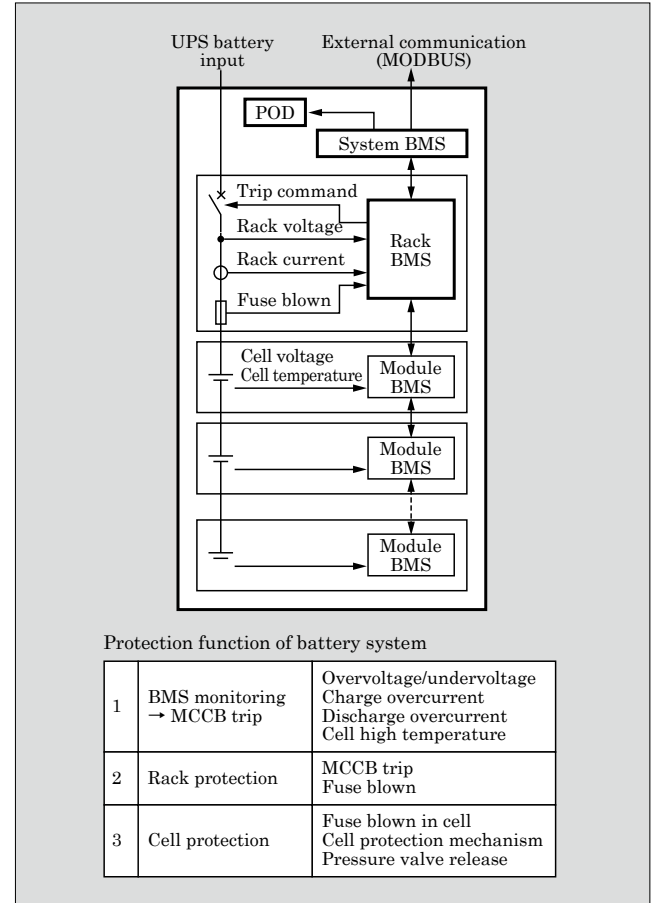


Fig.3 Safety protection of LIB system

Table 3 Protection function of battery system

Item	Major failure	Minor failure
Cell overvoltage	○	—
Cell undervoltage	○	—
Rack overvoltage	○	—
Rack undervoltage	○	—
Voltage imbalance	—	○
Voltage detection sensing error	—	○
High temperature	○	—
Low temperature	—	○
Temperature unbalance	—	○
Charge overcurrent	○	—
Discharge overcurrent	○	—
Communication failure 1	—	○
Communication failure 2	—	○
MCCB failure 1	—	○
MCCB failure 2	—	○
Current detection abnormality	—	○
Fuse blown	—	○

the UPS, and minor failures that only cause an alarm. The major failures include cell overvoltage, cell undervoltage, rack overvoltage, rack undervoltage, high battery cell temperature, charge overcurrent and discharge overcurrent. The minor failure system moni-

tors voltage imbalance, low temperature and temperature unbalance, and monitors abnormality of the systems detecting any voltage sensing error, current detection abnormality, communication abnormality and MCCB abnormality. On the other hand, the battery system is protected from short circuit by the fuse in the rack. Furthermore, the cell unit, provided with several protection mechanisms, disconnects abnormal cells from the circuit at the time of overcharging and overheating. The mechanism that lowers the cell's internal pressure (safety valve) operates as a final protection. These protection systems allow safe use.

2.3 Maintenance service

The number of racks is determined with the design lifespan of LIBs as 15 years, but we also provide a capacity guarantee service of 15 years in accordance with the lifespan of the UPS systems. To get the capacity guarantee of 15 years, it is essential that the actual ambient temperature and the discharge conditions meet the specifications. The depth and number of times of discharge has a sufficient margin in comparison with the actual normal blackout, and LIBs are unlikely to be used under the condition exceeding the set discharge conditions. On the other hand, the ambient temperature may change depending on the installation location and arrangement and setting temperature of air conditioners; therefore, temperature monitoring is vitally important. In the case of the capacity guarantee of 15 years, it is necessary to periodically replace the switchgear, SMPS assembly and fuses. Fuji Electric is responsible for performing the maintenance service.

The deterioration of the capacity can be checked by analyzing the data in the BMS.

3. Characteristics of Employed LIB Manufactured by Samsung SDI Co., Ltd

The applications of LIBs and materials of positive electrodes, negative electrodes and electrolytes of LIBs differ by manufacturers. The employed LIB manufactured by Samsung SDI Co., Ltd. consists of a positive electrode made of lithium manganese oxide, which is a composite oxide of lithium transition metal, a graphite negative electrode, and an electrolyte made of a water-insoluble organic solvent. To be used for UPSs, LIBs are required to have high voltage, high energy density and a high discharge rate. The employed LIB has a cell voltage of 3.8 V and an energy density of 135 Wh/kg, which are higher than those of other LIBs, contributing space saving. The LIB also has a rated capacity of 67 Ah and discharge rate^{*3} of 6C or more, and its 3 to 4 parallel connection system is sufficient for a UPS having a single-unit capacity of 500 kVA. Thus, it is suitable for UPS applications.

The LIBs manufactured by Samsung SDI Co., Ltd are widely used and it has a top share in the usage for automobiles and cellular phones in the global market.

They were quickly used for UPS applications also and have been widely used in Asian countries including South Korea since 2011. The LIBs are also low-cost when compared with lead batteries in terms of the life cycle cost of a 15-year design lifespan of UPS systems. Thus, judging comprehensively, we use the LIB manufactured by Samsung SDI Co., Ltd having a performance suitable for UPS applications, abundant track records, and cost advantages.

4. Advantages and Disadvantages

The following refers to the advantages and disadvantages of LIBs and high-rate discharge lead storage batteries, which have been conventionally used, for UPSs.

4.1 Comparison of battery characteristics

The design lifespan of lead storage batteries is 7 to 9 years. In contrast, LIBs can be used for 15 years and can be replaced at the same time of UPS system replacement. When the capacity of lead storage batteries goes below 80%, the capacity starts to decrease rapidly; therefore, the period for replacing the battery needs to be determined appropriately. However, the capacity of LIBs decreases approximately constantly during the lifetime, and the period for replacing the battery can be determined easily beforehand. LIBs also have good capacity decrease characteristics with respect to temperature. Lead storage batteries follow the Arrhenius' law, and the capacity becomes 50% when the temperature increases by 10°C. In contrast, when the temperature increases by 10°C, the capacity of LIBs after 15 years decreases by approximately 10%.

Another significant advantage of using an LIB for UPS is that the discharge capacity that can be taken out is stable. Regarding lead storage batteries, the capacity that can be taken out decreases as the discharge current increases. The capacity that can be taken out also decreases as the temperature decreases. Furthermore, when the discharge current is small, management of final voltage and slow discharge becomes necessary. On the other hand, a capacity decrease due to the difference in discharge current and ambient temperature for LIBs is low.

The disadvantage of LIBs is that the maximum discharge current is lower than that of lead storage batteries. The high-rate discharge lead storage batteries for UPS can supply a large current such as 1.2 C/5 sec. Meanwhile, the maximum discharge current of

^{*3}: Discharge rate: Discharge rate (C rate) = discharge current (A) / battery capacity (Ah). For example, when the capacity is 67 Ah (1-hour rate), the discharge rate of the battery 1 C indicates that the battery discharges for 1 hour at a current of 67 A. Note that C does not indicate a coulomb.

Table 4 Comparison of LIB and high-rate discharge lead storage battery

Items	High-rate discharge lead storage battery	LIB
Capacity	350 Ah (10-hour rate)	201 Ah (1-hour rate)
Design lifespan	7 to 9 years	15 years
Storage unit dimensions	W4,000 × D1,000 × H2,350 (mm)	W2,100 × D700 × H2,350 (mm)
Installation area ratio	100%	53%
Weight	9,600 kg	2,100 kg
Weight ratio	100%	22%

LIBs is 6.7 C.

4.2 Comparison of LIB and high-rate discharge lead storage battery

Table 4 shows the comparison of an LIB and a lead storage battery for high-rate discharge. Conditions during the design lifespan are set as follows: a backup time of 5 minutes, a load capacity of 500 kVA, a power factor of 0.9 and an ambient temperature of 25 °C. The number of discharge times was calculated simulating several times of discharge a year for lead storage batteries and a 5% discharge 24 times a year and 100% discharge 2 times a year for LIBs. As a result, LIBs have a footprint ratio of 53% and a weight ratio of 22%, and can save the space needed for an electric room.

5. Safety Measures

The safety standards for LIBs are established in the IEC standards, JIS, and the Electrical Appliance and Material Safety Act. In addition, the UN Recommendations on the Transport of Dangerous Goods stipulates the safety of land, sea and air transportation. In December 2011, “Examination report on the approach to safety measures concerning lithium ion batteries in dangerous facilities” was issued by the Dangerous Goods Safety Office of the Fire and Disaster Management Agency of the Ministry of Internal Affairs and Communications. To reexamine the fire risks, LIBs were demonstrated and tested for the report in terms of 3 items: the fire risks before and after sealing, safety measures for storage batteries, and safety during storage. On the basis of the result, the approach to safety measures for dangerous facilities that store or handle the LIBs are formulated.

5.1 UN Recommendations on the Transport of Dangerous Goods (UN3480)

The LIBs have passed the safety tests related to battery modules that are specified in UN3480, which are altitude simulation test T1, temperature test T2, vibration test T3, impact test T4 and external short-circuit test T5. In Japan, the LIBs are transported in storage cases that meet a UN standard and the battery

modules are installed in the rack on site to stabilize quality.

5.2 IEC standards and JIS

Samsung SDI Co., Ltd has been certified as meeting the international standard IEC 62619 for battery cells, battery modules, and BMS. The test items, conditions and judgment method of JIS C 8715-2, the “Secondary Lithium Cells and Batteries for Use in Industrial Applications,” established in 2012 are equivalent to the ones of IEC 62619 as shown in Table 5. Thus, the products conform to JIS C 8715-2. The product is determined to be conforming if it satisfies either of the thermal runaway resistance test and the fire spread resistance test.

Further, it is particularly important to prevent contamination by foreign substances during a cell process. An internal short-circuit test assuming contamination by foreign substances is specified. In the internal short-circuit resistance test, a charged single cell is disassembled, and a nickel piece is placed between the separator and the positive electrode active material at the outermost periphery or between the separator and the negative electrode active material. The test piece is then verified whether the initial voltage drops by 50 mV or more while being pressurized in a pressurizing device. In this test, Samsung SDI Co., Ltd has confirmed that it does not drop voltage and does not cause internal short circuit even when pressurizing up to 400 N.

5.3 Electrical Appliances and Materials Safety Act

In 2008, the Order for Enforcement of the Electrical Appliances and Materials Safety Act was revised, and LIBs that meet certain requirements came to be subject to the Electrical Appliances and Materials Safety Act. This standard has the same test items as IEC 62133 (JIS C 8712 stipulates similar safety standards as IEC 62133) and JIS C 8714 have. The volume density of the LIB per cell is 261 Wh/L, which is

Table 5 Comparison of JIS C 8715-2 and IEC 62619

Applicable	JIS C 8715-2	IEC 62619
Cell	External short-circuit test	External short-circuit test
	Impact test	Impact test
	Drop test	Drop test
	Thermal abuse test	Thermal abuse test
	Overcharge test	Overcharge test
	Forced discharge test	Forced discharge test
	Thermal runaway resistance test	Internal short-circuit
System	Fire spread resistance test	—
	Overcharge control of voltage	Overcharge control of voltage
	Overcharge control of current	Overcharge control of current
	Overheating control	Overheating control

smaller than 400 Wh/L, and the LIB is not subject to this Act.

5.4 Handling of LIB under the current Fire Services Act

The electrolytes of LIBs correspond to water-insoluble substances that fall into dangerous goods class IV second oil division, and the quantity is specified to be 1,000 L. The electrolytes also need to conform to the technical standards of dangerous materials stipulated in the government ordinance. For dangerous materials of less than specified quantity, storing or handling must follow the fire prevention ordinance of each municipality.

5.5 Safety measures for dangerous facilities that store or handle LIBs

The safety measures related to the storage and handling of storage batteries are stipulated as follows on the basis of the fact that the fire risk is greatly reduced by the UN Recommendations on the Transport of Dangerous Goods, the Electrical Appliances and Materials Safety Act, IEC standards and JIS, and certain knowledge has been obtained by experiments.

When a storage battery meets the following (1) to (2), it is not necessary to take the following measures:

- (1) Impact test (limited to storage batteries that are not subject to the Electrical Appliance and Material Safety Act) specified in T4 of the United Nations Recommendation (UN 3480) 38.3,

Or, safety is secured against the external burden by crushing test prescribed in the Electrical Appliance and Material Safety Act.

- (2) In case of leakage or flammable vapors are not confirmed from the inside of the storage battery in the drop test from the height of 3 m.

The LIB is conforming because it passed the recommendation of the United Nations and the 3-m drop test. Therefore, the LIB does not have to meet the following requirement for dangerous facilities or the small-amount dangerous facilities that store or handle liquid dangerous materials.

- (a) The electrical equipment shall have an explosion-proof construction.
- (b) Floors shall have structure that doesn't allow hazardous substances to permeate, and the floor shall be inclined and fitted with a collection drain (a catch-basin).
- (c) Equipment shall be installed for discharging

flammable vapor and particulates outside from a high position.

5.6 Regulation on storage of dangerous materials according to use districts

For buildings that store and process dangerous materials, the Building Standards Act stipulates "unit regulation" associated with securing fire prevention safety of the building itself and "use regulation" associated with geographical conditions. The City Planning Act and the Building Standards Act are provided with a use district designation system for creating a good urban environment and securing functional urban activities by appropriately arranging residential, commercial and industrial districts in the city. This system determines land use as a general framework of residential, commercial and industrial urban areas. The use districts are classified into 12 types, and a restriction is imposed for each use district. The LIB corresponds to dangerous materials to be subject to the use regulation, and it is necessary to keep the restricted amount of storage in accordance with the use district. According to this, it is permitted to store 50 times the specified quantity in quasi-industrial districts, 10 times the specified quantity in commercial districts, and 5 times the specified quantity in quasi-residential districts.

The general LIB capacity of the UPS7000HX Series and the UPS6000DX Series is below the above restricted amount of storage, and the products are not subject to the regulation.

6. Postscript

The "UPS7000HX Series" and "UPS6000DX Series" having lithium ion batteries have been described. The UPS conform to safety standards and regulations related to dangerous material storage. Thus, we would like to offer these UPSs to data centers to contribute to their space saving. We will be expanding the applications to overseas projects and medium-capacity UPSs of 100 kVA or lower.

References

- (1) Yamagata, Y. et al. "UPS 7000HX Series" of High-Efficiency, Large-Capacity UPS Products Using AT-NPC 3-Level for Data Centers. FUJI ELECTRIC REVIEW. 2012, vol.58, no.4, p.207-211.

“XS Series” 650-V Discrete IGBTs

HARA, Yukihiro*

Global energy demand is increasing steadily and further energy conservation is called for.

In this situation, there is a strong demand for switching devices with a lower loss in order to improve the efficiency of uninterruptible power systems (UPSs) for equipment requiring high-quality power and power conditioning systems (PCSs) that convert direct current power generated by photovoltaic systems into alternating-current power.

Fuji Electric has developed and launched the “XS Series” 650-V discrete IGBTs as a product line that improves the on-state voltage and switching loss trade-off characteristic to improve the efficiency of UPSs and PCSs.

1. Features

Figure 1 shows the appearance of the XS Series and Table 1 the line-up. The major features are as follows:

- (a) Recommended drive frequency $f_{sw} = 10$ to 50 kHz
- (b) On-state voltage $V_{CE(sat)} = 1.5$ V ($T_{vj} = 125^\circ\text{C}$)
- (c) Turn-off loss $E_{off} = 0.86$ mJ ($T_{vj} = 125^\circ\text{C}$, turn-off $dv/dt = 10$ kV/ μs)

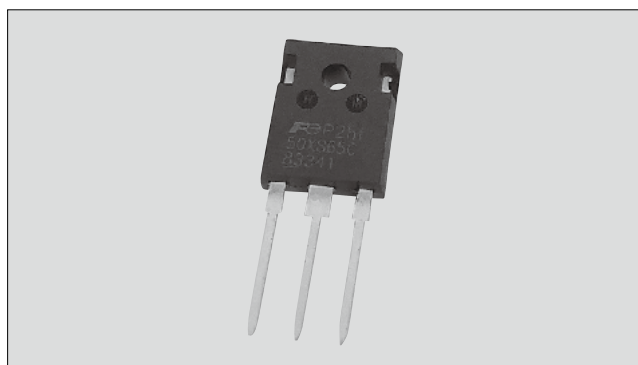


Fig.1 “XS Series” (TO-247 package)

2. Chip Technology

This product is based on the insulated gate bipolar transistor (IGBT) and free wheeling diode (FWD) chip technologies of the 7th-generation “X Series,” and it has the optimum design for discrete products used at f_{sw} of 10 to 50 kHz.

The IGBT uses the miniaturization and thin-wafer technologies of the 7th-generation chip technology as the basis and has a surface structure optimized for discrete applications and $V_{CE(sat)}$ reduced. The collector layer features hole injection control to decrease the switching loss. This has achieved a significant improvement in the trade-off characteristic from that of the conventional products with a 0.5-V reduction in $V_{CE(sat)}$ and an approximately 20% reduction in E_{off} , as shown in Fig. 2.

The FWD has also improved the V_F and E_{Tr} trade-off characteristic by making use of the thin wafer and lifetime optimization technologies of the 7th-generation chip technology as shown in Fig. 3. It also achieved a low surge voltage with a soft recovery characteristics and a reduction of V_F by approximately

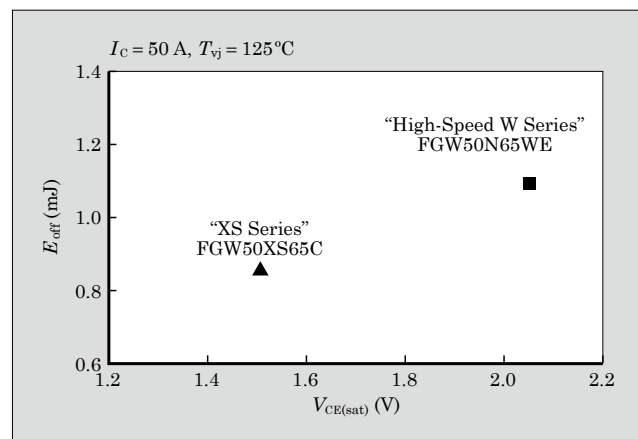


Fig.2 Trade-off characteristic (IGBTs)

Table 1 “XS Series” line-up

V_{CE}	Package	I_C ($T_c = 100^\circ\text{C}$)				Built-in FWD
		30 A	40 A	50 A	75 A	
650 V	TO-247	FGW30XS65	FGW40XS65	FGW50XS65	FGW75XS65	None
		FGW30XS65C	FGW40XS65C	FGW50XS65C	FGW75XS65C	Provided
	TO-247-4L	—	—	—	FGZ75XS65C	Provided

* Electronic Devices Business Group, Fuji Electric Co., Ltd.

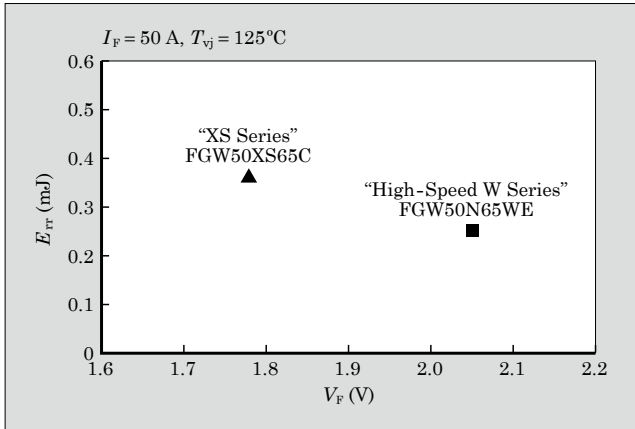


Fig.3 Trade-off characteristic (FWDs)

0.3 V from conventional products.

3. Package

As with conventional products, the industry standard TO-247 package has been employed. For the solder to connect between the chip and lead frame, lead-free solder is used, which conforms to the RoHS Directive*1 (EU2011/65/EU).

4. Effect of Application

UPSs and PCSs of a few kilovolt-amperes to 50 kVA often use discrete IGBTs to compose the inverter circuits with 3-level inverters (I-type and T-type) shown in Fig. 4.

Figure 5 shows the calculation result of the generated loss in the discrete IGBT of the I-type 3-level inverter. As compared with the "High-Speed W Series," a conventional product line, the XS Series has the loss reduced on the outside (T1 and T4) and the inside (T2 and T3) by improving the $V_{CE(sat)}$ and E_{off} trade-off characteristic.

Figure 6 shows the result of calculating the gener-

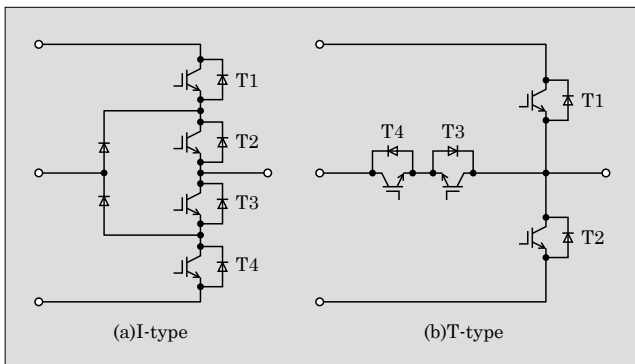


Fig.4 3-level inverter (I-type and T-type)

*1: RoHS Directive: A European Union (EU) directive on the restriction of the use of certain hazardous substances in electrical and electronic equipment

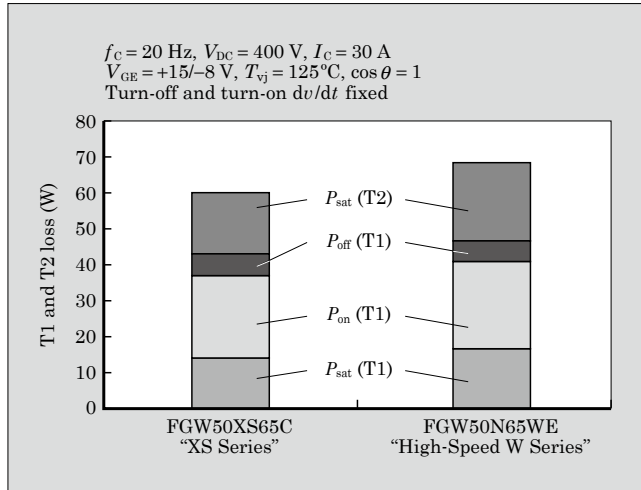


Fig.5 Device loss (3-level inverter I-type)

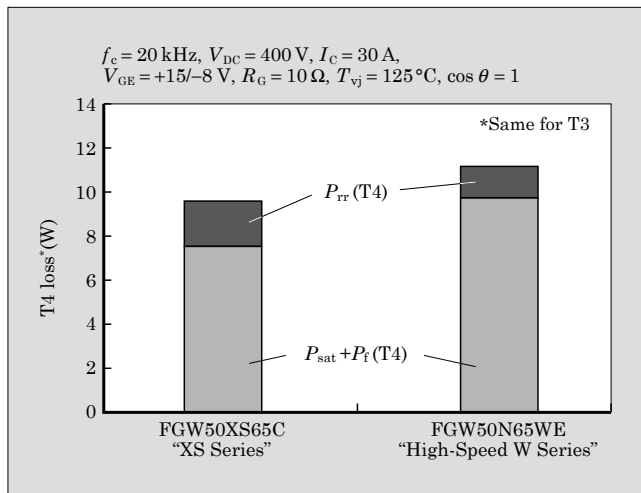


Fig.6 Device loss (3-level inverter T-type)

ated loss in the IGBT and FWD in the AC switch (T3 and T4) of a T-type 3-level inverter. The loss generated in the devices of the AC switch is composed of the conduction loss of the IGBT and FWD and the recovery loss of the FWD. As compared with the High-Speed W Series, the XS Series has a lower on-state voltage of the IGBT and FWD and features lower loss with the T-type as well.

Launch time

September 2018

Product Inquiries

Sales Department I, Sales Division,
Electronic Devices Business Group,
Fuji Electric Co., Ltd.
Tel: +81 (3) 5435-7152

7th-Generation “X Series” RC-IGBT Module “Small-2B”

TAKASAKI, Aiko* YAMANO, Akio* ICHIKAWA, Hiroaki*

Recently, as a solution to the energy resource depletion and global warming issues, expectations are rising for power electronics technology that contributes to the efficient use of energy. Above all, demand is increasing for insulated gate bipolar transistor (IGBT) modules, which are major components of power conversion equipment used in a wide range of fields including the industrial, consumer, automobile and renewable energy ones. A lowered power dissipation and improved reliability are strongly required of these IGBT modules. To make equipment smaller, there is also high demand for increasing the output current while maintaining the same package size as conventional products. However, increasing the output current of an IGBT module causes the operation temperature of IGBT and free wheeling diode (FWD) to rise, possibly leading to lower reliability. Accordingly, it is essential to have technological innovation for achieving both high output and high reliability.

Fuji Electric has developed the 7th-generation “X Series” semiconductor chips and packages to commercialize high-reliability IGBT modules. For this series, Fuji Electric has newly developed a reverse-conducting IGBT (RC-IGBT).

This RC-IGBT has the conventional IGBT and FWD functions integrated into one chip, as is shown in Fig. 1, making the chip area per rated current smaller. This has made it possible to mount more chips, which has resulted in a larger output as compared with conventional products that use the same package.

This paper describes the “Small-2B,” an RC-IGBT

module integrating this RC-IGBT chip.

1. Technologies Applied

1.1 Chip technology

The X Series IGBTs have the collector-emitter saturation voltage $V_{CE(sat)}$ significantly reduced because the surface gate structures have been miniaturized as compared with the “V Series” 6th-generation IGBTs. The products formed into a thin wafer have achieved an improved trade-off relationship between the turn-off loss and $V_{CE(sat)}$. On the other hand, a thin wafer causes a voltage oscillation at turn-off energy and reduces the breakdown voltage in case of without technical considerations. Therefore, we have solved this problem by optimizing the field stop layer, which

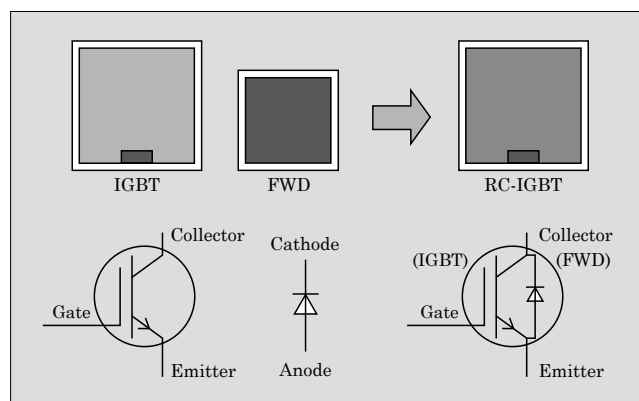


Fig. 1 Schematic drawings of RC-IGBT chips and equivalent circuits

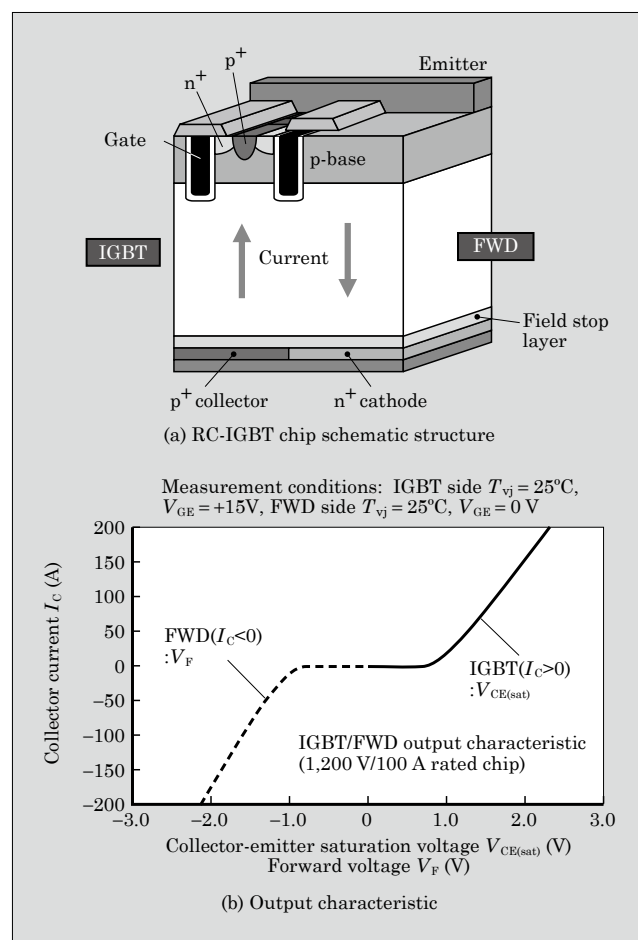


Fig. 2 Cross-sectional view and output characteristic of X Series RC-IGBT chip

* Electronic Devices Business Group, Fuji Electric Co., Ltd.

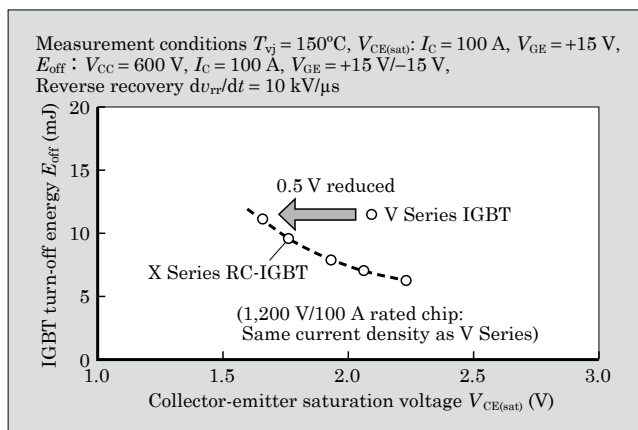


Fig. 3 Trade-off characteristic of X Series RC-IGBT chip

is the voltage withstanding structure on the back side of semiconductor chips.

The following describes the RC-IGBT to which the X Series technology has been applied. Figure 2(a) shows a schematic structure of the X Series RC-IGBT chip and Fig. 2(b) the output characteristic. An RC-IGBT has the structure of both IGBT and FWD in one chip and allows a current to flow in both the forward (solid line) and reverse (dotted line) directions.

As shown in the IGBT turn-off energy and $V_{CE(sat)}$ trade-off characteristic of the X Series RC-IGBT in Fig. 3, $V_{CE(sat)}$ has been reduced by approximately 0.5 V from that of the conventional V Series.

1.2 Package technology

In order to realize a high output current, the X Series IGBT module has increased the guaranteed continuous operating temperature from the conventional 150°C to 175°C . A higher output current increases the current variation arising from load fluctuation. This in turn causes a larger temperature fluctuation and thermal stress variation as well. Therefore, persisting in the conventional structure may cause the aluminum wire bonding on the semiconductor chips and solder under the chips to deteriorate, thus shortening the product life, and may cause lower reliability. The silicone gel filled inside the products for ensuring insulation performance is exposed to high temperature for a long time and the insulation performance may be deteriorated. With the X Series, we have optimized the aluminum wire layout, solder under the chips and silicone gel to solve these problems.

2. Product Line-Up

Table 1 compares the V Series, X Series and X Series RC-IGBT of the “Small-2B” line-up. Up to now, the maximum rated current was 35 A for the V Series and the X Series. The RC-IGBT technology has newly been applied to increase the maximum rated current to 50 A.

Table 1 “Small-2B” line-up comparison

		Rated current (A)			
		15	25	35	50
Small-2B	V Series	V-IGBT + V-FWD			
	X Series	X-IGBT + X-FWD			
Package appearance		(Unit: mm)			

3. “Small-2B” Characteristics

Figure 4 shows the result of calculating power dissipation in an inverter using the X Series RC-IGBT module Small-2B 1,200 V/50 A. As compared with using the V Series IGBT module Small-2B 1,200 V/35 A, power loss of the X Series RC-IGBT module is approximately 15% lower.

Figure 5 shows the result of calculating the IGBT junction temperature against the inverter output cur-

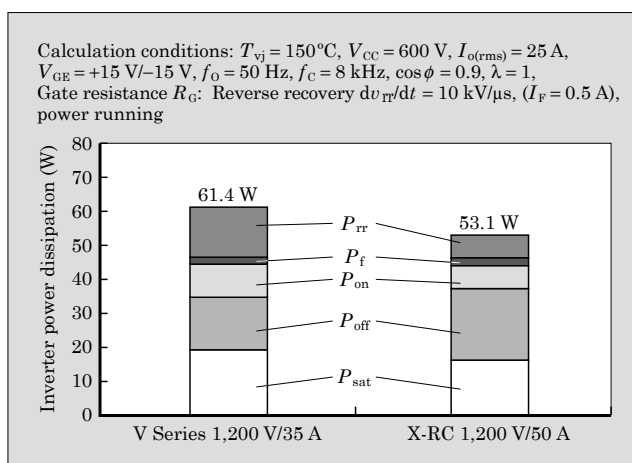


Fig. 4 Result of inverter power loss calculation

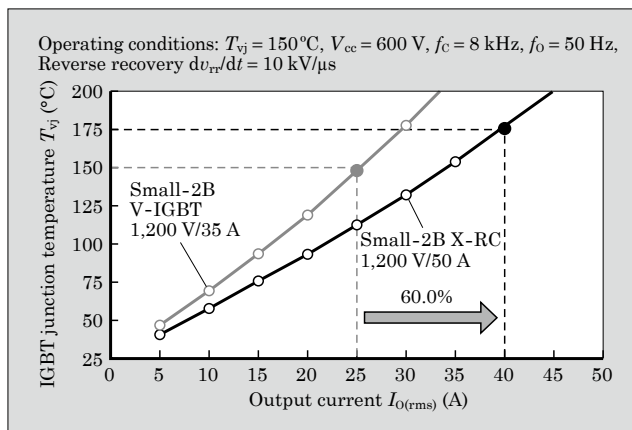


Fig. 5 Relationship between output current and IGBT junction temperature

rent. We have reduced the inverter power dissipation and raised the guaranteed continuous operating temperature from 150°C of the V Series to 175°C of the X Series to successfully achieve a 60% increase in the output current of products with the same package.

Launch time

September 2018

Product Inquiries

Sales Department I, Sales Division,
Electronic Devices Business Group,
Fuji Electric Co., Ltd.
Tel: +81 (3) 5435-7152



High Speed Hybrid Modules Combining High Speed IGBTs with SiC-SBDs


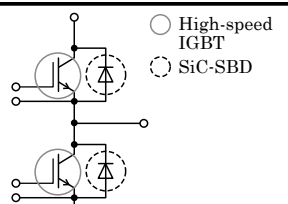

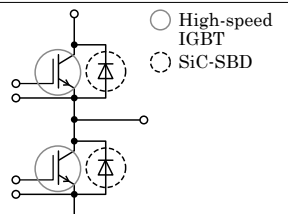
USUI, Ryosuke* KATO, Yoshiharu*

In recent years, there has been greater demand to reduce emissions of greenhouse gases such as CO₂ as a measure to suppress global warming. In order to achieve this, it has become necessary to promote a higher degree of energy savings in a variety of fields. Innovation of components such as power devices, circuits, and control mechanisms is required to advance energy savings in power conversion equipment typified by inverters, and it has become an important goal to achieve even less power dissipation in power devices. Moreover, in order to realize further miniaturization and better efficiency in power conversion equipment, an increasing number of applications are performing power conversion at high frequencies, and there is greater demand for high-speed low-loss switching. It is against this background that Fuji Electric has developed and commercialized high-speed hybrid modules that incorporate a high-speed insulated gate bipolar transistors (IGBT) that can operate at a switching speed of 20 kHz or higher and Schottky barrier diodes (SiC-SBD) into a conventional package (see Table 1).

1. Features

The high-speed hybrid module, which combines high-speed IGBTs and SiC-SBDs, makes use of the same package as conventional Si modules in order to maintain compatibility. The diode makes use of a Fuji

Table 1 High-speed hybrid module

Package	Equivalent circuit
 Standard 2-in-1 M276	 <p>○ High-speed IGBT ○ SiC-SBD</p>
 Dual XT M254	 <p>○ High-speed IGBT ○ SiC-SBD</p>

* Electronic Device Business Division, Fuji Electric Co., Ltd.

Electric SiC-SBD chip (withstand voltage of 1,200 V) while the IGBT makes use of a chip optimized for high-speed switching based on the 6th-generation "V Series." In 1,200-V/200-A rated products, loss is reduced by approximately 56% compared with the 7th-generation "X Series" Si modules.

1.1 Product line-up

Table 2 shows the product line-up for the high-speed hybrid module. Fuji Electric has recently developed a module with a 2-in-1 circuit configuration.

1.2 Generated loss of inverter

In this section, as an example, the generated loss of an inverter equipped with a 1,200-V/200-A hybrid module that utilizes an M276 package is described. Figure 1 shows the result of simulating generated loss in the inverter. In the high-speed switching region with a switching frequency of 20 kHz or higher, the generated loss of the inverter equipped with the high-speed hybrid module was approximately 56% less than that of the X Series Si module. Furthermore, the rate of reduction increased in correlation with increases

Table 2 High-speed hybrid module product line-up

Package	Circuit configuration	Dimensions	Rated voltage (V)	Rated current (A)
		W × D × H (mm)		
Standard 2 in 1	2 in 1	62.0 × 108.0 × 30.9	1,200	200
				300
Dual XT	2 in 1	62.0 × 150.0 × 20.5	1,200	300

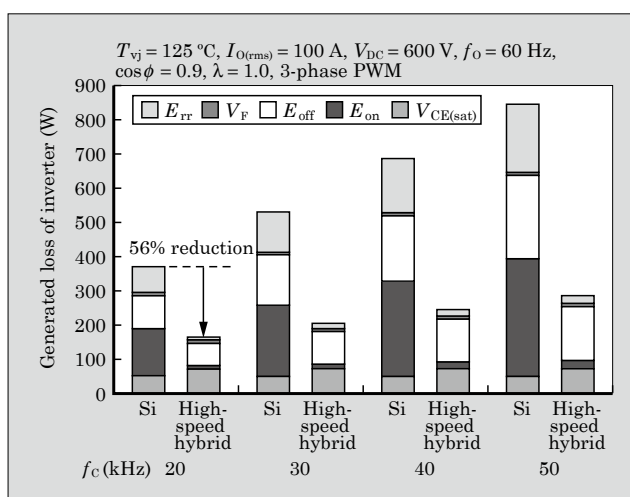


Fig.1 Inverter generated loss simulation results

in switching frequency, and it can contribute to high-efficiency operation and miniaturization through the high-frequency operation of the inverter.

2. Supporting Technologies

2.1 SiC-SBD based reduction of turn-on loss and reverse recovery loss

Figure 2 shows a comparison between reverse recovery waveforms of the high-speed hybrid module and X Series Si module. The high-speed hybrid module has a considerably small reverse recovery current peak value. This is explained by the fact that SiC-SBD is a unipolar device, and so it causes no minority carrier injection. Compared with the X Series Si module, the 1,200-V/200-A high-speed hybrid module reduces reverse recovery loss by 92%.

Furthermore, the peak value of the reverse recovery current in the free wheeling diode (FWD) is reflected in the peak value of the turn-on current in the IGBT of the opposing arm. As the peak value of the reverse recovery current gets smaller, the peak value of the turn-on current reduces, allowing the IGBT to reduce turn-on loss. Figure 3 shows a comparison between turn-on waveforms of the high-speed hybrid module and X Series Si module. Similar to reverse recovery waveforms, the peak value of the turn-on current is quite small. Compared with the X Series Si module, the 1,200-V/200-A high-speed hybrid module reduces turn-on loss by 84%.

2.2 High-speed IGBT based reduction of turn-off loss

The high-speed IGBT is based on existing V

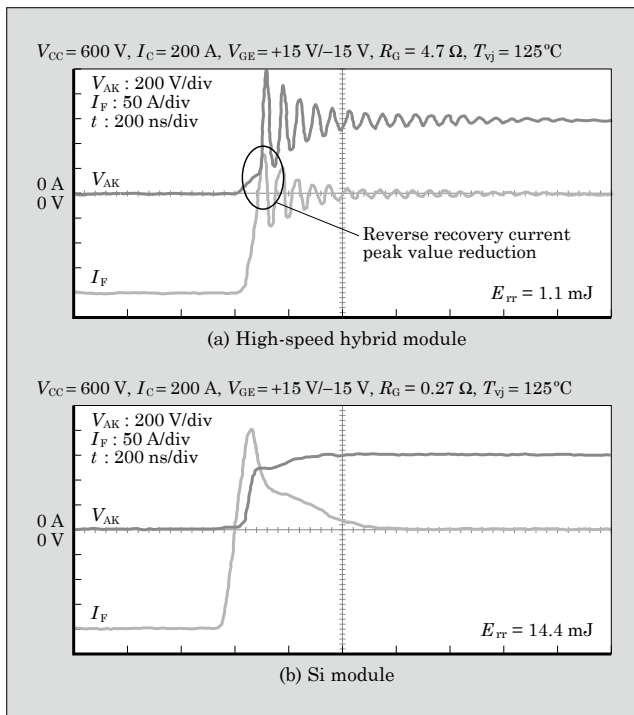


Fig.2 Reverse recovery waveforms

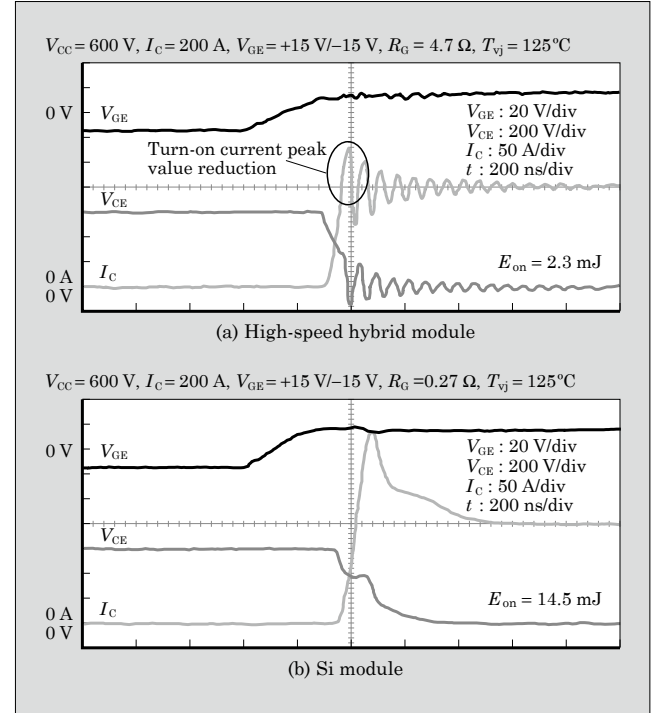


Fig.3 Turn-on waveforms

Series IGBT. It reduces turn-off loss by using an active structure that significantly reduces parasitic capacitance and by reducing the concentration of impurities in the collector layer responsible for suppressing hole injection. Figure 4 shows a comparison between turn-off waveforms of the high-speed hybrid module and X Series Si module. Compared with the X Series Si module, the high-speed hybrid module achieves a

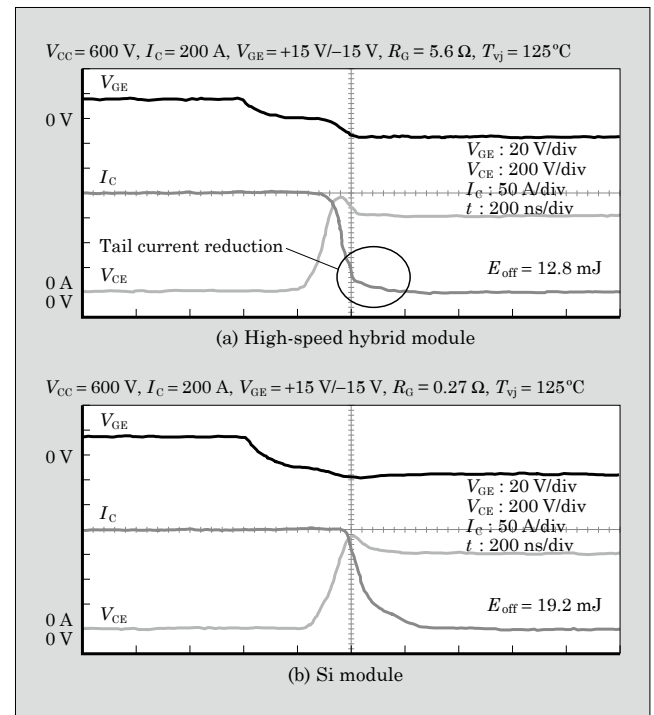


Fig.4 Turn-off waveforms

33% reduction by greatly improving tail current during turn-off.

Launch time

August 2019

Product inquiries

Sales Department I, Sales Division,
Electronic Devices Business Group,
Fuji Electric Co., Ltd.
Tel: +81 (3) 5435-7152



Overseas Subsidiaries

* Non-consolidated subsidiaries

America

Fuji Electric Corp. of America

Sales of electrical machinery and equipment, semiconductor devices, drive control equipment, and devices

Tel +1-732-560-9410

URL <https://americas.fujielectric.com/>

Reliable Turbine Services LLC

Repair and maintenance of steam turbines, generators, and peripheral equipment

Tel +1-573-468-4045

Fuji SEMEC Inc.

Manufacture and sales of door opening and closing systems

Tel +1-450-641-4811

Asia

Fuji Electric Asia Pacific Pte. Ltd.

Sales of electrical distribution and control equipment, drive control equipment, and semiconductor devices

Tel +65-6533-0014

URL <http://www.sg.fujielectric.com/>

Fuji SMBE Pte. Ltd.

Manufacture, sales, and services relating to low-voltage power distribution board (switchgear, control equipment)

Tel +65-6756-0988

URL <http://smbe.fujielectric.com/>

Fuji Electric (Thailand) Co., Ltd.

Sales and engineering of electric substation equipment, control panels, and other electric equipment

Tel +66-2-210-0615

URL <http://www.th.fujielectric.com/en/>

Fuji Electric Manufacturing (Thailand) Co., Ltd.

Manufacture and sales of inverters (LV/MV), power systems (UPS, PCS, switching power supply systems), electric substation equipment (GIS) and vending machines

Tel +66-2-5292178

Fuji Tusco Co., Ltd.

Manufacture and sales of Power Transformers, Distribution Transformers and Cast Resin Transformers

Tel +66-2324-0100

URL <http://www.ftu.fujielectric.com/>

Fuji Electric Vietnam Co., Ltd. *

Sales of electrical distribution and control equipment and drive control equipment

Tel +84-24-3935-1593

URL <http://www.vn.fujielectric.com/en/>

Fuji Furukawa E&C (Vietnam) Co., Ltd. *

Engineering and construction of mechanics and electrical works

Tel +84-4-3755-5067

Fuji CAC Joint Stock Company

Provide the Solution for Electrical and Process Control System

Tel +84-28-3742-0959

URL www.fujicac.com

PT. Fuji Electric Indonesia

Sales of inverters, servos, UPS, tools, and other component products

Tel +62 21 574-4571

URL <http://www.id.fujielectric.com/>

Fuji Electric India Pvt. Ltd.

Sales of drive control equipment and semiconductor devices

Tel +91-22-4010 4870

URL <http://www.fujielectric.co.in>

Fuji Electric Philippines, Inc.

Manufacture of semiconductor devices

Tel +63-2-844-6183

Fuji Electric (Malaysia) Sdn. Bhd.

Manufacture of magnetic disk and aluminum substrate for magnetic disk

Tel +60-4-403-1111

URL <http://www.fujielectric.com.my/>

Fuji Furukawa E&C (Malaysia) Sdn. Bhd. *

Engineering and construction of mechanics and electrical works

Tel +60-3-4297-5322

Fuji Electric Taiwan Co., Ltd.

Sales of semiconductor devices, electrical distribution and control equipment, and drive control equipment

Tel +886-2-2511-1820

Fuji Electric Korea Co., Ltd.

Sales of power distribution and control equipment, drive control equipment, rotators, high-voltage inverters, electronic control panels, medium- and large-sized UPS, and measurement equipment

Tel +82-2-780-5011

URL <http://www.fujielectric.co.kr/>

Fuji Electric Co., Ltd. (Middle East Branch Office)

Promotion of electrical products for the electrical utilities and the industrial plants

Tel +973-17 564 569

Fuji Electric Co., Ltd. (Myanmar Branch Office)

Providing research, feasibility studies, Liaison services

Tel +95-1-382714

Representative office of Fujielectric Co., Ltd. (Cambodia)

Providing research, feasibility studies, Liaison services

Tel +855-(0)23-964-070

Europe

Fuji Electric Europe GmbH

Sales of electrical/electronic machinery and components

Tel +49-69-6690290

URL <https://www.fujielectric-europe.com/>

Fuji Electric France S.A.S

Manufacture and sales of measurement and control devices

Tel +33-4-73-98-26-98

URL <https://www.fujielectric.fr/en>

Fuji N2telligence GmbH *

Sales and engineering of fuel cells and peripheral equipment

Tel +49 (0) 3841 758 4500

China

Fuji Electric (China) Co., Ltd.

Sales of locally manufactured or imported products in China, and export of locally manufactured products

Tel +86-21-5496-1177

URL <http://www.fujielectric.com.cn/>

Shanghai Electric Fuji Electric Power Technology (Wuxi) Co., Ltd.

Research and development for, design and manufacture of, and provision of consulting and services for electric drive products, equipment for industrial automation control systems, control facilities for wind power generation and photovoltaic power generation, uninterruptible power systems, and power electronics products

Tel +86-510-8815-9229

Wuxi Fuji Electric FA Co., Ltd.

Manufacture and sales of low/high-voltage inverters, temperature controllers, gas analyzers, and UPS

Tel +86-510-8815-2088

Fuji Electric (Changshu) Co., Ltd.

Manufacture and sales of electromagnetic contactors and thermal relays

Tel +86-512-5284-5642

URL <http://www.fujielectric.com.cn/csfe/>

Fuji Electric (Zhuhai) Co., Ltd.

Manufacture and sales of industrial electric heating devices

Tel +86-756-7267-861

URL <http://www.fujielectric.com.cn/fz/>

Fuji Electric (Shenzhen) Co., Ltd.

Manufacture and sales of photoconductors, semiconductor devices and currency handling equipment

Tel +86-755-2734-2910

URL <http://www.sz.fujielectric.com.cn/>

Fuji Electric Dalian Co., Ltd.

Manufacture of low-voltage circuit breakers

Tel +86-411-8762-2000

Fuji Electric Motor (Dalian) Co., Ltd.

Manufacture of industrial motors

Tel +86-411-8763-6555

Dailan Fuji Bingshan Vending Machine Co., Ltd.

Development, manufacture, sales, servicing, overhauling, and installation of vending machines, and related consulting

Tel +86-411-8754-5798

Fuji Electric (Hangzhou) Software Co., Ltd.

Development of vending machine-related control software and development of management software

Tel +86-571-8821-1661

URL <http://www.fujielectric.com.cn/fhs/>

Fuji Electric FA (Asia) Co., Ltd.

Sales of electrical distribution and control equipment

Tel +852-2311-8282

Fuji Electric Hong Kong Co., Ltd.

Sales of semiconductor devices and photoconductors

Tel +852-2664-8699

URL <http://www.hk.fujielectric.com/en/>

Hoei Hong Kong Co., Ltd.

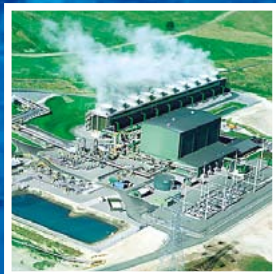
Sales of electrical/electronic components

Tel +852-2369-8186

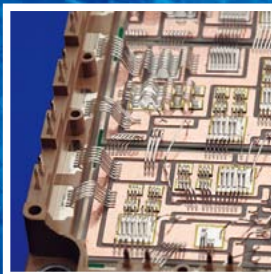
URL <http://www.hoei.com.hk/>

Innovating Energy Technology

Through our pursuit of innovation in electric and thermal energy technology, we develop products that maximize energy efficiency and lead to a responsible and sustainable society.



Corrosion Resistant, Material, and Hot Water Utilization Technology
Geothermal Power Plants



Device Technology
Power Devices (IGBT)



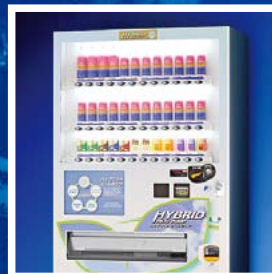
Power Electronics Technology
Power Conditioning Systems (PCS)
for Megasolar Plants



Power Electronics Technology
Inverters



Power Electronics Technology
Uninterruptible Power Supply
Systems (UPS)



Heat Exchange and Refrigerant Control Technology
Hybrid Heat Pump
Vending Machines

F Fuji Electric